# Nano-engineering polymer topographies for biological response manipulation of stem cells and bacteria

Felipe Viela Bovio

Supervisor: Dra. Isabel Rodríguez Fernández

# Contents

# Resumen

La influencia del entorno físico de una célula o bacteria en su respuesta biológica se ha convertido en uno de los campos de investigación con mayor interés por su potencial aplicación en diferentes campos de la medicina regenerativa. El estudio de la influencia de la superficie en la respuesta celular requiere un preciso control y manipulación del entorno extracelular.

El desarrollo de nuevas técnicas de nanofabricación ha proporcionado nuevas herramientas con las que controlar y estandarizar de forma precisa el entorno celular, permitiendo el estudio cuantitativo de la influencia de los parámetros físicos de la matriz extracelular, como por ejemplo la topografía, en las funciones celulares.

En esta tesis, con el objetivo de estudiar la influencia topográfica en la respuesta celular y bacteriana, utilizamos la técnica de nanoimpresión. Ésta técnica nos permite fabricar superficies poliméricas micro y nanoestructuradas a bajo coste, para el estudio sistemático de la influencia de diferentes parámetros topográficos en la respuesta celular. Además, esta técnica de nanoimpresión se ha utilizado para desarrollar un nuevo proceso de fabricación de nanocompuestos nanoestructurados.

Esta tesis está organizada en 3 capítulos principales. El capítulo 3, en el que se presenta un estudio comparativo de la respuesta celular de células madre neuronales cultivadas sobre micro y nanopilares poliméricos de alta relación de aspecto. En este trabajo se ha estudiado la influencia de estas dos topografías en la capacidad proliferación y adhesión así como la morfología y migración

celular. Además, se ha utilizado una nueva técnica combinada de microscopía electrónica de barrido y litografía de haz de iones focalizados para cuantificar las fuerzas de tracción que ejercen las fuerzas sobre los pilares durante su migración. Los resultados obtenidos demuestran una clara influencia de la topografía en las funciones celulares. Las células cultivadas sobre nanopilares demuestran una ligera disminución de su capacidad proliferativa y una reducción en el área celular proyectada. Sin embargo, tal y como se observa en células cultivadas en una superficie plana la migración sigue siendo aleatoria y rápida.

En el caso de las células cultivadas sobre micropilares, la capacidad proliferativa también se ve disminuida, y la morfología celular esta significativamente afectada, observándose células con una morfología circular y una área proyectada muy reducida así como una significativa deformación del núcleo. En este caso la migración celular está afectada de forma significativa, observándose una migración lenta pero con una alta direccionalidad. La cuantificación de las fuerzas de tracción revela un aumento proporcional de éstas con la rigidez de los pilares. Observándose mayores fuerzas de tracción en las células cultivadas sobre micropilares que sobre nanopilares. En este trabajo se demuestra la aplicabilidad de las topografías poliméricas de alta relación de aspecto para controlar la respuesta celular mediante las propiedades mecánicas de la superficie.

En el capítulo 4, se presenta la fabricación de una topografía polimérica inspirada en el ojo de la polilla y la caracterización de sus propiedades bactericidas. Los resultados obtenidos demuestran que esta topografía es capaz de reducir la proliferación bacteriana en un 50% tanto de cepas Gram

positivas como de Gram negativas, mediante la ruptura de la pared bacteriana cuando las bacterias se adhieren a esta superficie. Paralelamente, se ha estudiado la proliferación de queratinocitos y la influencia en su morfología. Los resultados demuestran la idoneidad de esta superficie para el crecimiento de queratinocitos. En este capítulo, demostramos la potencial aplicabilidad de superficies poliméricas inspiradas en el ojo de la polilla para su uso en la fabricación de materiales para aplicación biomédica, como por ejemplo implantes médicos.

En el capítulo 5, se presentan dos nuevos nanocompuestos nanoestructurados con alto poder bactericida. Continuando con los resultados del capítulo 4, para mejorar las propiedades bactericidas de las superficies poliméricas inspiradas en el ojo de la polilla, utilizamos un nuevo proceso de fabricación de nanocompuestos basado en la técnica de nanoimpresión, para incluir nanopartículas antibacterianas de $TiO_2$ y ZnO dentro de las nanoestructuras. Los resultados obtenidos demuestran que la inclusión de nanopartículas en la superficie funcional polimérica aumentan el potencial bactericida alcanzando valores del 90%, debido a la acción sinérgica de la acción bactericida de la topografía y el estrés oxidativo derivado de la presencia de nanopartículas. Sin embargo, los resultados demuestran que estas superficies mantienen su biocompatibilidad. Estos nanocompuestos nanoestructurados con alto poder bactericida aparecen como nuevos materiales para aplicaciones biomédicas y también para aplicaciones en el campo de la construcción o envasado.

# Abstract

The understanding of the cell-environment interaction and the influence of this interaction on the cell response have become a subject of intense research due to the impact in many areas of regenerative medicine. To fully understand the interaction between cells and surfaces, a precise control over the environmental parameters that influence the cell response in the extracellular matrix is required and this includes the micro and nano topography. With the development of nanofabrication technologies, new tools have emerged where the control of the cellular surroundings can be standardized and established with more precision. These micro and nano tools provide for specific spatial and mechanical cues to which cells respond and allow to perform quantitative biological investigations of cell responses to ultimately decipher the role of the matrix nanotopography as a regulator of cell function and fate.

To this end, in this thesis, functional micro and nano topographies were designed and fabricated on polymeric substrates using nanoimprinting. This nanofabrication technique allows fabricating with high reproducibility functional topographies for systematic biological studies. The imprinting methodology was established and a new process to fabricate nano-engineered nanocomposites was developed. The specific studies performed on the polymer imprinted surfaces include the response of neural stem cells to high aspect ratio nanopillars and the adhesion and viability of bacteria onto the moth-eye mimetic topography.

This thesis is organized in three main chapters. Chapter 3, “Biomechanical control by high aspect ratio nanopillars of neural stem cells”, presents a

comparative study of the neural stem cell response to high aspect ratio micro and nanopillar polymer topography. The response to these topographies in terms of cell proliferation, cell morphology, cell adhesion and migration was characterized and the cell traction forces measured by a new approach that combines scanning electron microscopy and focus ion beam. The results show evidences of a strong influence of the topography on neural stem cell behaviour. Cells cultured on nanopillared topography exhibited a somewhat reduced proliferation and cell spreading compared to the cell seeded on flat surfaces. However, the migration speed increased compared to flat surface, while the directionality was random. On the other hand, cells cultured on the micropillar topography exhibited a reduced proliferation rate, with a significant decrease of the cell spreading and large nucleus deformation and a slow but a directional persistent migration. The quantification of cells traction forces revealed an increase of the force magnitude related as well to the increase of surface stiffness. The traction forces displayed by the cells seeded on micropillars were accordingly much higher than those observed on nanopillars. Therefore, this work demonstrates the suitability of high aspect ratio polymer topographies to elicit distinct mechanical forces able to direct discernible basic cellular responses. Thus, high aspect ratio micro topographies appear to be effective tools to probe cellular and nuclear biomechanics.

Chapter 4, “Bactericidal and biocompatible moth-eye mimetic polymer topography”, presents the fabrication of moth-eye mimetic topography on poly-methylmethacrylate (PMMA), and the bactericidal attributes of this nanotopography against Gram positive and Gram negative bacteria. The results show the ability of moth eye mimetic topography to provoke the mechanical

rupture of bacteria membrane with an efficacy of 50%. Simultaneously, the moth-eye topography is biocompatible and supports the growth and proliferation of human keratinocytes. Therefore, the results substantiate the suitability of this material for applications as a non-resistance causing bactericidal material for biomedical implants.

Chapter 5, “Bactericidal biocompatible moth eye mimetic nanopatterned nanocomposites”, presents a highly effective bactericidal surfaces based on moth-eye nanopatterned nanocomposites fabricated on one-step processing. Following the results obtained in Chapter 4, this chapter demonstrates the enhanced bactericidal properties of nanostructured nanocomposites due to the synergistic effect between the nanotopography and the oxidative action of metal oxide nanoparticles reaching bactericidal effectiveness of 90%. Nonetheless, the surfaces supported keratinocytes development thus, remained biocompatible. The nanopatterned nanocomposites, with high bactericidal efficacy would be beneficial in applications in the biomedical field and other sectors like food packaging or construction.

# Chapter 1

# Micro and nanotopographies for cell and bacteria manipulation

## 1. Introduction

*In vivo,* cells and bacteria are exposed to a three-dimensional (3D) micro and nanostructured environment. In general, cells live attached to a surface and many of their biological responses are determined by the chemical and physical characteristics of this surface. By now, it is widely recognized that cells respond to the biochemical make-up and mechanical properties of the substrate, such as stiffness and deformability, and to the micro and nano topographical parameters such as geometry and density of the topographical features.[1-4]

The realization that cells respond to mechanical forces has led to a new area of research termed Mechanobiology. This emerging research area includes mechanosensing, which refers to the mechanisms that the cell has to sense the mechanical properties of their environment and mechanotransduction, which refers to the biomolecular mechanisms taking place leading to the cell response.[5-7]

Cells probe the mechanical properties of their environment and subsequently transduce this information into a specific molecular response that ultimately determines the cell fate. Cells can also alter their motility and metabolic functions in response to the mechanics of their surroundings. However, many challenges remain to fully understand the relationship between matrix mechanics and its role in cell function and regulation.[6] Design of effective artificial cell culture conditions to elicit the desired cell responses is a subject of intense research in the biomaterial field for application impacting areas of regenerative medicine such as prosthetics or tissue engineering as well as

fundamental in vitro studies of cell biology and biomechanics with implication on a variety of pathological process such as cancer or degenerative diseases.

An important component to study the cell-environment interaction is to create, characterize and manipulate cell microenvironments *in vitro*. During the last years, different micro and nanoengineering tools have been successfully applied in biological and biomedical research, generating a rich micro and nano toolbox for cell manipulation.[8] The implementation of micro and nanofabrication technologies to biological research has opened up the door for the controlled manipulation of the biological environment providing a useful technology to investigate the cell response to external physical stimuli. These new fabrication technologies have allowed to create surfaces with defined physical characteristics, including the geometrical arrangement, density, shape or dimensional parameters that allow to produce a large range of stimuli and to study the response to them by cells.[9, 10] Micro and nanotopographies have become indeed very valuable tools for the study and prediction of the cellular interaction and response to their micro and nano environments, these include cell behaviors such as adhesion, morphology and cytoskeletal organization, orientation, migration and proliferation.[11-13]

Micro and nanofabrication allow to accurate design and reproducibly fabricate cellular surroundings making possible systematic studies of the cell response to specific physical and mechanical characteristics of substrates.[14] Lately, high-throughput screening platforms have started to appear that allow to characterize the influence on cell response of a large range of varied topographical parameters in a high throughput manner.[15]

## 2. Micro and nanotopographies for cell manipulation

The rationale why cells respond to topographical parameters has been given in terms of energy barriers seen by cells on the surfaces they grow. In general, it is admitted that cells, using their surface receptors, filopodia or other cell appendages, are able to identify physical or chemical discontinuities on the surface.[13] These discontinuities can be described as energy barriers that are visible to cells through the interrupted continuity of proteins adsorbed on the surface and the abnormal presentation of these to cell surface receptors.[16]

In this situation of discontinuity, cells would tend to minimize interaction with the high-energy barriers and modify accordingly their adhesion, spreading, migration and orientation.

Micro and nanofabrication can create physical surface discontinuities with high precision and as such topographical features can be employed to modulate precisely the response of cells on surfaces.[8, 14, 16, 17]

### 2.1. Micro and nanotopographies to control eukaryotic cells response

Eukaryotic cells development takes place in a three dimensional dynamic environment. Therefore, cells sense and respond to the physical and mechanical cues of their surroundings and adapt their phenotype. Cells have a number of proteins and cellular structures, such as cell membrane or organelles, that are capable to sense mechanical properties of their environment, which are the so called mechanosensors.[18] Mechanosensors can translate a mechanical input into a biochemical output, initiating a mechanoresponsive-signaling pathway.[19] Thus, the large number of cellular structures that respond to physical or mechanical stimuli such as ion channels, glycocalix, cell-cell

junctional receptors or even the nucleus, evidences the importance of mechanosensing and mechanotransduction in cell biology. [20, 21]

Cells in general act in response to the physical and mechanical properties of their microenvironment in two different ways: with a physical response (e.g. cytoskeleton rearrangement), or with a biochemical response (e.g., activation intracellular or extracellular signaling cascades). These complex cellular mechanisms lead to the final cellular behaviors observed such as generation of traction forces or focal adhesions, cell alignment, morphological changes, apoptosis etc.

Therefore, a large number of efforts in cell mechanics have been directed to understand the interactions and decipher the mechanisms between the topographical mechanical stimulus and the induced cell response.

Micro and nanofabrication technologies provide the appropriate tools for this purpose because these technologies can produce topographical designs with high precision and reproducibility, which allow performing systematic studies of different variables at the time.[9]

The topographical parameters that influence these cell behaviors include: feature size and geometry (e.g. post or ridges) isotropy or anisotropy, density and interspacing, aspect ratio, and material related stiffness.[22]

Micro and nanoengineered topographies have enabled the manipulation and study of cell behavior in terms of motility,[23] morphology,[24] adhesion,[25] migration,[26] differentiation[27] and proliferation.[28]

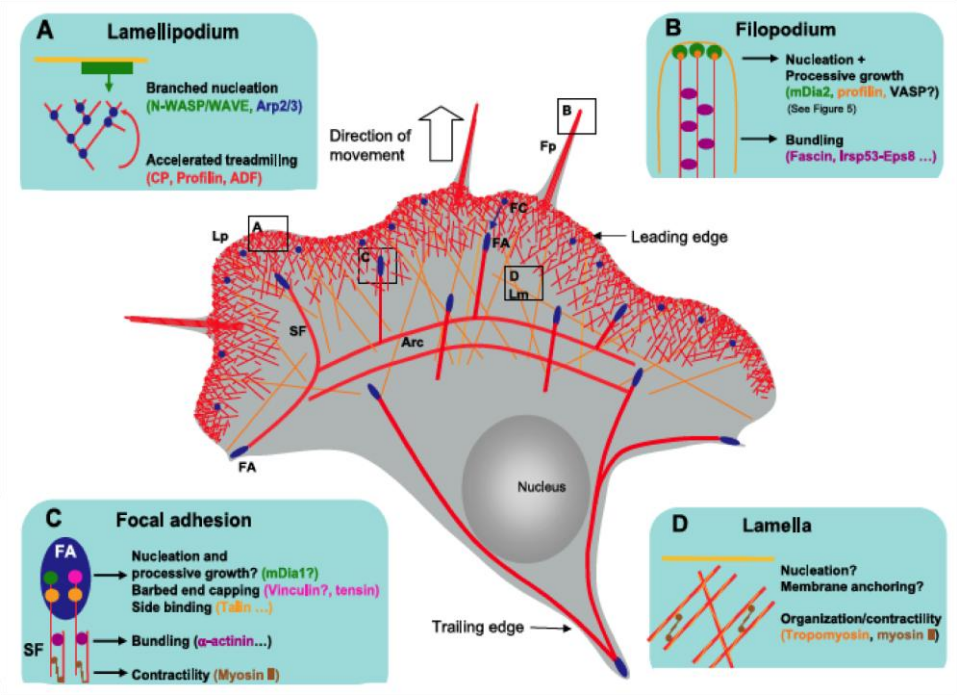


*Figure 1. Schematic illustration of the actin cytoskeleton and focal adhesions in a migrating cell. Image reproduced with permission from Ref.*[29]

### 2.1.1. Cell adhesion

Cell adhesion is the interaction between neighboring cells or with the underlying substrate (*in vivo*, the extracellular matrix), through specialized multi-protein adhesive structures.

Most cell types derived from tissues (except blood cells) need to adhere to other cells or to the extracellular matrix (ECM) to survive. Thus, the quality of adhesion is critical for their survival, proliferation and differentiation. Adhesion is mediated by transmembrane glycoprotein scaffolds, known as focal adhesions (FA), which are connected to the cytoskeleton.[30, 31] FA are receptors that act as mechanosensors allowing the cell to sense the environment and together with the cytoskeleton respond by triggering specific biochemical pathways which will determine cellular parameters such as morphology, migration and adhesion.[32]

Cell adhesion is one of the most influenced cellular functions by topography. The topographical parameters that influence cell adhesion include: feature size, geometry, density and interspacing. In this regard, micro and nanotopographies have been used to determine the impact of surface physical parameters on cell adhesion.[4]

The micro and nanostructures' feature size strongly influences cellular adhesion. Whereas, in smooth surfaces focal adhesions are randomly established, promoting the formation of disorganized connected stress fibers. Micron size scale topographies induce an organized arrangement of focal adhesions around micropillars, promoting an organized stress fibers formation, which ultimately dictates cell morphology (Fig. 2).[33, 34] On the other hand, nanometer size range features minimize the contact area between cell an surface and deter the formation of mature focal adhesions, decreasing cell spreading.[35, 36]

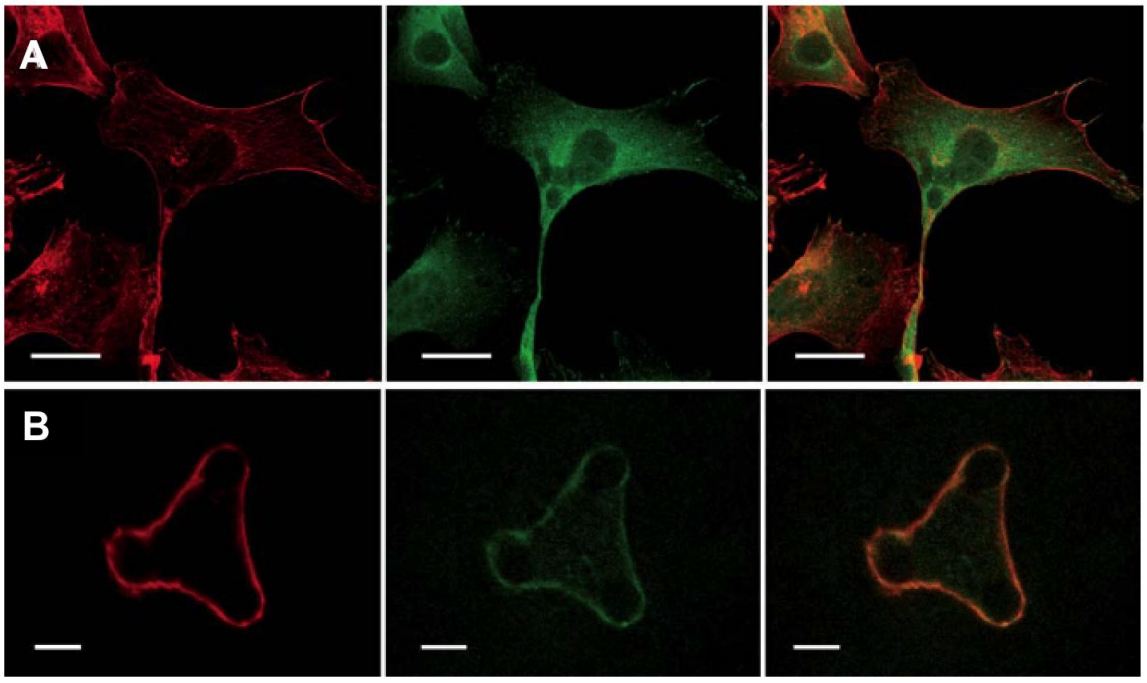


*Figure 2. Fibroblast cytoskeleton (red) and paxilin (green) reorganization when cells are cultured on smooth PDMS (A, Scale bar 15 µm) or micropillared PDMS (B, Scale bar 5 µm). Image reproduced with permission from Ref. [34]*

The influence of micro and nanostructures' density or interspacing on cell adhesion is related to the ability of the cells to reach or not the underlying substrate. It has been observed that medium and low-density micro or nanotopographies can promote cell adhesion while high-density nanotopographies can reduce it.[4, 37] Despite density is one of the most influencing factors on cell adhesion; nanostructures' interspacing appears also as an important driving factor of cell adhesion. Modifying the distance between nanostructures, one can determine if cells remain attached to nanostructures' top or it starts to sink towards the underlying substrate.[38]

### 2.1.2. Cell morphology

Cell morphology is the basic structure and appearance that a cell exhibits. Modifying the cell morphology using micro or nanostructured surfaces leads to the modification of the cellular internal organization which has a direct influence on gene expression and as such can determine cell functions such as cell survival, cell signaling and differentiation.[4]

Cell morphology can be quantified in terms of cell area, aspect ratio, circularity and solidity to quantitatively compare the morphological changes. Micro and nanostructured surfaces have been useful tools to influence the cell morphology.[2, 39, 40] Typically, on nanostructured topographies, cells exhibit a rounder aspect with smaller projected area compare to flat substrates (Fig. 3).[41-43] A pronounce decrease of cell spreading is observed when the height or aspect ratio is increased.[4, 41, 43]

High aspect ratio nanopillars have been used to determine the impact of nanotopography on cell morphology. In general, the higher aspect ratio of

nanofeatures the smaller the projected cell area.[36] This morphological influence is apparently due to the reduced contact area that high aspect ratio nanopillared topographies provide, hindering the formation of stable focal adhesions and consequently cell spreading.[42, 44-46]

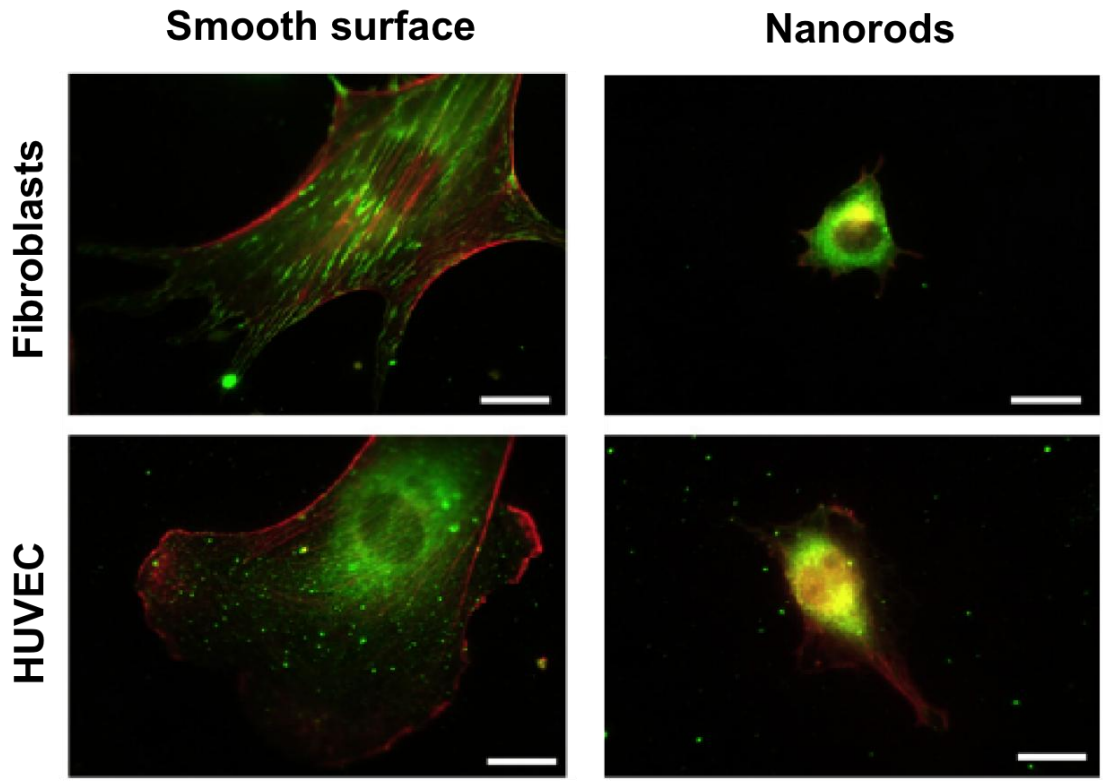


*Figure 3. Fibroblasts and endothelial cells cultured on high aspect ratio nanotopographies exhibit a reduced cell area. Scale bar 20 μm. Image reproduced with permission from Ref.[36]*

Topography can also be employed to study cell nucleus mechanics. The topography derived external forces driving the remodeling of the cell architecture can be transmitted through the cytoskeleton to the inner cell organelles, including the nucleus.[47] The cell nucleus is much stiffer than the cell cytoplasm; nonetheless, it shows viscoelastic properties and deformability.[48] Nuclear deformation has been seen during cell migration, or

during metastasis when cancer cells suffer severe deformations to invade new tissues.[49] Topographical substrates have allowed performing a qualitative characterization of nucleus deformability *in vitro*. Using a micropillared surface, it was found the nucleus of tumor cells can be deformed to much larger extent than healthy cells, indicating a reduced nuclear stiffness on cancer cells which is directly connected with their invasive capacity (Fig 4).[48, 50]

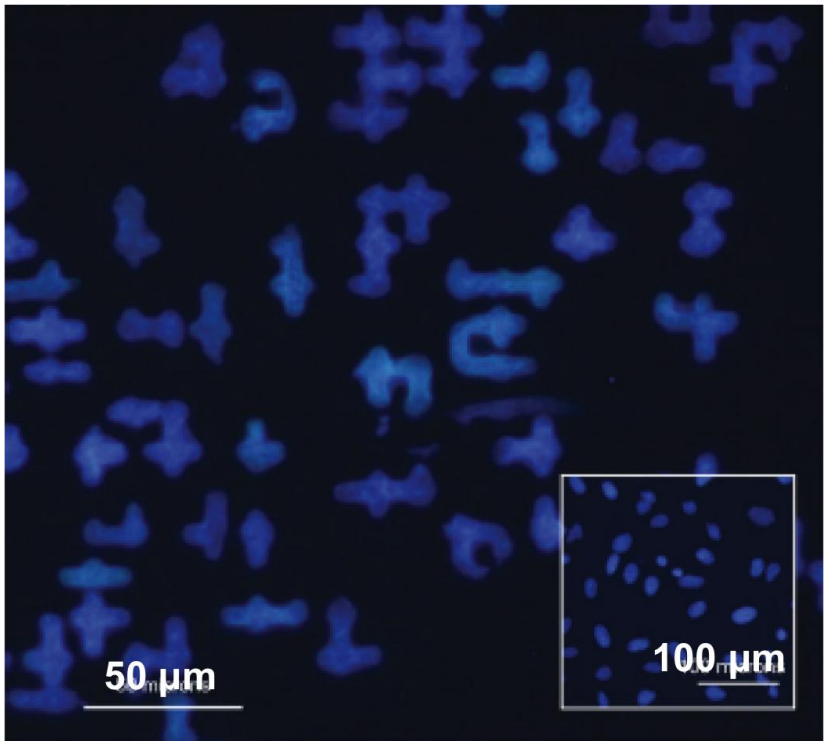


*Figure 4. Deformation of cell nuclei cultured on micropillars. The inset shows typical nucleus's morphology of cells cultured on flat substrates. Image reproduced with permission from Ref.[48]*

### 2.1.3. Cell migration

Cell migration is the broad term to refer to the cell translation from one location to another. Cell migration is an inherent process in cells and it is essential for processes such as morphogenesis, wound healing and immune responses.

Cell migration occurs in response to many factors and situations, for example the need to feed. Either as single cell or group of cells, migration is a sequential process in which cell polarization, protrusion and adhesion, translocation and retraction of the rear are required to complete a displacement.[51, 52]

For the investigation of the influence of the physical environment on the cellular migration, the application of micro and nanotopographies has been extremely useful. Studies have demonstrated that surface topography can regulate the velocity and directionality of individual cells.[53] Generally, cells are observed to elongate and migrate along a particular direction in anisotropic topographies such as channels.[54, 55]

Nanogratings and nanopillared topographies have been used to study cell adhesions and cell migration. By tuning the geometrical parameters of surfaces, it has been possible to correlate the size of the cell focal adhesions with cell migration.[56] It was found that nanoscale topographies have the capability to impair the focal adhesion maturation, turning them into transient adhesions, and seemingly increasing cell migration rate.

Cell migration implies the generation of traction forces exerted over the substrate to perform the cell translation. Thus, during cell movement, cell polarizes into a front protrusion leading the migration and a rear edge that retracts to follow the displacement (Fig 5).[57] Micro and nanotopographies have allowed studying the influence of substrate rigidity on cell migration, speed and direction. Pillars' mechanical properties can be tuned independently of the bulk materials characteristics by varying their dimensions.[58] Thus, cell culture on micro and nanopillared topographies has enabled also the quantification of

traction forces through the bending of flexible pillars caused by the cell when it moves.[34, 59, 60] Cell traction forces are essential for cell migration, but they are also used by cells to control their shape and maintain cellular homeostasis.[61, 62]

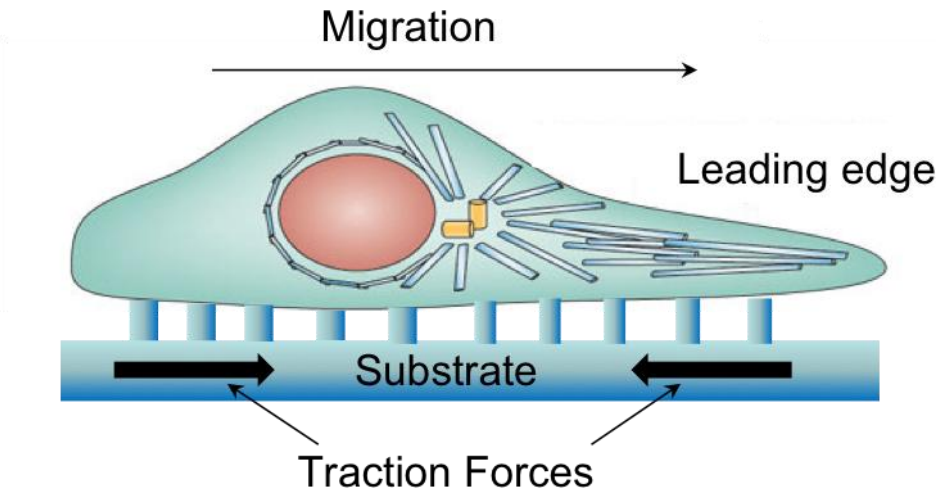


*Figure 5. Cell polarization during migration. The bending of and the flexible pillars during the cell migration allows the quantification of cell traction forces effected by cells on the underlying substrate.*

### 2.1.4. Cell differentiation

Stem cells are undifferentiated cells that own a great ability to proliferate and the potential to differentiate into different cell types.[63]

In physiological conditions, stem cell differentiation is controlled by the surrounding three dimensional environment, also known as stem cell niche, including biochemical and biomechanical signaling.

Traditionally, in vitro cell differentiation studies are based on the action of soluble factors but mechanical influence of cell environment on stem cell differentiation is still not well understood.[64-68]

There are evidences that the mechanical stimulus exerted by specific topographies have an influence on mesenchymal stem cells (MSC) differentiation.[16, 22, 69-71] And there are a few other works describing the effect of topography on cell lineage differentiation towards neurons[27] or endoderm cells.[68]

Due to the high potential of stem cells to proliferate, self-maintain and differentiate, the investigation of the influence of topographies on stem cell fate has been focused on these aspects.[69, 70]

Ultra high aspect ratio polymer nanopillars have been used to successfully direct human embryonic stem cells differentiation towards endoderm cells.[68] Besides, low aspect ratio polymer nanopits have been used to address the differentiation of mesenchymal stem cells. Dalby and coworkers studied the influence of ordered and disordered pillared geometries on MSC differentiation.[69] They concluded that highly ordered topographies have a negligible effect on cell adhesion and differentiation, while disordered topographies promote MSC differentiation towards osteocytes.

Therefore, due to the high potential of micro and nanotopographies to control or manipulate the behavior of stem cells, micro and nanopatterned substrates have emerged as a promising alternative to develop smart materials for regenerative medicine, tissue engineering, or for biological in vitro studies of mechanical influence on a wide variety of pathological process.

### 2.2. Micro and nanotopographies to modulate the bacterial response

Like eukaryotic cells, bacterial function is also influenced by surface topography. Bacteria have a natural tendency to adhere as nutrients tend to accumulate on surfaces in liquid environments.[72-74]

Consequently, bacteria have evolved the means to sense and adapt to their environment by chemical and physical sensing mechanisms. For instance, attached bacteria usually produce large amounts of extracellular-polymeric-substances (EPS), allowing them to create a matrix-protected biofilm providing a better growth environment.[75, 76]

Bacteria respond to their environment through changes in tension of the cell membrane upon bacteria-surface attachment. The established bacteria-surface interaction generates a mechanical stress yielding membrane deformation (Fig. 6A).[77-79] Mechanosensitive channels (MC), which are sensitive to membrane tension, are opened in response to this membrane deformation (Fig. 6B). MCs translate the mechanical stimuli into a biological response triggering the modification of gene expression to adapt bacteria from planktonic phenotype to surface-adhering phenotype.[76, 80, 81]

Stress sensitive (SS) proteins present on bacterial membrane mediate an alternative mechanism. SS proteins sense and response to a variety of signals described as membrane perturbations, such as periplasmic protein misfolding. When SS proteins are activated, they trigger a phosphorylation cascade that activates regulatory proteins that bind bacterial DNA and modify gene expression to adapt their phenotype to the new environment (Fig. 6C).[76, 81, 82]

Therefore, either by external forces acting on bacterial wall or the adhesion force arising from the surface interaction, bacterial membrane deformation upon attachment has been acknowledged as the main mechanosensing mechanism that determines the changes on the bacterial phenotype.

The bacterial ability to respond towards physical environmental factors has been an intense subject of research through the use of micro and nanostructured topographies. These have largely focused on the development of topographies that prevent bacterial colonization or proliferation to avoid biofilm formation as one of the most important problems derives from infection.

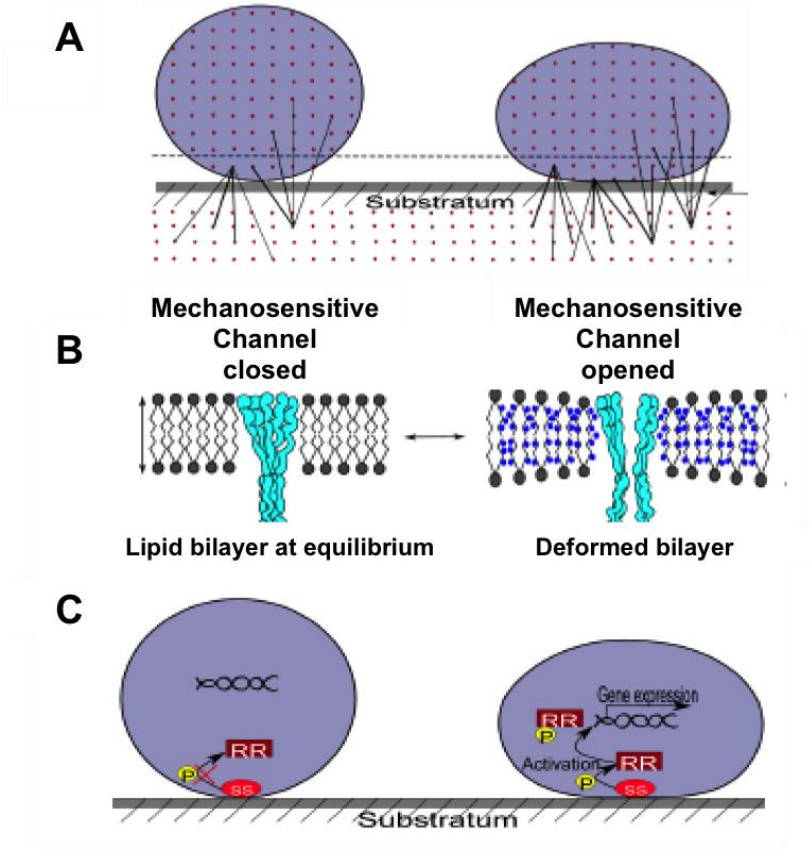


*Figure 6. Bacterial wall deformation and mechanosensing. A) Bacteria-substrate long-distance interaction causes cell wall deformation. B) Mechanosensitive channels act as mechanotransductor of membrane tension by opening upon membrane deformation. C) Membrane deformation activate of stress sensitive proteins regulating gene expression. Image reproduced with permission from Ref.*[76]

Bacteria attachment to surfaces has been reported to be influenced by the surface feature geometry,[83] dimensions,[84] interspacing,[85] or roughness.[86] Micro and nanotopographies have been used to show that bacterial adhesion is influenced by the surface geometrical factors and the topography determines the bacteria orientation during the initial settlement and in some works disrupt the formation of biofilm (Fig 7).[87, 88]

However, a direct correlation between surface parameters and bacterial response cannot be established and the results published are sometimes controversial.[89-94] It has been found a tendency such that superhydrophobic surfaces are antibacterial while hydrophilicity promotes bacterial adhesion, but this it not always the case.

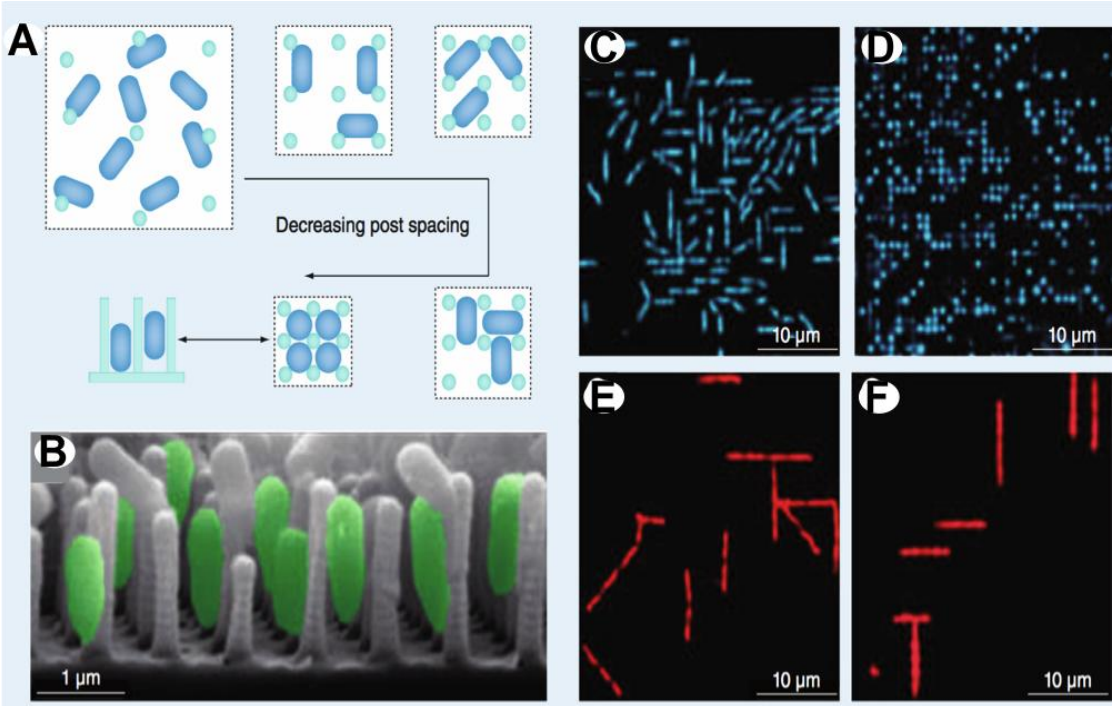


*Figure 7. Nanotopographies to control bacterial attachment. A) Schematic representation of the influence of interpillar space on P. aeruginosa adhesion. B) SEM imaging of attached P.aeruginosa to nanopillars. C, D, E, F) Fluorescence imaging of bacterial attachment to nanopillared topographies. Image reproduced with permission from Ref.[85].*

In addition to modulating adhesion, topography has also an influence on the viability and proliferation of attached bacteria to a surface. This effect was found on natural topographies such as the cicada wing[95] and subsequently on dragonfly wings[96] gecko skin,[97] or shark skin.[98] These species display a nanocone topography that reduces bacterial adhesion and renders them non viable (Fig 8).[98-102] These findings have opened the door to the use of advanced nanofabrication techniques to design natural mimetic topographies to develop new smart materials that can effectively prevent the bacterial adhesion or proliferation without causing resistance.

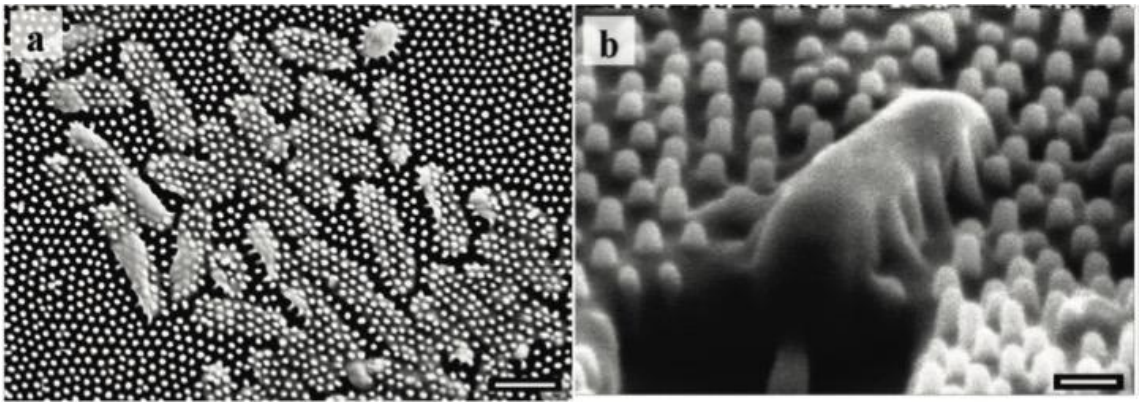


*Figure 8. Bactericidal effect of natural topographies. A) SEM image of P.aeruginosa attached on cicada wing surface, death bacteria exhibit a squashed appearance due to the interaction with the naotopography (Scale bar 1 µm). Ion milled cross section of bacteria attached on cicada wing topography (Scale bar 200 nm). Image reproduced with permission from Ref.[102]*

## 3. Objectives

The overall objective of this thesis is to engineer functional micro/nano topographies in polymers to influence the biological response of eukaryotic cells and bacteria with potential applicability as materials for regenerative medicine and medical implants.

Another objective is to develop a practical and reproducible nanofabrication process based on polymer nanoimprinting to produce with high precision micro and nano polymer patterned surfaces that allow for biological systematic studies

The specific main objectives can be summarized as follows:

1. To develop the nanoimprinting fabrication process to create the appropriated nano and micro topographies to elicit desired cell behavior.
2. To perform a quantitative study of stem cell cellular and nuclear biomechanics on high-aspect-ratio micro and nanopillared polymer topographies.
3. To create bactericidal surfaces based on non-resistance causing natural bactericidal topographies, which at the same time show biocompatibility and allow eukaryotic cell development.

The specific objectives are covered in three different chapters. Chapter 2 covers the influence of high aspect ratio micro and nanopillared topographies on neural stem cell functions. Chapter 3 covers the developmental of bactericidal surfaces based on the moth eye mimetic topography including as well, the investigation of the biocompatible properties. Finally in chapter 4 present a new method to

fabricated nanoparticle enhanced moth-eye bactericidal surfaces and the impact on eukaryotic viability.

# Chapter 2

# Nanofabrication techniques for biological applications

## 1. Micro- Nano fabrication for biomanipulation

Micro and nanofabrication devices have emerged as important tools to precisely manipulate biological entities. The capability to handle and manipulate cells *in vitro* with precision has enabled a number of advancements in quantitative cell biology research and directly impacts fields including tissue engineering, regenerative medicine, drug-screening and medical diagnostics.

Micro-nano tools have become essential for quantitative cell biology because they allow to standardize and reproduce the environmental parameters of *in vitro* assays and to perform programmed investigations altering these parameters to qualitatively and quantitatively qualify the effects on cell behavior. As such, micro and nanotools have provided a better understanding of surface bio interactions and mechanobiology processes.[8, 103]

A number of techniques have been employed for the fabrication of micro-nano devices for cell manipulation. These can be classified on direct writing techniques and replication techniques

### 1.1. Direct writing techniques

#### 1.1.1. Electrospinning and 3D printing

One of the most widely employed techniques to construct cell scaffolds is electrospinning. This technique makes use of an electric field to pull out of a nozzle micro or nanofibers that eventually form a mesh.[104] (Fig. 1A) This technique has been employed widely because of its practicality and low cost to produce nano-sized fibers and scaffolds with large ratio between area and volume on a large variety of materials, ranging from composites to proteins or

polysaccharides.[105, 106] Electrospinning has been frequently used for the fabrication of scaffolds for cell culture and antibacterial materials.[107-109] However, the lack of control of internal architecture and topology of electrospun fibers, have shifted the attention to other techniques that allow the fabrication of more controlled architectures. Recently, 3D printing or additive manufacturing has emerged as a revolutionizing manufacturing technology. Additive manufacturing can produce three dimensional objects through fusing, crosslinking or depositing materials, such as polymers, ceramics, metals, liquids, powders or even live cells, layer by layer to create the 3D object which have been previously designed by computer software.[110, 111] Typically, a computer-controlled stage moves a pattern-generating head while depositing material till a 3D object is reproduced (Fig. 1B). Different patterning heads based on laser optics or ink-based print-head, can be used for 3D printing. Patterning heads based on laser optics provide a number of alternatives for 3D fabrication, such as stereolithography (SLA) of photocurable resins or selective laser sintering of polymeric powder.[111] Ink-based printer heads allow further extending the number of materials that can be used for 3D printing by droplet- or filament based printing. Moreover, 3D printing can be used to directly fabricate three-dimensional structures using live cells as primary source. In a bioprinting process, live cells can be deposited together with materials to form in vitro scaffolds for cells, [112] tissues or even whole human organs, providing an important fabrication technique for tissue engineering and medical field.[104, 113] However, up to date, there are still some important technical limitations for its applicability. Firstly, it is the lack of resolution of the current processes, which is in general above the micro-scale. The second limitant factor is the materials,

there are only a few suitable which can be used with the current instrumentation.

Ultimately, the succesful integration of an implant requires the vascularization and this is far from realized today.[104, 111]

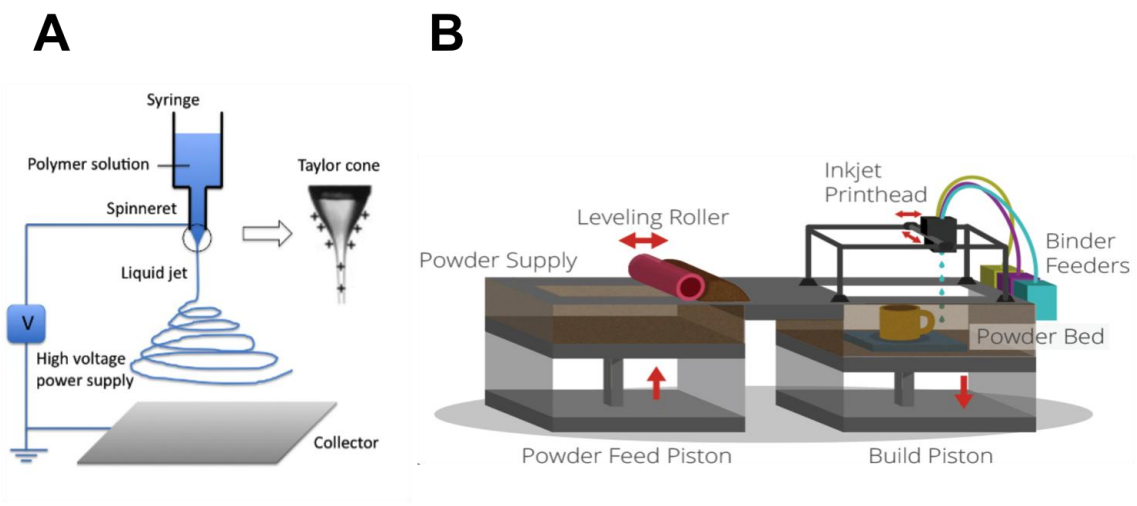


*Figure 1. Set up for electrospun polymer nanofibers fabrication (A) and 3D printing (B). Image reproduced with permission from A) Ref.[114] B) https://3dprintingindustry.com/3d-printing-basics-free-beginners-guide/processes/*

### 1.1.2. Photo and e-beam lithography

Lithographic techniques are the most widely employed technologies for the fabrication of micro and nanopatterned materials due to their ability to reach up to 5 nanometer resolution with a precise control of the geometrical and dimensional parameters of the features.

Photolithography, have been routinely used to fabricate micro and sub-micron scale features on semi-conductor materials including silicon wafers, glass and

quartz. Photolitography, also named as optical lithography or UV lithography, creates patterns using a UV light source. After substrate's conditioning a polymer light sensitive thin film (photoresist) is spin coated onto the substrate, then the wafer is heated to remove the remanant solvent (soft bake). Then it is exposed to UV light through a photo mask previously designed to create the patterned.. After exposure the UV exposure, the photo resist is generally baked and finally developed. Subsequently, the wafer is postporecess by dry or wet etching proceses to transfer the micro or nanopatterns from the photoresist to the substrate (Fig. 2). The smaller feature size that can be achieved with photolithography is ~0.3 μm due the light diffraction limit. Hence, for the fabrication of features below 500 nm, electron beam lithography (EBL) is generally employed. Advanced ion beam lithography (IBL) techniques are used for to achieve sub-10 nm resolution.[115]

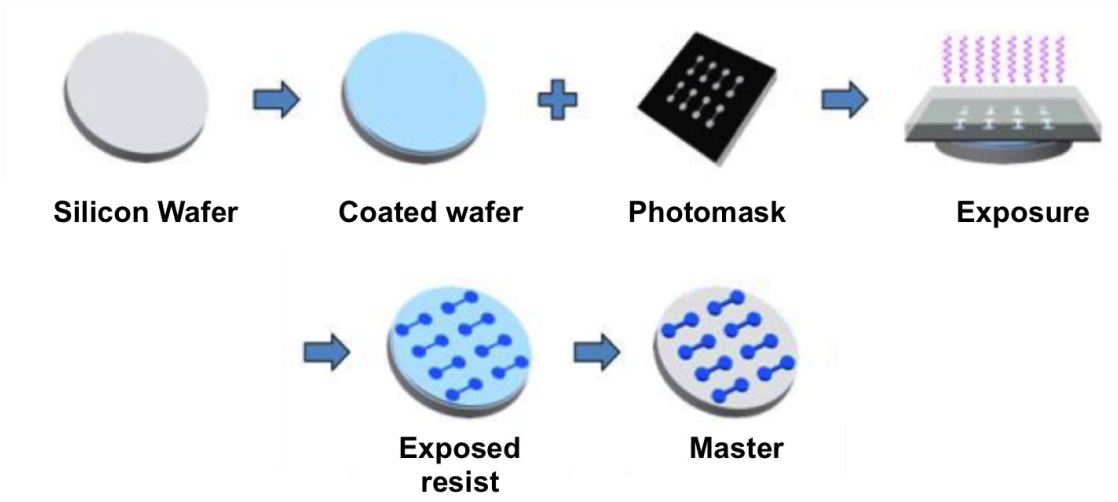


*Figure 2. Sequential procedure for mold fabrication by photo and e-beam lithography. Image modify from http://www.openwetware.org/wiki/Photolithography*

## 1.2. Replication techniques

Micro and nanofabrication techniques with higher precision and versatility have been principally developed by the electronic industry which traditionally employ hard inorganic materials. These materials in most cases are not suitable for cell culture and bio applications due to their hard, brittle and, frequently opaque properties. Thus, other technologies have emerged that allow replicating with high fidelity lithographic patterned templates into soft polymeric materials, which are more biocompatible.

### 1.2.1. Soft lithography

Soft lithography is a replication technique to transfer the nano or microstructure from a master mold or template, previously fabricated by photolithography or e-beam lithography, into a silicon elastomer, poly-dimethyl-siloxane (PDMS).[8, 103] PDMS replicas are fabricated by casting a liquid mixture of the pre-polymer and crosslinker, into a master mold. Then, the polymer is thermally cured and peeled off from the master mold, obtaining a PDMS replica of the micro or nanopatterned master mold (Fig. 3).[116]

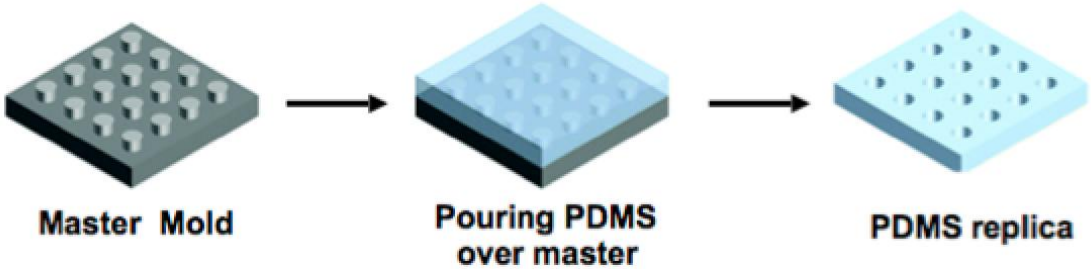


*Figure 3. Soft lithography process*

PDMS is a thermostable polymer with low surface energy, which prevents adhesion to other surface materials. For this reason, in this thesis soft

lithography has been employed to replicate the master molds and subsequentely the PDMS master molds replicas are employed for nanoimprinting. This intermediate step allows preserving master molds.

Soft lithography has been one of the most popular techniques for transferring micro and nanopatterns to compatible materials for biological applications at low cost.[117-119]

Different techniques derived from soft lithography have emerged for biological research. One of the most useful has been microcontact printing (μCP). This technique has been extensively used to create protein patterns on surfaces and to make cell patterned arrays.[120-122] In the process, the PDMS stamp is inked on the protein solution and then, upon contact, the inked mold transfer the protein patterned on to a surface (Fig. 4 D, E, F).[123] μCP has been extensively applied in biological research, the diffusion of the molecular inks and the molecular disorder at the pattern edges, limits the resolution of this technique to 100-200 nm.[124, 125]

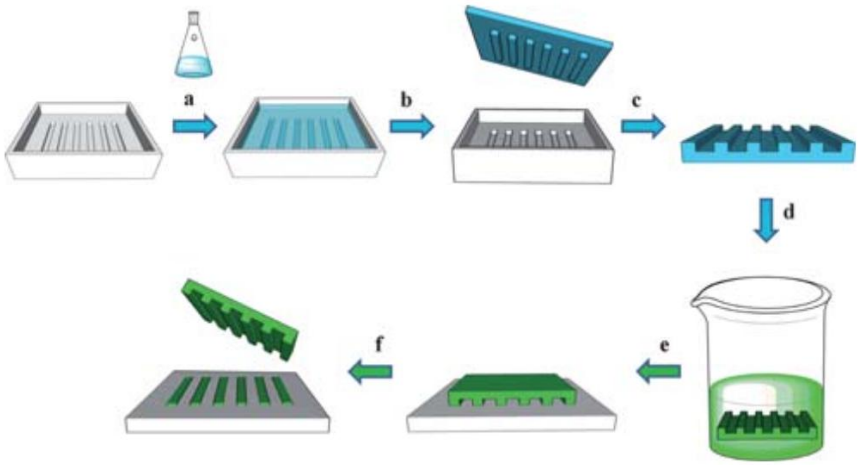


*Figure 4. Soft lithography (top), micro-contact printing process (bottom). Image reproduced with permission from Ref.[123]*

### 1.2.2. Nanoimprint lithography

Nanoimprint lithography (NIL) was introduced in 1995 by Chou *et al.,* firstly as thermal nanoimprint lithography process (tNIL) using a thin thermoplastic film as a resist material.[126] Subsequently, the process is also carried out using UV curable liquid resins to improve resolution and further extend its applicability.[127]

Typically, NIL has been used as replication method to fabricate nanometer scale patterns onto an imprint resist which then is processed to transfer the pattern from the resist to the underneath substrate.[126] However, NIL can be also used as fabrication technique of functional polymer topographies by direct replication of a master mold in any thermoplastic or UV curable polymer. In this thesis, NIL is used for direct replication of nanostructure onto polymers to obtain functional topographies, which is in fact a nano-hot embossing process. Hence, in the following sections NIL will be termed as nanoimprinting.

Nanoimprinting is a replication technique that allows transferring micro or nanostructures from a master mold, typically made of silicon or nickel, to a thermoplastic polymer or resin. Nanoimprinting starts with the loading of the mold on to the polymer films. Polymers are heated over the glass transition temperature. As the polymer is heated up, it becomes soften into a molten stage, where it will fill in the mold cavities under sufficient imprinting pressure which typically ranges between 20 and 40 bars. Finally, the mold-polymer assembly is cooled down and the demolding is performed (Fig. 5). NIL is a cost effective nanofabrication technique that allows the replication of micro and nanofeatures on a wide variety of polymers with high reproducibility, precision and throughput. Thus, nanoimprinting allows the mass production of well-

defined micro and nanotopographies in large number of substrates which is advantageous for systematic and reproducible biological studies.[128] The replication of functional nanostructures onto polymers is attracting interest for applications in the biomedical filed. Many polymers, such as silicones, methacrylates such as PMMA, polyesters (polycarbonate (PC) or poly lactic acid (PLA)) and polyolefins (polypropylene (PP) or polyethylene (PE)) are currently used for the fabrication of biomedical devices[129] and can be processed readily by nanoimprinting. Other important advantage of nanoimprinting is the high throughput production and the readiness of the technology for up scaling via roll-to-roll processing.

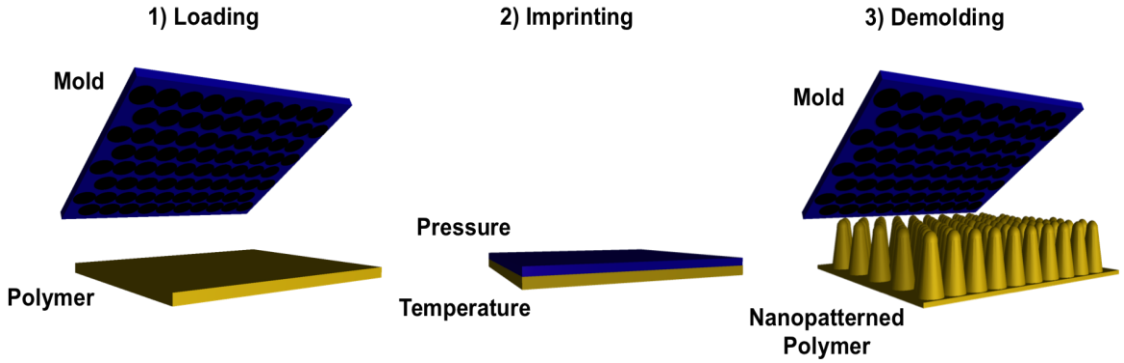


*Figure 5. Schematic representation of nanoimprinting replication process.*

### 1.2.3. Roll-to-roll nanoimprinting

Roll-to-roll nanoimprinting manufacturing consist of an imprinting roller with a patterned surface or wrapped with a flexible mold, which is used to imprint onto a flexible substrate set on a supporting roller (Fig. 6).

Thermal R2R process consist of a continue film of thermoplastic polymer, which is heated at the surface and pressed against the imprinting roller to transfer the

features of the mold continuously at the same time that the roller mold detaches on the other side liberating the features (Fig. 6A).

UV R2R process (Fig 6B), requires a substrate, such as polyethylene terephthalate (PET), to be coated with a thin film of UV curable polymer which is pressed against the imprinting roller, at the same time that is exposed to UV light to cure the resist before separating the film from the mold.[130]

Roll-to-roll nanoimprinting is a suitable technique for mass-production of nanostructured polymers or resins in a continuous and high throughput manner. This technique can be combined with other industrial processes such as chemical vapor deposition, sputtering or coating set ups in nano manufacturing facilities.[131, 132]

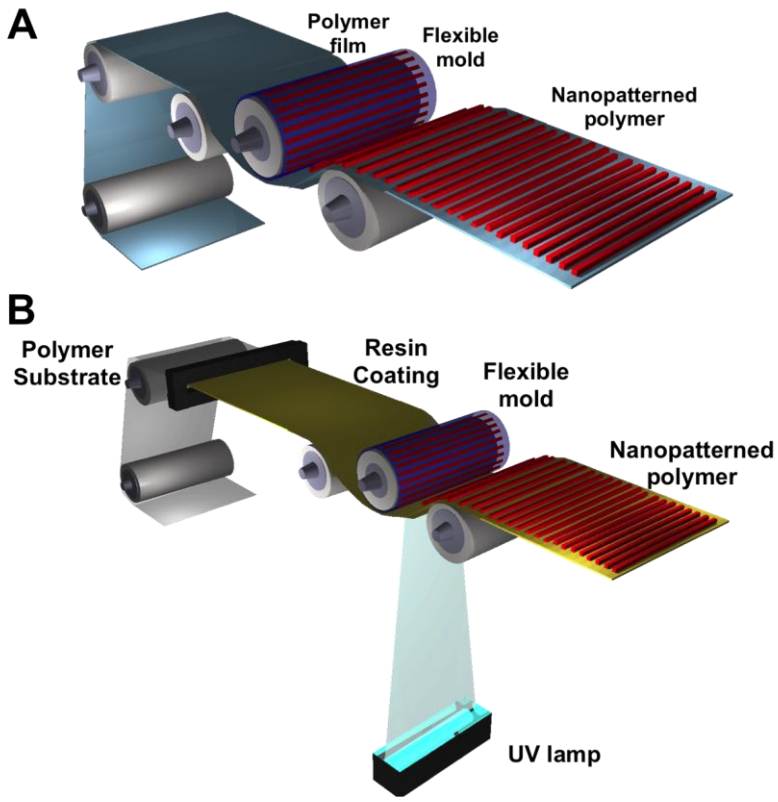


*Figure 6. Thermal (A) and UV (B) roll-to-roll units for mass production of micro and nanopatterned polymer films.*

In this thesis, nanoimprinting has been employed to prepare patterned topographical substrates for bio-interaction and mechano-biology studies. As mentioned, nanoimprinting offers a number of advantages such as material versatility, high resolution and replication fidelity, possibility for high throughput or upscale processing which allows the production of nanoscale devices at very low cost and disposable as it is required in these studies.

# Chapter 3

# Biomechanical control by high aspect ratio nanopillars of neural stem cells

## 1. Introduction: Mechanosensing on cellular physiology and pathology

Traditionally, research in biology has been performed focused on the biochemical aspects, using molecular and genetic techniques. Accordingly, pathological processes have been considered as an alteration of biochemical signaling.[49] However, during the last years the realization that the composition, the mechanical properties and surface topography of the extracellular matrix (ECM) provide surface cues which are a key influencing the cell fate and response, has change the way cell biology is performed.

Today, there is an extensive activity on biomaterial´s research where the composition, mechanical properties, surface topography including geometry and dimensionality are designed to elicit desired cell responses and ultimately control the cellular response.[16, 22, 133]

Micro and nanofabrication techniques are extremely useful providing precise and affordable tools for the precise control of a single environmental parameter, allowing researchers the standardization of environmental conditions.[9] The regulation of cell behavior by physical material attributes without the need for specific chemical factors will provide for very low cost and practical means of regulating *in vitro* the biological activity. This will be of great advantage in applications for fundamental *in vitro* studies of cell biology and biomechanics as well as in regenerative medicine.[22]

In this field, stem cells (SC) are the most promising cell sources for tissue engineering due to their ability for proliferation, self-renewing and differentiation.[134] More recently, it has been observed that the ECM physical

attributes can also regulate the gene expression and cell differentiation of stem cell.

### 1.1. Mechanosensing by stem cells

Stem cells (SC) are undifferentiated cells that are capable of proliferation, long-term renewal and differentiation towards specific cell phenotypes (Fig 1). *In vivo*, SC functions are controlled by a 3D microenvironment within the tissue, name as ‘stem cell niche’, in this location stem cells can reside for a indefinite period of time producing progeny while self-renewing.[63, 135] The chemical and physical characteristics of stem cells niches are important key factors in the control of their fate and function.

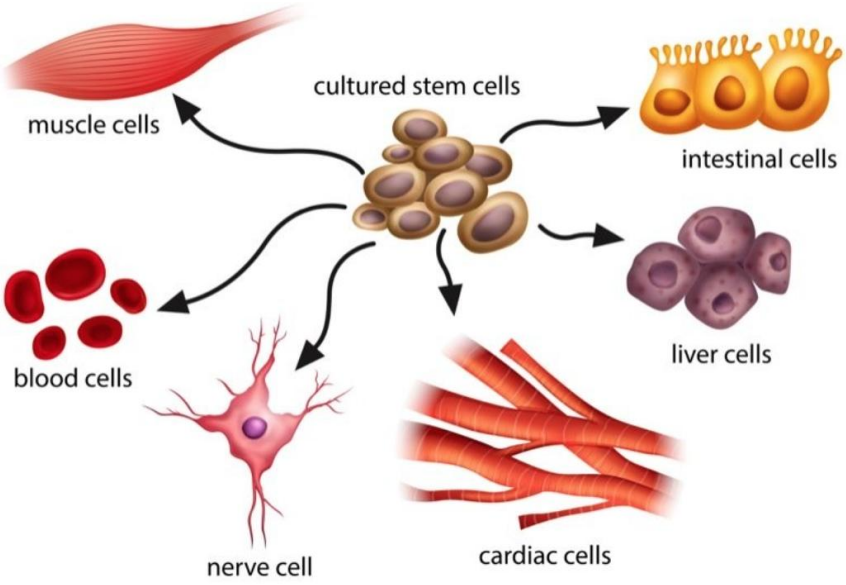


*Figure 1. Stem cells can differentiate towards different phenotypes, from blood cells to neurons. Image taken from https://www.cryo-cell.com/cord-blood/about-stem-cells.*

The influence of stiffness[136, 137], nanotopography[39, 69] and chemical functionalization[138-140] of a substrate on the stem cells fate have been previously reported.[63] However, much more research is needed to elucidate

the complex processes giving rise to the mechanical stimulation of differentiation pathways. The understanding of the response of stem cells towards a mechanical stimulus is crucial for the *in vitro* control and differentiation of stem cells towards specific cell phenotypes. In the replacement of damaged cells, tissues or even organs, new regenerative medicine approaches based on the physical cell microenvironment would benefit enormously from a low cost and practical means to obtain differentiated cell cultures.[141, 142]

Recently, neural stem cells (NSC) have raised great interest due to promising applications in the treatment of neurodegenerative disorders such as Alzheimer's, ischemia or Parkinson's diseases. Mouse neural stem cells C17.2, have been employed as model due to their ability to differentiate in astrocytes, oligodendrocytes or neurons and their potential application in regenerative medicine to repair neurological damages and brain injuries.[143, 144] Neural stem cells differentiation mediated by biochemical signaling has been extensively studied.[145] Nevertheless, a deeper understanding is required to use mechanical cues as regulation parameters of stem cell differentiation towards specific cell phenotypes to facilitate the use of these cells for developmental studies or cell-based regenerative therapies.

**2. Micro and nanostructured topographies to control stem cell response**

*In vitro* model systems have been applied to study the influence of external mechanical forces on stem cell fate and to gain further understanding of the stem cell biology.

With this aim, there have been numerous approaches to develop materials with fine control of the topographical features using micro and nanofabrication techniques.[146] These technologies enable the fabrication with nanoscale precision and high reproducibility, of cellular instructive micro and nano topographical environments. Nanoimprinting exhibit many advantages over other fabrication techniques such as the ability to pattern a large variety of materials and geometrical features form micro to nano scale with high precision, at large scale and cost effectively.[128] These characteristics are essential to produce feature-controlled substrates in large number to permit repeatable studies in large numbers. Well-controlled extensive studies will allow gaining a wider understanding of the mechanotransduction mechanisms involved in cell adhesion and the interplay between surface topography and cellular response, which appears to be an important step towards the development of next generation of smart surfaces for biomedical applications. Most studies of cell behavior on topographical surfaces have been performed on low aspect ratio features.[54, 70, 147-149] Studies of cell behavior on high aspect ratio (HAR) features are scarcer; presumably because of the more challenging fabrication process compared to low aspect ratio features. Studies of cell response on HAR pillars include silicon substrates, [42, 150] semiconductor nanowires,[151] metallic pillars,[44, 100] and polymers.[45, 46, 100] Nanopillars and nanowires in rigid materials have been commonly employed to gain intracellular access for delivery or as diagnostic probes.[4] Recently, nano pillars were employed as tool to probe nuclear mechanics[152] and furthermore, embryonic stem cell differentiation onto definitive endoderm was demonstrated on HAR polycarbonate pillars.[68]

HAR structures offer an additional number of physical cues or parameters that could be tuned to trigger desired cell responses. Cell behavior on HAR topographies has been reported to be influenced by the substrate specific geometry and feature size,[153] the feature height,[42, 45] aspect ratio and linked effective stiffness[33] as well as feature density.[4, 42] Cells on HAR pillar arrays of high density generally appear to present lower rates of adhesion and proliferation[4] with a possible explanation that cells experience reduced available contact area and or less stable focal adhesions.[154] In contrast, the trend observed for cells seeded on low density HAR arrays is an enhancement of cell adhesion.[41] In these substrates cells are seen to reach the underlying substrate, where the HAR structures act in many cases as anchor points of focal adhesions.[35] Nonetheless, most of cell behavior studies on HAR substrates have focused on morphological changes and cell orientation, whereas other aspects such as cell proliferation and migration dynamics have received much less attention.

Despite the many efforts, numerous challenges remain to fully understand the complex cellular-matrix interactions and their role in cell function regulation. In this work, to bring further insights to the field of stem cell nanomechanics, the response of progenitor neural stems cells to HAR dense pillared topography in two different scales, the nano and the micro is characterized. Detailed characterization of the cell adhesion, viability and proliferation rate, cell morphology, cell migration dynamics and traction forces is performed. Each topographical scale elicited a distinct behavior. Cells seeded on the micro scale HAR topography showed a more confined morphology and large cytoplasmic

penetrations into the HAR topography with reduced mobility and high traction adhesive forces. Conversely, cells on the nanotopography showed high rate of proliferation, a large cell spread, high mobility with random migration altogether with low traction forces.

## 3. Experimental section

**3.1. Patterning of HAR topographies: HAR pillar structures were patterned** by thermal nanoimprinting. The required silicon templates were fabricated through standard clean room processes of photolithography and reactive plasma etching. The templates were coated with a Perfluorodecyltrichlorosilane (FDTS) (Alfa Aesar) through vapor deposition as release agent to facilitate the demolding process. Imprinting was performed using a CNI nanoimprinter (NIL Technology). The substrates employed were polycarbonate films (Lexan 8040, Sabic) with a thickness of 175 µm. The PC films were imprinted at 180°C and 6 Bars of pressure for 20 minutes. The polymer-mold assembly was allowed to cool down to 80°C before the pressure was released and demolding was performed. Nanopillars of 500±15 nm in diameter and 2 µm height and micropillars of 2±0.5 µm in diameter and 10 µm in height were produced. Scanning electron microscope (SEM) imaging was carried out using an Auriga FIB-SEM system (Zeiss). The wetting behavior of the substrates was evaluated by measuring the contact angle (CA) of 5 µl of water drops using a tensiometer (Theta Lite system, Biolin).

**3.2. Nanopatterned surface conditioning**: The imprinted substrates (four substrates of each topography) were cut to size (7 mm in diameter) and fixed on a 24-well-plate. Subsequently, the substrates were sterilized and then incubated in 0.5% Gelatin (Sigma-Aldrich) solution for 30 minutes at 37°C and

in 5% $CO_2$ atmosphere. The excess of gelatin solution was removed by aspiration and the substrates were rinsed with PBS twice (Fisher Bio reagents).

*Cell Culture*: Mouse Neuronal Stem Cells C17.2 were cultured in Dulbecco's modified Eagle's medium (DMEM, Invitrogen) supplemented with 10% Fetal Bovine Serum (Gibco), 5% Horse Serum (Sigma) and 1% penicillin-streptomycin (Gibco) at 37°C and 5% $CO_2$ atmosphere.

**3.3. Cell Viability Assay**: The assay was conducted in triplicate for each of the substrates tested and in two independent assays. Cells were seeded on the prepared substrates at a density of 15000 cell/ml. The cell viability was assessed by colorimetry using the test kit *CellTiter 96® $AQ_{ueous}$ One Solution Cell Proliferation Assay* (Promega). The data given correspond to the 1st, 4th, 5th, 6th and 8th day of growth and were obtained using a H4 hybrid micro plate reader (BioTek). Population Duplication Time (PDT) was calculated from the viability test data obtained using equation 1.

$$\mathrm{PDT} = \mathrm{t} \times \frac{\mathrm{Ln}(2)}{\mathrm{Ln}(\mathrm{Cellf} - \mathrm{Celli})} \qquad \text{(Equation 1)}$$

Were *t* is the incubation time, *Cellf* is the number of cells at a given incubation time, and *Celli* the initial number of cells seeded on the substrate.

**3.4. Cell migration**: Cell velocity and direction were evaluated by time-lapse imaging**.** Cells were seeded and cultured on the substrates for 72 hours with appropriate media and this was replaced before beginning the imaging experiments. Imaging was carried out using a AF6000 LX microscope (Leica) equipped with an incubation chamber at 37°C and a 5% $CO_2$ atmosphere. Images were collected every 5 minutes over a period of 1200 minutes using a 10x magnification objective. The migration of cell was analyzed using the

MTrack J macro included in the Image J image analysis software form NIH. Initially the cell locations in the time-lapse movies were tracked, 50 random cells per substrate were analyzed. Using Diper, the software-macro developed by Gorelik *et al.,* cellular tracking data were computed to obtain the average speed, profile speed, directionally ratio and corresponding plotting.

**3.5. Immunofluorescence cell staining**: Cells were seeded and cultured during 72 hours at 37°C and 5% of CO2. The culture media was then aspirated and cells were rinsed with PBS buffer and fixed with 4% paraformaldehyde (Sigma-Aldrich) for 15 minutes. Subsequently, the cells were permeabilized with 0.1% Triton X-100 (Sigma-Aldrich) for 2 minutes, rinsed with PBS and incubated with a 1:500 mouse antivinculin dilution (Sigma-Aldrich) for 1 hour. Following, the substrates were rinsed with PBS and incubated with 1:500 Alexa-647 rabbit anti mouse IgG dilution (Molecular Probes) for 1 hour in darkness. Cells were then rinsed with PBS and incubated with ActinGreen (Molecular Probes) and Dapi (Molecular Probes) for 30 minutes in the dark. Finally, the substrates were rinsed and mounted on FluorSave reagent media (Calbiochem) and imaged using a LSM710 confocal fluorescent microscope (Carl Zeiss) at 40x and 63x magnification. All the incubation steps were carried out at room temperature.

**3.6. Quantification of cellular morphology**: The individual morphology was analyzed using the Image J image analysis software by NIH. Cells were seeded and cultured on the different substrates, and collected after 72 hours. Five independent trials with three replicates of each substrate were analyzed. Three

different parameters were taking into account for quantification of cellular morphology: area, circularity and elongation. Circularity was defined as $4\pi \times [Area/(Perimeter)^2]$. Elongation was defined as [*Major Axis*/*Minor Axis*] as the cells are fitted to an ellipse. Flat PC substrates were used as control.

**3.7. Cell tractions characterization by SEM and FIB**: Cells cultured on the patterned substrates for 72 hours were fixed with 4% paraformaldehide. The substrates were then rinsed in DI water and dehydrated using a series of ethanol dilutions with increasing concentration from 50% to 100% for 5 min in each dilution. Prior to imaging, the substrates were air-dried and sputter-coated with a thin layer of gold-palladium. Imaging was carried out using an Auriga FIB-SEM system (Zeiss). FIB was employed to mill the cross-sections of cells adhered to the nanopillars and SEM to image precisely the bending of the nanopillars due to the cell tractions on them across the cell length from the leading to the receding edge. The traction forces for cells seeded on the micropillars were obtained directly from the SEM images. The bending angle of the pillars was obtained from the images of cells with visible connections to the topography using Image J (NIH). Using the bending angle data, the deflection (x) of the individual pillars from the initial position was calculated, assuming an initial position of $90^o$ as observed in pillars without cells. The cellular traction force (*F*) was calculated using Hooke's Law (Equation 2), in which the deflection ($\Delta x$) corresponds to the bending distance of a pillar.

$$F = k\Delta x \qquad (Equation\ 2)$$

The stiffness (*k*) of a cantilever (Equation 2) dependent on the Young`s modulus (E), the moment of inertia (I) and nanopillar's length (L) was calculated by the Euler-Bernoulli beam theory:

$$k = \frac{3EI}{L^3} = \frac{3\pi ED^4}{L^3} \qquad (Equation\ 3)$$

## 4. Results

### 4.1. Fabrication and characterization of HAR pillars substrates

The HAR pillared substrates were fabricated on standard polycarbonate (PC) films for its high transparency. Nanoimprinting of the topographical features allowed for the accurate and reproducible replication of the large number of substrate required for the tests performed during this study. Two different topographies were studied; 500 nm x 2 µm and 2 x 10 µm pillars (Diameter (D) x Height (H)) with aspect ratio corresponding to 4 and 5 respectively. In both cases, a square arrangement of the pillars with an inter pillar distance equal to 1D was employed. These topographies correspond to a dimensional range in the micro and nano scale. We chose two scales to determine the differential impact of the on the cell response and possibly gain a broader insight on the impact of HAR topographies on cell behavior. In addition, the selected features allow testing the true effect of the topography without interfering effect from the underlying substrate as the cells cannot reach to it. Images of the nanoimprinted HAR topographies carried out by scanning electron microscopy (SEM) are shown in Figure 2A. The images reveal well-defined nanopatterned features. The dimensions of the topographies are tabulated in Figure 2B.

A

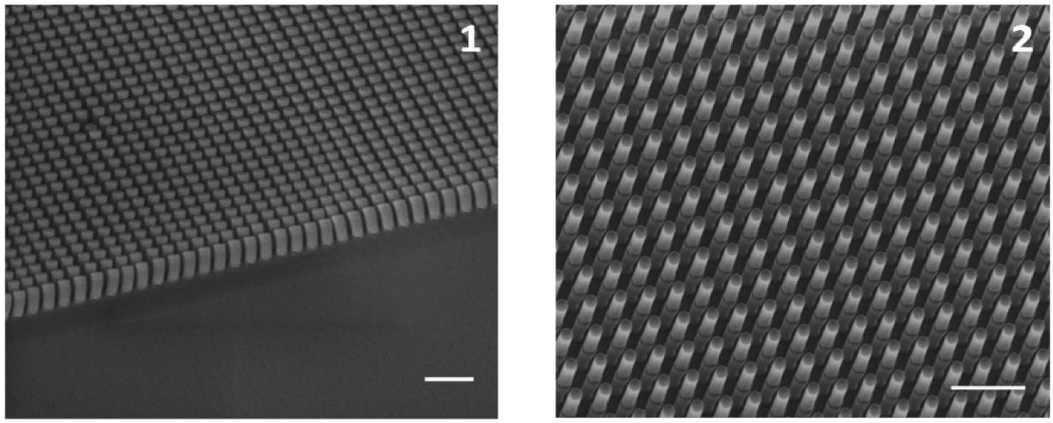


B

| Substrate [Pillar diameter] | Aspect Ratio [Height: Diameter] | Density [pillars cm-2] | WCA Mean [°] | WCA Mean + Gelatin [°] | Interspacing [µm] |
|---|---|---|---|---|---|
| 500 nm | 4 | 1.2x108 | 147.5±1.3 | 28.8±0.2 | 0.5 |
| 2 µm | 5 | 7.4x106 | 148.9±3.4 | 25.2±0.4 | 2 |

*Figure 2. A) SEM images of the topographies fabricated by polymer nanoimprinting 1) 500 nm pillars and 2) 2 µm pillars. B) Summary of the physical characteristics of the patterned substrates. Scale bar 2 µm (1), 10 µm (2)*

Generally, surfaces in contact with biological media are eventually covered with proteins. However in this work, to have a homogeneous chemical surface within all the substrates under test from the start and to be able to ascribe the difference on cell behavior on the different substrates solely to the topography, before cell seeding, the substrates were covered with protein from gelatin to provide a cell adhesive surface on the entire pillared topography. To test the protein coverage on the substrates, contact angle measurements were performed. The values obtained are summarized in Figure 2B. The data reveal that the substrates turned hydrophilic upon the treatment with gelatin solution

indicating the adsorption of the protein onto the surface and its completed coverage.

### 4.2. Cell viability

At the initial experiments, the ability of cells to adhere and proliferate onto the HAR topographical substrates was assessed. The growth pattern obtained depicted in Figure 3A shows that the pillared substrates supported cell division following the characteristic cell growth profile. As it is plotted in **Figure 3**A, cells on all the substrates enter the logarithmic growth phase on the fourth day of culture, reaching the highest development level on the fifth day. Subsequently, they lose viability and enter death phase on the sixth day when the growth medium was exhausted. The substrates showed marked differences in proliferation rates compared to the control. Cells growing on 500 nm pillars reached higher growth values than cells seeded on 2 μm pillars, but in both cases, the growth rates were lower than that of the control. This fact is also supported by the data obtained for population duplication time (PDT) plotted in Figure 3B. It can be seen a similar trend for all substrates. However, the PDT values were higher for the topographic substrates compared to the flat controls indicating a lower cellular growth rate and among these, cells seeded on the 2 μm pillar substrates show the highest duplication time. These results indicate that while all substrates support cell adhesion and proliferation, the HAR topography increased the cell duplication time hence, the growth pattern. And in the case of cells seeded on the 2 μm pillars, the proliferation rate was substantially reduced.

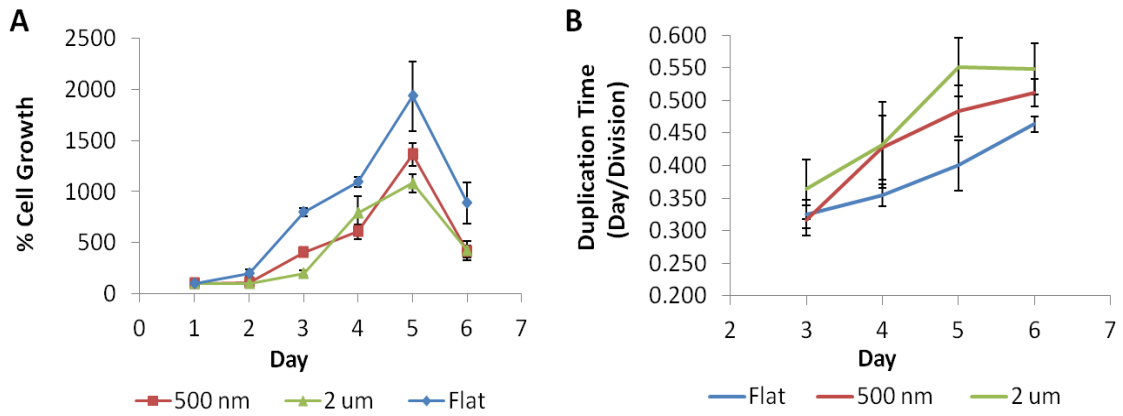


*Figure 3. Proliferation rate of the C17.2 cells during 6 days on the 500 nm and 2 µm pillar topographies comparatively to a flat control. (A) Proliferation rate plot profile (B) Quantification of population duplication time (PDT). Error bars represent standard deviation.*

### 4.3. Morphological cell response

The morphology of cells seeded on the HAR pillars was assessed comparatively to the cells seeded on flat control substrates through fluorescence images. To have a more quantifiable measurement of the morphology differences induced by the topography, the area, circularity and elongation were calculated. Very distinctive morphologies were observed on the three substrates. As seen on the fluorescence images displayed in Figure 4, cells cultured over flat substrates appeared well spread and elongated and they showed large spreading area and the lowest circularity value and elongation. Conversely, cells grown on 2 µm pillars showed a considerable reduction of the projected cell area up to 5-fold and displayed higher values of circularity and lower of elongation. Cells on this substrate grew projections frequently extending as far as three times the cell body diameter along one specific pillar lattice direction. In contrast, the morphology observed for cells cultured onto the

500 nm pillars was more spread, less circular and with higher levels of elongation. In addition, these cells showed numerous filopodia extending in every direction while being more prominent on the advancing cell edge.

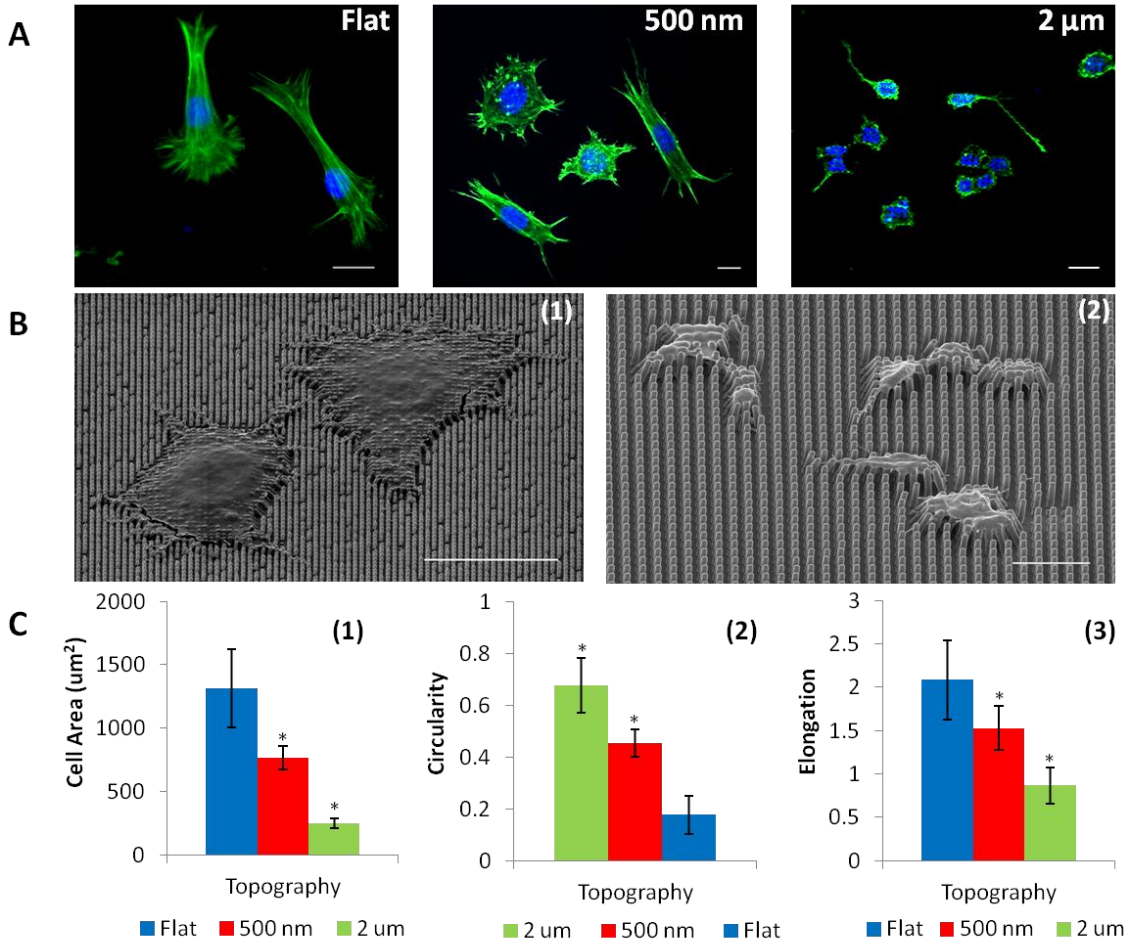


*Figure 4. Changes in cell adhesion and morphology with the topography. (A) Fluorescence images of C17.2 cells cultured over a flat, 500 nm and 2 µm HAR pillar topographies. (B) SEM images of cells cultured over (1) 500 nm pillars and (2) 2 µm pillar topographies (C). Quantification and comparison of cellular morphological parameters in terms of (1) cell spreading, (2) circularity and (3) elongation. The statistical significance ($p < 0.05$) after performing t-tests marked as (*) indicates a significant difference between the topographies compared to a flat control. Scale bar 20 µm. Error bars represent standard deviation.*

Consistent with findings reported before,[4, 42, 45] these observations indicate that the dimension, the density and the interspacing distance between pillars strongly determine the morphology of cells cultured on HAR pillar substrates. A critical spacing dimension of 2 µm between the nanopillars was determined before by Bonde et *al*.,[4] below which, cells are unable to reach and adhere onto the underlying surface. Further, SEM imaging of the cell body arrangement on the HAR topographies was performed to corroborate these findings. As shown in Figure 3B, cells seeded on 2 µm pillars, presented cell bodies suspended within the bed of pillars with large cytoplasmic penetrations. In some instances, cell adhesions were seen onto the side of the pillars but in any of the substrates analyzed, the cell body reached the underlying substrate. Nano pillar impalement onto the plasma membrane was also observed on cells seeded onto the 500 nm pillar topography. However, this was much less pronounced and restricted to the periphery of the plasma membrane while cells remained largely suspended on top of the pillars. This effect was seen from the third day of culture.

To gain further insight on the cytosol and cytoskeletal rearrangement on the pillared surfaces, immunofluorescence staining for actin and vinculin was performed. Confocal microscopy images of cells seeded on both topographies were taken on an optical plane just below the pillar surface (Figure 5). Due to the high aspect ratio of the topography, the cytoskeleton structures appeared spread along several focal planes. Therefore, at high resolution, it was not possible to visualize discrete vinculin stained focal adhesions or continuous actin filaments. However, the images reveal other interesting aspects of the interaction of cells with the pillar structures and resulting morphological changes.

In Figure 4 A(1) it can be observed that the 2 µm pillars appear delimited by a strong fluorescent ring outlining the pillars perimeter. This stronger fluorescent emission is due to the increase on the concentration of fluorophores indicating that there is a increase of green-stained actin stress fibers clustered around the pillars.[152] On the other hand, the vinculin fluorescent signal (Fig 5B (2)) and signal from the nucleus stained with DAPI (Fig 5A (3)) faded from the pillar caps´ centers and it shows as black circles on the confocal images. These observations indicate that the cell membrane was intact resting on the top of the pillars and that the cytoplasm was mostly embedded within the topography with the nucleus undergoing a large deformation as it is enclosed and confined within the topography not only on the normal direction but on the lateral direction within the 2 µm interpillar gaps.

Previous studies indeed have shown that stem cells have very soft nuclei as they contain less chromatin in condensed configuration and in addition, the expression level of lamin-A and lamin-C is much lower than that for differentiated cells. [155, 156] Our observations corroborate these studies; it was found that the stem cell nuclei underwent large deformations in both the axial and lateral directions (Fig 5A). Particularly on migrating cells, the nucleus can be seen markedly elongated and constrained within the pilar gaps reducing substantially the nucleus projected area and showing a circularity factor 0.4± 0.13.

Immunofluorescence imaging of the cells seeded on the 500 nm pillars (Figure 5B (1,2) also showed cytoplasmic penetrations but of a lesser degree. In many of the cells analyzed, it was observed that only at peripheral areas, pillars had impelled onto the plasma membrane. The nucleus of these cells rested atop of

the 500 nm pillars and showed slight pillar impalement as denoted by the black-dotted DAPI fluorescence images of Figure 5B (3). However, in many of the cells analyzed, the nucleus retained the typical oval morphology (circularity factor 0.7±0.1). These observations indicate that the nucleus conformed to the topography on the normal direction but it was not compressed laterally into the topography. The gap within the pillars (i.e. 500 nm) is indeed too small for the cell nucleus to constrain within such small dimension; this observation is in line with previous reports.[4, 42, 45] It is plausible that the dense 500 nm topography may appear more like a continuous surface where cells can establish an adequate number of adhesions where the disjointed topography only adds a small fraction of tension to the cytoskeleton.

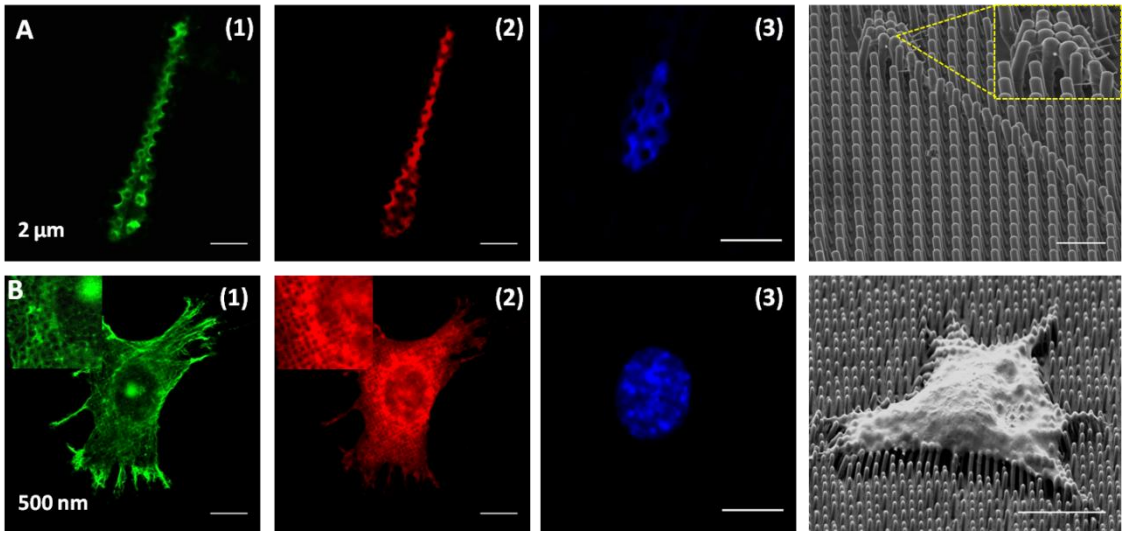


*Figure 5. Confocal inmunofluorescent images of C17.2 cells showing the cytoskeletal arrangement (stained by 1) actin-green and 2) vinculin red) and nuclei morphology (stained by 3) DAPI) adopted by A) cells seeded on a 2 µm HAR pillar substrate and B) cells seeded on s 500 nm HAR pillar substrate. Scale bar 10 um. Cells on the 2 µm pillares appear embedded into the HAR topography showing a reduced cell projected area and a nucleus constrained laterally and axially. Cells on the 500 nm pillars show pillar impalement onto the cytoplasm and the nucleolus denoted by the dark spots on the fluorescent areas. However, the cell projected area remains largely unchanged indicating that the cell spread atop the topography.*

### 4.4. Cell Migration and dynamics of adhesion

Cell movement or migration is the outcome of three interrelated processes: adhesion, protrusion driven by actin polymerization and actomyosin contraction for cell body translocation.[157] Many studies have demonstrated that these processes are especially sensitive to extracellular mechanical cues such as stiffness and topography.[53, 158] Accordingly, both parameters have been investigated extensively to design cell instructive substrates to direct and orientate cell migration.[159]

In this study it was assayed how the cells sense pillars´density or interspacing in order to determine the dimensionality of a textured surface that cells perceived as continuous or discrete and how these variables impact on cell migration. With this aim, the migratory patterns of the cells cultured over both HAR pillar substrates and a flat control were investigated through time-lapse imaging during 20 h. The cell trajectories obtained from video frames, were tracked and the data was analyzed using Image J. The cells´ trajectories together with the speed profile and average speed on each of the substrates are shown in Figure 6.

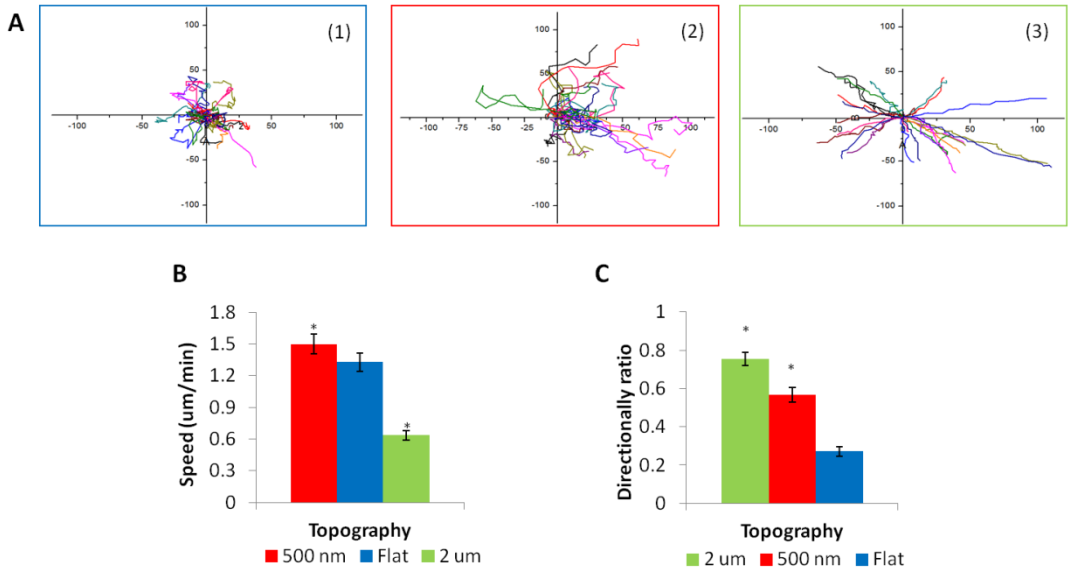


*Figure 6. Cell migration patterns. (A) Wind rose plots of cell trajectories in (1) Flat control surface (2) 500 nm pillars (3) 2 µm pillars. (B) Average speed profiles and (C) directionally ratio of the cell migrating trajectories on the tested substrates. The statistical significance ($p < 0.05$) after performing t-tests is marked by * indicating a significant difference between the two topographies compared with a flat control. Error bars represent standard deviation.*

The windrose plots of the cell trajectories overlaid at origin (Figure 6) indicate that cells cultured on 500 nm pillars display a random migration similar to that on the flat substrate with a continuous fast movement. Due to the isotropic character of the topography, a random migration is predictable. Noteworthy of these cells is the high migration speed and active exploration of the environment by the numerous filopodia growing in all directions. On average it was observed a remarkable 15 % increase in cell speed over the cells seeded on flat substrates. The filopodia have an exploratory function for cells to probe their environment and once a suitable area is located, lamellipodia are formed to relocate the cell to the desired location.[160] It was hypothesized that the high dynamic filopodia activity of cells seeded on the 500 nm pillars is possible because this topography offers a pillar density or inter-pillar distance suitable for

the filopodia to sense adjacent pillars but on the other hand, the cells may also sense the discontinuity on the substrate and develop weaker, less stable adhesions compared to cells seeded on flat surfaces.

Conversely, cells seeded on the 2 μm pillars did not exhibit such high exploration activity; the active formation or filopodia or lamelipodia could not be observed distinctively. This topography in fact imposes a geometrical hindrance to the cell movement. As we have seen above, within an interpillar distance of 2 μm, cells became confined within the HAR micro pillars with large cytoplasmic and nuclear penetrations into the topography. Accordingly, the required cytoskeleton rearrangement and contractile force to lift the cell nucleus for the migration to advance was greater. Moreover, these cells exhibited what it appears to be a different migration mechanism. They generally developed a long protrusion that eventually was successful in pulling the cell body forward due to the increased tension created. The migration pattern of cells seeded over the 2 μm pillar substrate was characteristically quasi-directional with a cell velocity on average 50% slower than that on the flat control. The motion was also discontinuous with alternating periods of no apparent mobility followed by a sudden jump to a new location preceded by a long protrusion and typically along the pillar lattice.

### 4.5. Cellular traction forces

To further substantiate these findings, the cell traction forces on the HAR topography were measured. Because of the small magnitude of cell traction forces in the nN range, it is a challenging task to determine cell traction forces accurately. In particular, when the medium topography is on nanoscale, optical visualization methods are ineffective. Hence, in this work, ion and electron microscopy techniques were employed to image the cell-nanopillars´ interaction and measure from the images, the deflection of pillars due to the cell tractions. The deflections then serve to quantify the traction forces generated by the cells applying the Hooke´s law.

To quantify these traction forces, the deflection of the pillars situated at different locations under the cell membrane was measured. For this, cells seeded on the 500 nm pillars were finely ion milled from the front to the rear using a FIB (Figure 7A). The pillars´ deflection was measured from the cross-section SEM images. During the force measurement and experiment analyses, cell images were segregated according to the migration state in relation to their round or elliptical phenotype. The different phenotypes showed different traction force patterns (Figure 7B). For round, non-migrating cells, a symmetric traction force profile was obtained across the entire cell membrane indicating that the traction force exerted on both the cell edges had a similar magnitude (Figure 7C). For these cells, the maximum traction force exerted at the periphery was on average 0.75 µN. Conversely, elliptical migrating cells exhibited an asymmetric traction force profile being higher at the advancing edge and lower at the receding end (Figure 7D) with values of traction force over 2.5 µN at the leading edge, and a maximum receding force of 1.75 µN. The trend found generally

agree with what has been reported before[44] and indicate that traction forces generated by the cells are directed toward the center of the cell, with the strongest forces concentrating at the lamellipodia leading edge and steeply decaying towards the center of the cell.

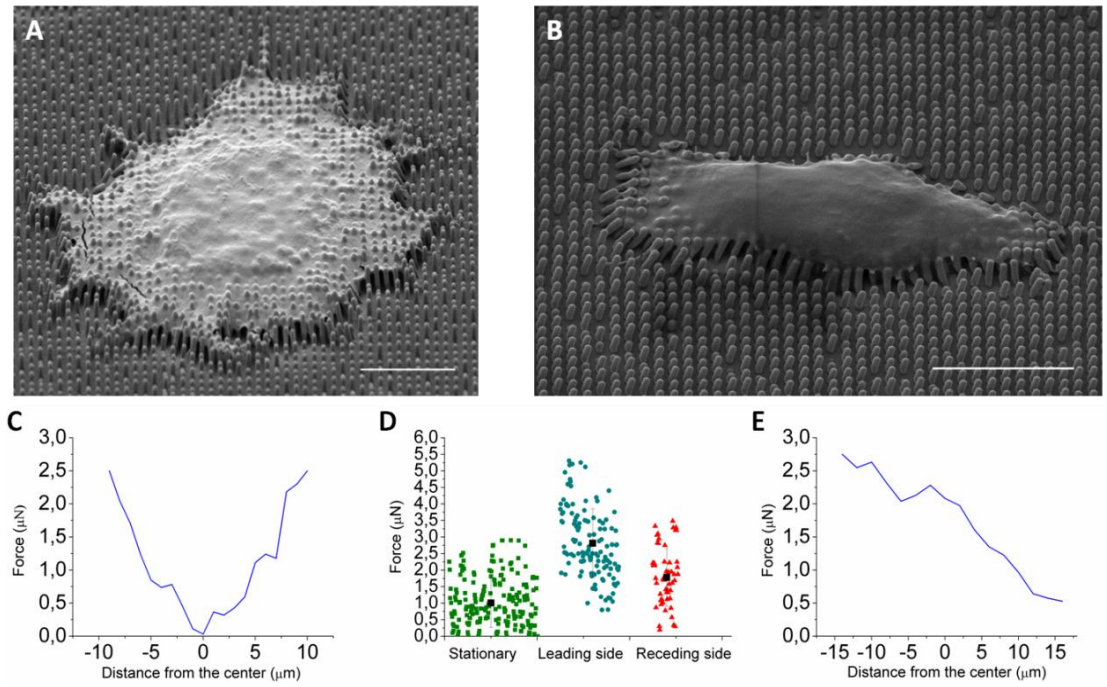


*Figure 7. Traction forces for cells on 500 nm HAR pillared substrates. (A) SEM image of stationary cell over 500 nm pillars showing no polarization. (B) SEM image of a polarized cell migrating on the 500 nm pillars showing the lamellipodia at the leading edge and a trailing edge. (C) Traction force profile across a stationary cell showing adhesive traction forces at the edges while no forces are detected at the center. (D) SEM image of a polarized cell migrating on the 500 nm pillars showing the lamellipodia at the leading edge and a trailing edge. (D) Distribution of traction forces measured exerted by stationary cell and migrating cell at the leading edge and at the receding edge. (E) Typical traction profile of a migrating cell showing high forces at the leading edge and lower the receding side. Scale bar 10 um.*

Quantification of the traction forces exerted by cells seeded on the 2 µm pillar substrates required also an independent analysis between migrating and non-migrating cells. Likewise, non-migrating cells with a round phenotype showed a symmetrical force profile with a mean traction force of 9 µN on average exerted at the periphery (Figure 8A). The pillar deflections caused by the cell main body or leading protrusion of migrating cells on the 2 µm topography were also evaluated independently (Figure 8B). The values of traction forces measured on the protruding edge were in the order of 5 µN while for the cell body the mean values were about 11 µN. These forces exerted by the cell body are one order of magnitude higher than those exerted by the leading protrusion, which is the direction of the cell motion. These results are in agreement with previous observations that the cellular contractility increases during cell migration.[34] Furthermore, the large magnitude of this compressive rear force is an evidence of the great contractile traction the cell body has to effect to lift the nucleus and pull the rest of cytoplasm embedded within the topography to allow for the cell translation to a new location. These large traction forces exerted by the cell cytoskeleton on the 2 µm pillars correlate with the large accumulation of actin stress fibers seen around the pillars as well as the nanopillars induced nuclear deformation investigated through the fluorescence staining experiments.

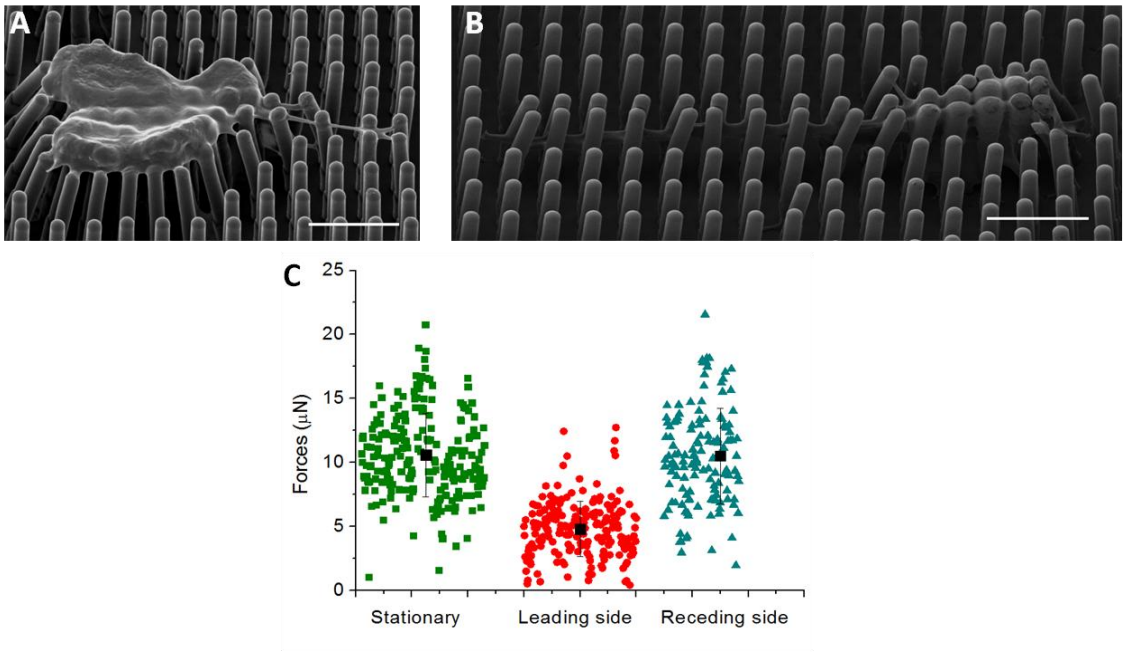


*Figure 8. Traction forces for cells cultured on 2 um HAR pillar substrates. (A) SEM image of stationary cell over 2 um pillars. (B) SEM image of a cell migrating within the 2 um pillar topography. (C) Distribution of the traction forces exert by a stationary cell at the periphery and migrating cell at the leading edge and at the receding edge. Scale bar 10 um*

## 5. Discussion

The HAR topography tested induced significant changes on cell response. Both substrates sustained adequate rates of adhesion and viability although the proliferation rate was somewhat reduced on the HAR topographies. On both substrates cell spreading was lesser than the flat control and it was remarkably reduced for cells seeded on the 2 µm substrates. A more striking effect of the HAR topography was found on cell morphology and behavior and it was very distinct for the nano or micro topography or the flat surface control. Cells seeded on the nano topography spread amply onto the HAR pillars and showed

a large degree of elongation with frequent cytoskeletal rearrangement. The data from confocal time-lapse microscopy experiments show that cells on 500 nm pillars moved constantly and randomly with quick changes to the direction of migration while filopodia explored the surface through cycles of protrusion–retraction that occurred on a timescale of a couple of minutes. Cells made contact adhesions onto the top of the pillars and remained largely atop of the topography although a certain degree of pillar impalement onto the cell cytoplasm and nucleus was observed. These cells while migrating showed a typical lamellipodial cell profile with higher traction forces of propulsion at the leading edge and lower on the trailing edge as mature adhesions released. These observations agree with previous reports [60] and the general trend observed whereby contractile forces generated by the cells are directed toward the center, with the strongest forces concentrating at the leading and receding edges and sharply decaying towards the central region.

Conversely, the cells cultured on 2 µm pillars, showed a very round cell projected area and apparent long periods of inactivity after which, they grew a characteristic unidirectional protrusion as cell leading edge. Cells on these substrates moved slowly with discontinuous migration of alternated periods of immobility followed by a sudden onset of motion. Migration was instead quasi-directional driven by a unique cytoplasmic protrusion. The timescale for the cells to move was about 10 minutes.

Previous studies have shown that the substrate topography significantly influences the exploration dynamics and substrate recognition of filopodia which ultimately guide cell functions such as cell adhesion, spreading, migration and division.[13, 161] Clear differences on the filopodia activity of cells seeded on the

500 nm pillars compared to the ones on 2 µm substrates was observed. Cells on 500 nm pillars grew numerous filopodia in every direction and moved rapidly showing 15% higher speed than cells seeded on the flat controls. It appears plausible that filopodia perceived the disjointed topography less conducive than a continuous surface to form stable adhesions as the pillars reduced the available area and confined the adhesive contacts to disjointed mechanical entities. In addition, having adhesive points on different mechanical entities may induce a certain degree of destabilization of the cell adhesion and mechanical stresses onto the cell plasma membrane. This presumed higher degree of instability together with a reduced adhesive contact area may account for the larger mobility seen for the cells on the 500 nm pillar substrate, as they appear to be like on a constant a search.

The filopodia activity of on cells seeded on 2 µm pillars appeared extremely reduced, they were less visible and for the most part of the cells, filopodia activity did not lead to cell spreading or cell motion. Cells fail to spread horizontally, but instead, they spread vertically into the topography and it was particularly evident for migrating cells (Fig 8A), where most of the cell volume appeared embedded within the topography. Cell adhesions were seen laterally onto the pillars´ wall to support the cell body. Migration was primarily driven by a unique cytoplasmic protrusion that extended generally unidirectional along the interpillar lattice as the most advantageous direction of drag to the movement.

Linked to the morphological changes and migration behavior, another notable influence of the HAR topography was on the organization and positioning of the cytoplasm components primarily the nucleus, and the traction forces generated

by the cells on the topographic surfaces. Both of these aspects are directly related to the actin cytoskeleton.

The general tendency of cells to maximize their contact area was observed. On both topographies, the cell membrane conformed to the topography within a feasible extent and at the same time, the cytoskeleton pulled the nucleus downwards against the pillars, which were observed to deform and impale onto the nucleus. For cells seeded on the 500 nm pillars, the cytoplasmic penetrations and nuclear deformation on the topography were relatively small. These cells displayed characteristic propulsive and contractile traction forces at the front and rear of the cells. On the micro topography with an aspect ratio of 4:1 and interpillar distance of 2 µm, cells were not able to establish sufficient adhesive contacts to spread onto the top surface of the pillars, neither were able to reach the underlying surface. Instead, to increase their contact area, cells embedded themselves within the topography making contact adhesions to the sides of the pillars while they pull the cytoplasm and nucleus inside of the topography. In many of the cells analyzed, the nucleus was deformed in the direction normal to the topography as the pillars impaled on to it. Moreover, commonly the nucleus was observed longitudinally deformed as it was drawn into the interpillar´s gaps. Consequently, cells seeded on the 2 µm topography displayed large propulsive tractions on the migrating leading edge and also exerted remarkably strong contractile axial forces at the cell main body region. The large magnitude of these forces provide evidence that cells on this topography required a more intricate reorganization of the force-generating filament components intertwined into the pillars and large contractile forces to lift to the cytoplasm and nucleus embedded within the HAR 2 µm pillars. These

results support the observations by Hanson *et al.* and Davison *et al*.,[48, 152] in that the topography induced plasma membrane deformation is transmitted to the nucleus by the cytoskeleton actin fibers resulting in nuclear deformation.

Another striking observation in this work is the large magnitude of the traction forces exerted by the cells on the HAR topography. Previous works on traction force sensing on pillar arrays (for multiple cell types and different substrate materials), have covered a range of forces from nN to µN.[44, 162, 163] In these works, the force level reported increased with the stiffness of the substrate for materials ranging from the elastomeric Polydimethylsiloxane (PDMS) with an elastic modulus of about 2 MPa to silicon with an elastic modulus of about 151 GPa.[163]

Previous works have also suggested that the matrix stiffness has a strong influence on cell traction forces and the general trend observed is an increase of cell force with substrate stiffness.[163, 164] However, in addition to increasing cell stresses, stiffness also influences the cell spread area which, indirectly influences the generation of cellular tractions.[165] The influence of these two parameters was decoupled by Han *et al*.,[166] who established that the role of substrate stiffness and spread area on traction force generation is *a priori* independent and demonstrated that substrate stiffness increases the average traction force, whereas cell spread area reduces the average force through an increase in the number focal adhesions. In line with this rationale, the large traction forces exerted by the cells on the HAR substrates may be directly linked with the higher substrate stiffness (compared to PDMS) and with the reduced cell spread seen compared to flat surface. While these results need further investigation, they provide further evidence of the enormous mechano sensing-

transduction capacity of cells, their ability to sense mechanical cues and adapt to different environments of substrate stiffness and geometrical features by modulation of the generated cytoskeletal forces within a wide range.

Generally cells have a tendency to maximize their contact area with the surfaces for reasons such as to achieve a stronger and more stable attachment, to increase the surface area for more effective membrane trafficking and absorption of nutrients. However, the question that emerged to us here is what are the physicochemical cues that steer the cells to undergo such large cytoplasm deformations and large compression of the nuclei into 2 µm gaps? Is it an active mechanism executed by the cell in order to maximize the adhesive contacts and surface area or, is it a conformation more favorable to decrease the cell membrane tension? Recent studies have indicated that the plasma membrane tension, exerting and responding to forces through the attached cytoskeleton is an important regulator of cell functions such as cell morphology and movement.[167, 168] And spreading correlates with an apparent decrease in membrane tension.[169] The results of this study point towards this end as spreading vertically into the topography appears more favorable for cells to release membrane tension than remaining in the round state or than bridging across the pillars at a distance of 2 µm. Further research will be necessary to underpin these assumptions and underlying mechanisms.

## 6. Conclusion

Nanoimprinted micro and nano HAR polymer topographies triggered very different stem cell responses. The dimensionality of the HAR topography in terms of pillar spacing and aspect ratio was a decisive factor to influence the cell fate. Aspect ratio and pillar spacing determined the possibility of the cells to reach the underlying substrate. With an aspect ratio of 4 and interpillar distance below 2 µm, cells were not able to reach the underlying surface and adhered only to the top of the topography. Hence, the cell responses observed derived merely from the topographical features and related mechanical stresses exerted onto the cells.

Cells on the nanotopography showed a somewhat lower rate of proliferation than those on the flat surface control together with a smaller cell spreading. In contrast, they showed higher mobility with random migration altogether with high traction forces. These responses are believed to arise from the ability of filopodia to sense the small disjointed areas as less conducive for the expansion of focal complexes into larger stable adhesive contacts.

Cells seeded on the micron scale topography showed yet a lower rate of proliferation and a round projected morphology. Nonetheless, cells spread vertically into the 2 µm interpillar gaps of the topography and migrating cells exhibited a large part of the cell volume embedded within the topography. These cells established contact adhesions laterally onto the pillars and the stress fibers pull the cytoplasm and nucleus into the topography. The marked morphological changes were associated with changes in migration and traction forces. The topography limited the cell migration due to geometrical restrictions to the movement of the nucleus embedded within the pillars, as such, migration

was slow and quasi-directional driven by a unique protrusion along a direction of less resistance. Cells on this topography effected large protrusion and contractile forces in order to lift up and shift the cell body to a new location.

The significance of these results relies on the possibility to attain with HAR pillars the true mechanical effect of topography without the influence of the underlying substrate, as cells were not able to reach to it. These substrates allowed us to observed *in situ* nuclear deformability of viable stem cells. It was shown that the nucleus of stems cells deforms readily and large changes on nuclear shape can take place during migration through confined spaces.

These large deformations observed for the nucleus correlated with the accumulation of the actin stress fibers around the pillars and the large traction forces measured which evidences the intricate coupling between the nucleus and the actin cytoskeleton. Another striking finding is the large traction forces the cells were able to exert to spread and migrate on the HAR topography. It was postulated that the membrane tension arising from the cell-topography interaction orchestrates the mechanical signals that trigger the formation of adhesive contacts by supporting cytoskeletal organization and membrane remodeling.

Hence, the results of this study indicate that HAR surface topographies are effective tools for in vitro cell manipulation and would be useful research tools in cell biology to probe cellular and nuclear biomechanics. Further, these results provide new insights for the understanding of stem cell response to artificial surfaces, which would be valuable in developing smart cell culture platforms for engineering the next-generation of regenerative biomaterials.

# Chapter 4

# Bactericidal Moth-eye mimetic polymer topography

## 1. Introduction

Bacteria are ubiquitous microorganisms that can be found literally everywhere on Earth. Its broad presence has forced all other living beings to develop different mechanisms to coexist with bacteria. As such, nature has evolved a large variety of strategies to fight against or take advantage of bacteria, these range from immune response, chemical destabilization by antimicrobial peptides or antimicrobial surfaces to the ability to use bacteria as food source or food factory.

Bacteria have caused the major deathly epidemics in human history and today have emerged again as an old-new threat due to the development of bacteria resistance. Methicilin-resistant *Staphylococcus aureus* (MRSA) and *Pseudomona aeruginosa* are the main bacteria involved in hospital-acquired/associated infections and the main cause of death derived from surgery complications.[170, 171] However, multidrug-resistant infections can leave the hospital and become part of the community flora if measurements are not taken.[172]

Although disease and pathogenesis are extremely distressing, bacteria can cause undesirable problems in many other fields, such as in food production, furnishing, shipping or construction. To fight bacteria, mankind has developed a number of strategies to contain the proliferation of bacteria into biofilms. These methods range from the development of antiseptics or antibiotics to processing methods such as heat or radiation treatments.

Despite these antibacterial strategies, bacterial colonization and biofilm formation on surfaces remain as important problems in the society and across all industrial sectors.

### 1.1. Adaptability of bacteria

The obstacle to control bacterial adhesion and proliferation lies on the great adaptability of bacteria to different environments. This high adaptability stems from the bacterial ability to acquire new genetic material and for their high duplication and growth capability. The mechanism developed to exchange or incorporate new genetic material is due to a process known as horizontal transfer. Three mechanisms are involved in horizontal transfer: bacterial transformation concerning the releasing of DNA molecules into the media by donor bacteria followed by incorporation by the recipient bacteria (Fig 1A), bacterial transduction where a bacteriophage acting as carrier, transports the genetic material from the donor to the recipient bacteria (Fig 1B) and bacterial conjugation where bacteria establish direct contact, through a membrane projection, which enables the direct exchange of genetic material between bacteria (Fig 1C).[173]

These mechanisms working together allow bacteria to efficiently tune their genome and through natural selection mechanism adapt to a wide variety of environments, including those with extreme conditions such as very high or low temperature surroundings, salty environments or even generate resistance to antibiotics.[171]

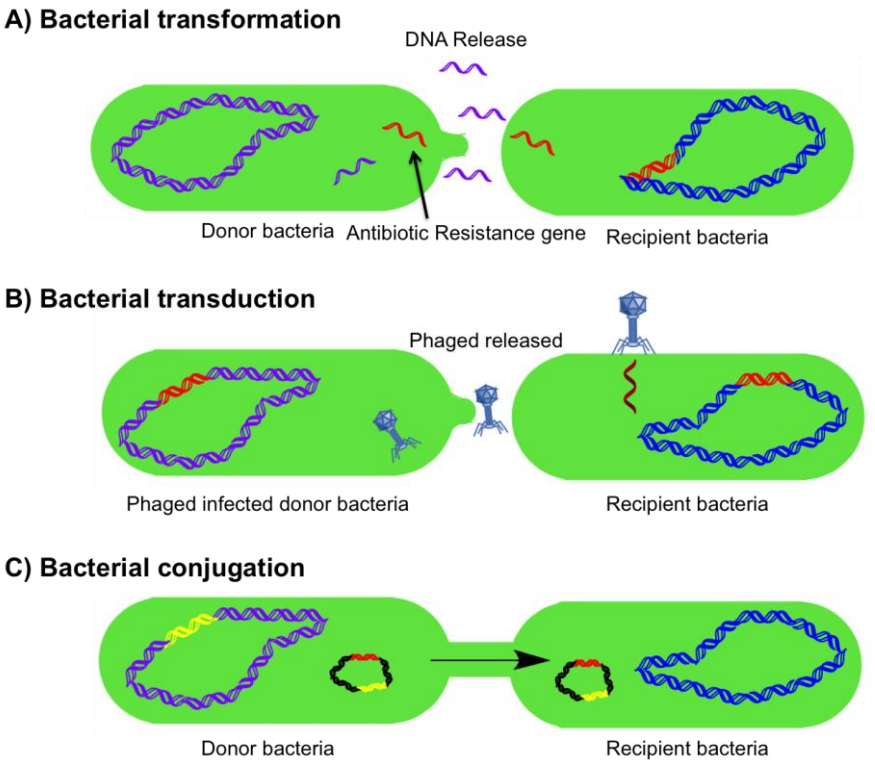


*Figure 1. Horizontal gene transfer mechanism between bacteria*

Apart from horizontal transfer, bacteria have evolved to form biofilms. Biofilms are sessile communities of bacteria attached to a surface, frequently embedded in a matrix of extracellular polymeric substances.[174] Bacteria obtain many advantages of being part of biofilm, including resistance to antibiotic and disinfectants and enhanced adaptability to the media since biofilm community regulates bacterial gene expression, allowing bacteria to adopt phenotypic changes according to the surrounding environment. Biofilms are the major cause of morbidity and mortality due to medical implant associated infection, and cause important economical loses in other industries.[170]

Biofilm formation is a sequential process of four different stages. The first stage involves the reversible interaction between bacteria and the surface material. This stage is driven by non-specific interactions, such as electrostatic, hydrophobic and Van der Waals forces. During this phase, bacteria are

passively attached onto material surfaces. In the second stage, the reversible interaction turns into irreversible, this is an active process mediated by Microbial Surface Components Recognizing Adhesive Matrix Molecules (MSCRAMMs) such as adhesines. During this phase, bacteria accumulate on the infected surface and the biofilm is progressively built up. The third step comprises the maturation of the biofilm. In the last step, the bacteria forming the biofilm shift their phenotype to planktonic state to begin a new invasive cycle (Fig2).[171, 175, 176]

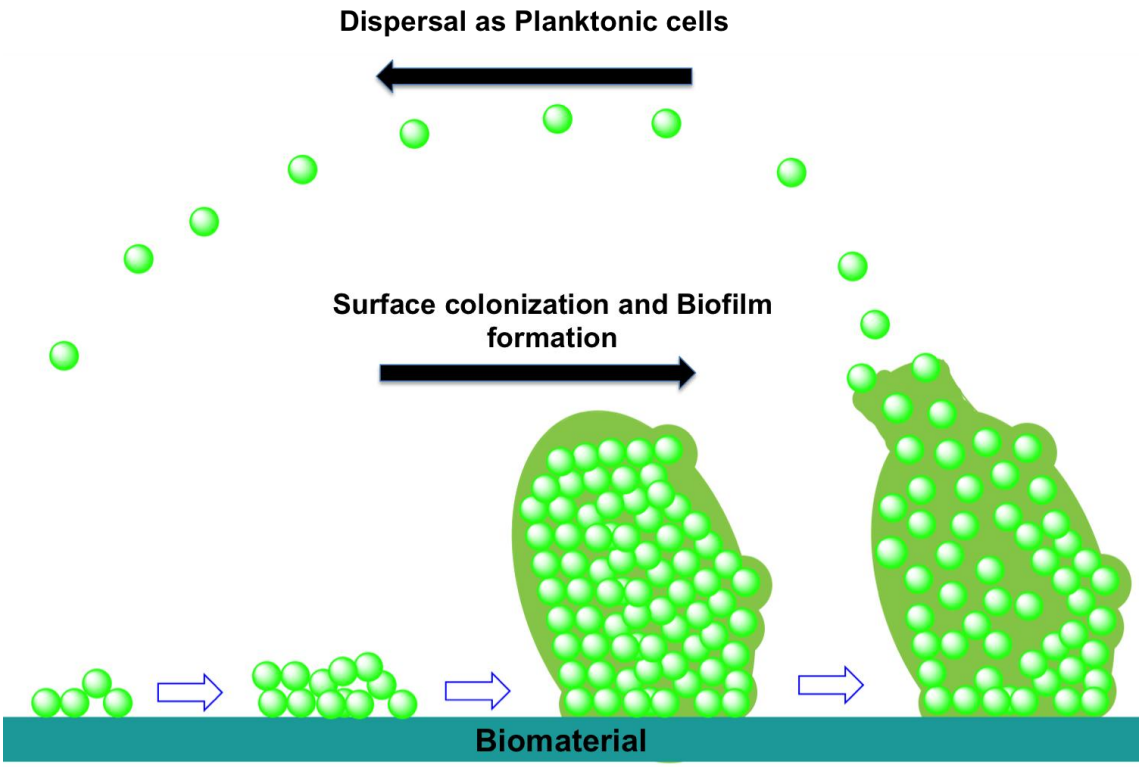


*Figure 2. Biofilm formation process. First bacteria attached to surface by reversible interaction, in the second step bacterial adhesion turns from reversible to irreversible. The following steps involve the development of the biofilm and the realising of planktonic bacteria to colonize a new area.*

## 1.2. Antibiotic Resistance

Multidrug resistance (MDR) bacteria have emerged as a direct consequence of the high ability of bacteria to adapt to many environments by the mechanisms previously described. Antibiotics are still the treatment of choice against infections.[177, 178] However, over-the-counter access and low prices of these drugs[179] along with the lack of precise infection-diagnosis have resulted in an overuse of antibiotics and the emergence of MDR bacteria.[177] Today, infections by MDR bacteria have become one of the most serious health threats impacting our society. The slow development of new effective drugs and the high rate of appearance of new strains of MDR bacteria are causing a fast increase in the rate of patient morbidity infection caused by these pathogens. Consequently, the emergence of MDR bacteria has become a global threat that requires the organized action of governments, industry and civil society to developed new strategies to stop and prevent MDR bacteria spreading.[180]

Bacteria have evolved a strong tendency to adhere to surfaces for survival reasons and as a matter of fact, bacterial adhesion has become a fundamental biological process. Surfaces provide important survival factors such as larger availability of nutrients as they accumulate on the surfaces [29, 30] and surfaces are also the platforms for forming protective biofilms.

It is now widely recognized that mechanosensing of the physical environment plays a key role on the biological response of bacteria.[16, 81] Surface-associated behaviours arising from mechanosensing include processes such as the production of EPS, biofilm formation, bacteria movement, virulence and most importantly viability.[76] The initial contact to a surface has been acknowledged as the mechanical cue that triggers intracellular signalling cascades that guide

the phenotypic changes and ultimately determine the bacterial adhesion regime.[74] There are three regimes of bacterial adhesion to surface (Fig 3) These regimes are defined by the magnitude of the adhesive forces operating between bacteria and surface. In the different regimes of adhesion forces, it is predicted that a bacterium will undergo different degrees of cell wall deformation, which will trigger specific metabolic activity and ultimately determine the behaviour of adhering bacteria. There is mounting evidence that bacterial viability is dependent upon the magnitude of the force through which they adhere to a substratum surface. A strong correlation has been found between high adhesion forces and bacterial deactivation suggesting that adhesive forces can generate high mechanical stresses on the bacterial membrane, which turn lethal to the bacteria.[181] These findings have brought the attention to new antibacterial strategies based on surfaces that can mechanically induce bacterial death.

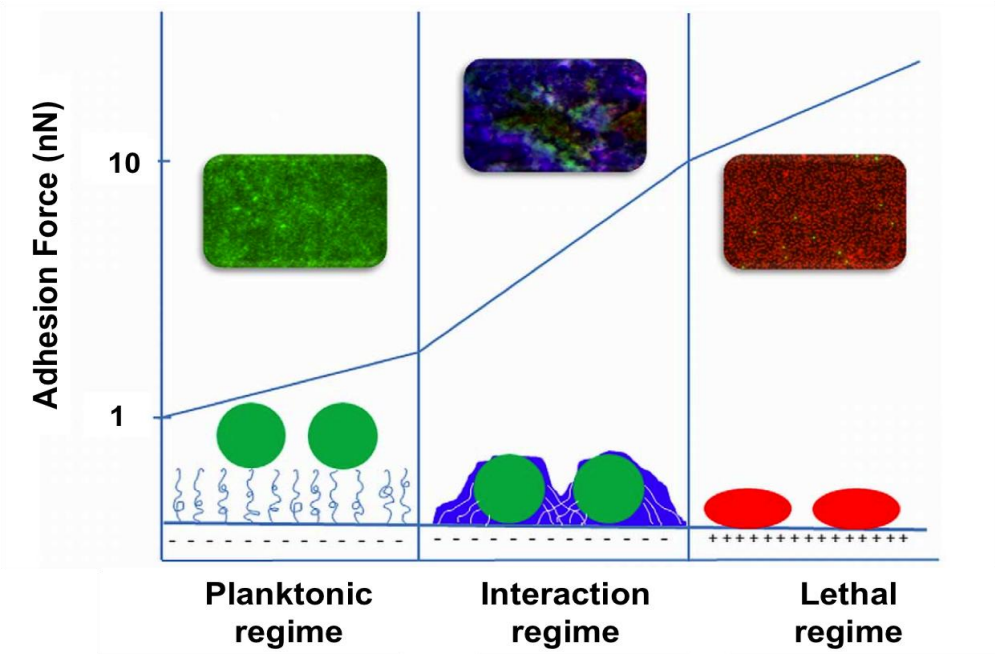


*Figure 3. Three regimes of bacterial adhesion to surface. Extremely low interaction forces characterize planktonic regime, low adhesion forces cannot induce phenotypical changes. Interaction regime is chacterized by the increase of adhesion forces that induce phenotypical changes, usually involving EPS production to create a protective biofilm. Lethal regime is defined by forces higher than 10 nN, which are typical when surfaces are positively charged, the strong interaction lead to the membrane deformation causing bacterial death. Image reproduced with permission from Ref.*[74]

### 1.3. Strategies against bacterial spreading

Commonly, the development of antibacterial materials has been based on the modification of chemical surface. However, chemical modification has several drawbacks, i.e. potential toxicity, short life performance due to the release of the chemical agent and potential immunogenicity. Moreover, the use of antibiotics as chemical agent for surface modification has been a common approach. However, this approach is temporary when the antibiotic load is depleted and moreover, it contributes to MDR bacteria emergence.[14] Other chemical coatings have been utilized like chitosan, quaternary ammonium compounds, and cationic surfactants, or inorganic compounds such as titanium oxide.[182]

Following the findings on the bacterial mechanosensing, the response to the physical characteristics of their surroundings and the influence of the adhesion force on bacterial viability, a new trend in the development of antibacterial materials has emerged.[74, 76] New strategies against bacterial spreading have shifted towards exploiting the physical properties of surface materials, including the topographical properties to prevent bacterial colonization.[183]

After Bartholott and Neinhuis in 1997, first described the self-cleaning properties of lotus leaf based on its topographical characteristics.[184] Scientists have turned to nature for the design of artificial inspired materials with surface functionalities derived from the physical topographic parameters.[170] In this regard, the development of new micro and nano fabrication technologies has provided the tools to produce these topographies and to better understand bacterial adhesion to surfaces.[183]

### 1.4. Natural Anti-bacterial Surfaces

Nature has been an endless source of inspiration for researchers. The development of micro and nanofabrication techniques during last decades has triggered the expansion of a wide variety of bioinspired functional materials that can mimic the functional properties such as self-cleaning, antireflective, antifouling or antibacterial effects found in plant leaves, animal skins or insects. In particular for antibacterial surfaces, nature has many different examples across the different species from insects, reptiles or fishes.[185]

### 1.4.1. Insects

Insects represent the 50% of eukaryotic species on Earth. They are made of by light-weight materials with different thickness ranging from 0.5 μm to 1mm.[186] Insects were first to develop powered flight, at least 90 million years before the earliest winged vertebrates.[171, 187] As an adaptation mechanism to environmental changes, insects have developed geometrical and non-smooth surfaces on their wings and eyes that allow them to reduce the contamination and retain the functionality of their surfaces.[102, 188, 189] The highly ordered structured surface, composed by micro- and nanometric features together with the organic composition of the insect cuticle provide them with interesting topographical properties such as superhydrophobicity, self-cleaning or antireflective surfaces.[171, 190]

Over the last years many efforts have been directed to the study of insect topographical surfaces and derived physical properties. Some of the relevant examples are described below.

#### 1.4.1.1. Cicada Wing

In 2012 Ivanova and coworkers, first reported the physical properties of the cicada wing. *Psaltoda claripennis*. The chemical composition characterized by X-ray diffraction was found to be mostly composed by chitin and waxes. [102, 191] Scanning electron microscopy (SEM) was used to characterize the cicada's wing surface. SEM imaging revealed well-defined conical nanopillars set in a hexagonal array, with a height of 200 nm, a cap of 60 nm and a pillar interspace of 170 nm. The study of the physical properties of cicada wing revealed a superhydrophobic surface with an effective bactericidal surface against

*Pseudomona aeruginosa*. The bactericidal effect was assessed with the actual cicada wings and also gold-coated. The attachment of bacteria to the nanopillars produced bacteria membrane disruption, which led to mechanical rupture and bacterial death. This result signified that the cicada wing bactericidal effect was dependent solely on the physical topographical surface characteristics.[102] Subsequently, other works have emerged regarding the bactericidal effectiveness of cicada wing. Bactericidal properties of Cicada wing have been tested against a set of bacteria Gram negative and Gram positive bacteria with rod-like and coccal morphology. The cicada wing topography demonstrated effective bactericidal action against Gram negative bacteria, but poor bactericidal performance against Gram positive bacteria.[95] Further research has been carried out to determine the bactericidal effectiveness of other cicada subspecies, which differ on the geometrical arrangement and nanopillars' dimensions on their wings. Kelleher *et al* correlated the bactericidal effectiveness with the physical dimensions of the cicada wing nanopillars. They analyzed height, diameter and interspacing of *Megaponia intermedia*, *Cryptotympana aguila* and *Ayuthia spectabile*. Although significant difference in height and diameter were seen, seemingly the most influencing parameter was interspacing. According to their results the higher spacing between pillars, the lower bactericidal effect against *Pseudomona aeruginosa*.[192]

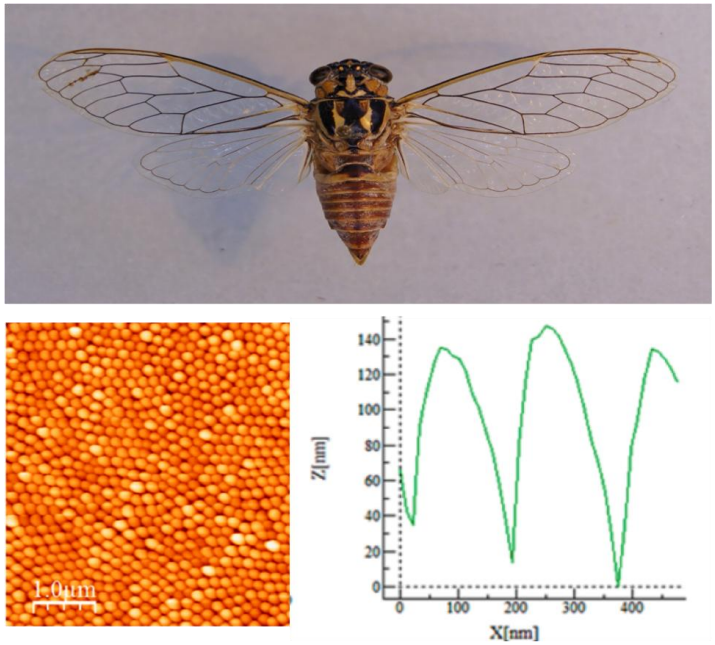


*Figure 4. Atomic force microscopy image and cross section profile of Cicada wing. Image reproduced with permission from Ref.*[192]

### 1.4.1.2. Dragonfly Wing

Following the findings of cicada wing bactericidal properties, dragonfly wing was the also characterized. The surface architecture of dragonfly wing was found to be a randomly organized nanopillared surface, which is connected at their bases establishing a network, while the nanopillars' caps remain disconnected or form clusters rendering hierarchical features. The mean value for nanopillars' height measured about 240 nm. The chemical composition of the surface was found to be the same to that of the cicada wing. The characterization of the physical properties of dragonfly wing showed similar superhydrophobic properties to the cicada wing.[193] The characterization of antibacterial effect revealed that the dragonfly wing is an effective bactericidal topography against Gram negative and Gram positive bacteria, showing higher efficiency for the Gram positive bacteria. This effect was attributed to the taller nanopillars' height.

As proposed by Mainwaring *et al.,* the increase in the height of the nanostructure provides an increased ability for the nanopillars to deform the thicker Gram positive bacteria membrane, making this surface effective against both Gram negative and Gram positive bacteria.[96]

*Figure 5. Scanning electron microscopy imaging of. Dragonfly wing (Scale bar 400 nm). Image reproduced with permission from Ref.[96]*

### 1.4.1.3. Moth-Eye

Another interesting topography derived property found in insects is the antireflective effect. For instance, insect compound eyes such as moth-eye, butterfly eye or fly eye present anti-reflection.[185] Therefore, the study of the antireflective properties of moth-eye has been an interesting subject of research for the interesting applications in optical devices. The natural moth-eye structure consists of highly ordered hexagonal arrays, with conical protuberances with height up to 250 nm and spacing between 200-250 nm. The smaller dimensions than the wavelength of light, allow a region of graded refractive index at the interface reducing the light reflected. This antireflective effect provides insects

an enhanced vision sensitivity even in low light conditions.[194] Conversely, no results have been reported before about antibacterial effect or superhydrophobicity of the moth-eye topography.

*Figure 6. Scanning electron microscopy imaging of Moth-eye (Scale bar 1 μm, Scale bar inset 100 nm). Image reproduced with permission from Ref.[185, 194]*

### 1.4.2. Gecko skin

During the last years, geckos have been object of intense research due to their adhesion properties.[97] Many works have focused on the fibrillar (setae) adhesive structures on the gecko's feet.[107, 195-197] In addition, the feet the gecko's skin comprises of a hierarchical topography[97, 198, 199] containing a hierarchical arrangement of ordered dome shaped microstructures with a diameter of 100-190 μm and 50 μm height, covered by high-aspect-ratio spinules with a height of 4 μm and a diameter ranging 10-30 nm. This hierarchical topography imparts on the gecko skin the properties of superhydrophobicity, self-cleaning, low adhesion and antibacterial function[97] Recently, the antibacterial properties were studied and it was reported to be an

effective bactericidal surface killing Gram positive and Gram negative bacteria.[99]

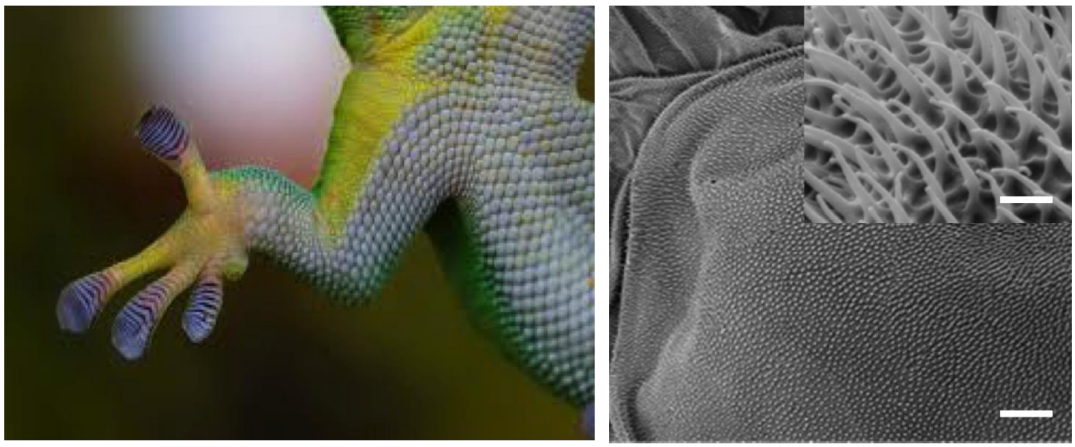

*Figure 7. Scanning electron microscopy imaging of hierarchical topography of gecko skin. Image reproduced with permission from Ref. [97, 99]*

### 1.4.3. Shark skin

Underwater animals are another example of natural functional surfaces. Marine animals, such as dolphins, sharks, whales, carps or crabs have evolved mechanisms to prevent undesirable fouling by microorganisms. Fish scales are covered by oriented micropapillae with nanostructures. This hierarchical topography turns fish scales into superoleophobic in water environment.[171, 185]

Shark skin can remain free from fouling organisms in spite of spending their entire lives under water. This fact has been object of study due to the interesting potential application in the design of antifouling surfaces. Shark skin is formed by very small tooth-like scales, consisting of a rectangular base with specially spaced riblets oriented parallel to swim orientation.[190] This hierarchical architecture minimize the adhesion of microorganism, reduce friction and decreased drag during shark gliding through water, which turn sharks into quick and efficient swimmers.[185]

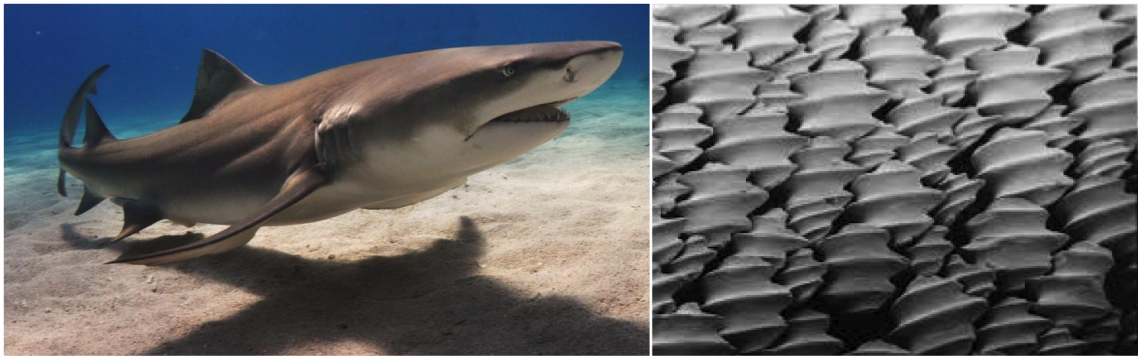

*Figure 8. Scanning electron microscopy imaging of Shark scales. Image reproduced with permission from http://asknature.org*

Therefore, these natural examples demonstrate the key role of surface topography to obtain specific functions.

## 2. Biomimetic antibacterial surfaces

Antibacterial natural topographies are growing increasing interest as non-resistance causing approach to prevent infections.

Bioinspired antibacterial surfaces have been fabricated on many different materials. Cicada wing topography has been reproduced on polymer and titanium and demonstrated to be effective against Gram negative bacteria.[100, 200, 201] Inspired topographies of the dragonfly wing have been successfully reproduced on silicon[193, 202] and titanium[203] and demonstrated to be bactericidal against Gram positive and Gram negative bacteria. Acrylic replicas of the nanotipped hairs on the gecko skin have been proven to be effective against Gram positive and negative bacteria.[99] Shark skin has been successfully replicated on epoxy resin,[186, 187] PDMS,[204] and polypropylene[205] and experimented for applications such as aircrafts,[191] ship hulls,[188] swim suits[206] or aeroengine components.[207]

The moth-eye topography has been described and studied as a natural antireflective surface. However, the study of the bactericidal activity of this natural surface has not been undertaken before. Hence, in this thesis, a study of the bactericidal properties of the moth-eye mimetic polymer topography produced via polymer nanoimprinting is presented. The bactericidal effect of the imprinted topography is evidenced against three different bacteria frequently involved in biofilm-associated infections including the Gram positive pathogen Staphylococcus *aureus* (S *aureus)* and Gram negative Pseudomonas *aeruginosa* (P *aeruginosa*) and Escherichia *coli (E. coli).* Furthermore, the biocompatibility of the topography towards human keratinocytes (HaCaT) is investigated through studies of proliferation capability and spread morphology of the HaCaT cells seeded on the nanocone topography. HaCaT cells have been used as *in vitro* model to assess the biocompatibility of polymeric scaffolds for skin implants.[208-210] Keratinocytes were chosen as an in vitro model due to their well-known role in epidermal tissue regeneration and wound healing[211, 212] and their sensitivity to direct contact with surfaces.[108, 196]

## 3. Experimental section

**3.1. Moth-eye mimetic topography fabrication.** The moth-eye nanostructures were fabricated on Poly(methyl methacrylate) (PMMA). Initially, PMMA thin films were produced on glass cover slips (18 mm in diameter). Prior to that, the glass cover slips surfaces were activated with oxygen plasma (Tepla 600) at 300 W for 5 minutes, to improve the adhesion between polymer and glass. On the surface, a solution of PMMA (Mw 120.000, Sigma Aldrich) on toluene (7.5 wt %) was spin coated at 1000 rpm for 1 minute and subsequently, the films were annealed at 100 °C. The nanocone structures were created by a thermal

nanoimprint process. Initially, a working mold with the moth-eye topography was prepared. For this a master nickel mold (HT-AR-02, Temicon) was replicated. This was accomplished using two layers of polydimethylsiloxane (PDMS). First, hard PDMS (h-PDMS)(PP2-RG07, Gelest) was mixed and casted onto the nickel mold and after 30 minutes standing for the filling of the cavities, the mold was spun (1000 rpm for 1 minute). Subsequently, the h-PDMS was partially cured in an oven for 10 minutes at 80 ºC. After that, the soft PDMS (Sylgard 184, Dow Corning) precursor and initiator were mixed, degassed and casted onto the partially cured h-PDMS layer and finally cured in an oven at 80 ºC for 24 hours. Lastly, the mold was peeled off and kept in a clean room environment. Using the replicated PDMS working molds, the prepared PMMA films were imprinting by pressing these molds at 170 º C at 45 bar or pressure for 5 minutes using an EITRE Nano Imprint Lithography system (Obducat). The polymer-mold assembly was cooled down to 70 °C before the pressure was released and the demolding was performed. The topography was imaged by SEM using an Auriga FIB-SEM system (Zeiss) and atomic force microscopy (AFM) using a Multimode 8 system (Bruker).

**3.2. Bacteria Culture and Live/Dead® Baclight™ Viability assays.** *Escherichia coli* (CECT 516), Pseudomona *aeruginosa* (CECT 4628) and *Staphylococcus Aureus* (RN 4220) (Colección Española de Cultivos Tipo, Universidad de Valencia), were used to assess the bactericidal properties of the topography. The glycerol stocks of bacteria were incubated at 37 °C in 50 ml of Luria-Bertani media (LB) overnight. The bacterial suspension obtained was diluted to an optical density, $OD_{600}$= 0.2. The imprinted and smooth PMMA substrates used for control were placed in 12 well-plates and incubated in static

conditions with 2 ml of bacteria suspension during 7 hours for *E.coli* and *S. aureus* and 5 hours for *P. aeruginosa*. After the incubation period, the PMMA substrates were gently rinsed using 1X Phosphate-buffered saline (PBS) (Fisher Scientific) and stained using Live/Dead® Baclight™ Viability Kit (Molecular Probes) (0.13 µl of stain diluted in 1 ml Tris-HCl) for 15 minutes in dark at room temperature. Finally, the PMMA substrates were rinsed with 1X PBS and mounted with *Bac*Light mounting oil for visualization. The substrates were imaged on a fluorescent microscope. Live and dead bacteria were counted using the Image J image analysis software (NIH Image). Four independent trials with three replicates of each substrate were run.

**3.3. Bacteria-Moth-eye topography interaction**. The interaction between bacteria and moth-eye mimetic topography was visualized by scanning electron microscopy (SEM). After the bacteria incubation period, all substrates were rinsed with 1X PBS prior to carry out the fixing process with 4% paraformaldehyde (PFA) (Sigma-Aldrich) for 15 minutes. Subsequently, the substrates were rinsed with increasing gradients of 0, 50, 75, 100% ethanol for 5 minutes each. These substrates were air dried and sputter-coated with a thin layer of gold imaging on an Auriga FIB-SEM system (Zeiss).

**3.4. Cell proliferation assay**. HaCaT cells expressing green fluorescent protein (GFP), were cultured in Dulbecco's modified Eagle's medium (DMEM, Biowest) supplemented with 10% fetal bovine serum (Gibco), 1% L-Glutamine (Biowest) and 1% penicillin–streptomycin (Biowest) at 37 °C and 5% CO2 atmosphere.
The growth and proliferation of the HaCaT cells was assessed on smooth PMMA and Polystyrene (PS) films and on the moth-eye imprinted topography. Three independent trials with three replicates of each substrate were run.

HaCaT cells were seeded at concentration of 20.000 cells/ ml. Cell viability was evaluated by a colorimetric method based on the reduction of Resazurin (blue) to resofurin (pink) due to the metabolic activity of viable cells. A solution of Resazaruin salt (Alfa Aesar) was prepared with a concentration of 10 µg/ml. Absorbance was measured during 15 days at 570 and 600 nm using a micro plate reader (H4 Hybrid Multi-Mode Microplate Reader, BioTek).

**3.5. Cell morphology imaging.** HaCaT cells were seeded and cultured on the different substrates, and collected after 10 days. The cells nuclei were stained using Dapi (Molecular probes) and the expressed GFP was used for cytoplasm visualization. Prior imaging, the substrates were rinsed with 1X PBS and mounted on FluorSave reagent media (CalBiochem). Images of the stained cells were obtained through a fluorescent microscope (Leica).

SEM imaging was also carried out to characterize the interaction between HaCaT cells and the topography. Before imaging, all substrates were rinsed with 1X PBS prior to the fixing process of bacteria with 4% paraformaldehyde (Sigma-Aldrich) for 15 minutes. Then the substrates were rinsed in increasing gradients of 0, 50, 75, 100% ethanol for 5 minutes in each dilution. These substrates were air dried and sputter-coated with a thin layer of gold. The cells on the substrates were imaged using an Auriga FIB-SEM system (Zeiss).

**3.6. Cellular morphology analysis.** The morphology of the HaCaT cells was analyzed individually using the image analysis software Image J (NIH Image). Three independent trials with three replicates of each substrate were analyzed. Two different parameters were taking into account for quantification: area and

elongation. Elongation was defined as [major axis/minor axis] as the cells are fitted to an ellipse. Smooth PMMA substrates were used as control.

## 4. Results and Discussion

### 4.1. Moth-eye topography characterization

PMMA was chosen as standard material to fabricate the moth-eye mimetic topography films because it is a polymer approved for medical applications and it is employed widely in intraocular lens implants.[213] It is also a commodity plastic used in a wide range of applications. The nanoimprinted moth-eye topography employed to quantify the bactericidal activity of the surfaces is displayed in Figure 9. The SEM (A) and AFM (B) images of the nanoimprinted substrates revealed a topography formed by well-defined nanocones disposed on hexagonal arrangement with dimensions close to those of the natural moth-eye structures.[194] The array of nanocones shows a mean height of 350 nm and a feature width on the cap of 80 nm with a pitch of 250 nm and aspect ratio of 4.3 (Fig. 9). The moth-eye topography exhibits similar nanofeatures' dimensions to those of the dragonfly wing[96] and the equal hexagonal arrangement of the cicada wing. [95, 192]

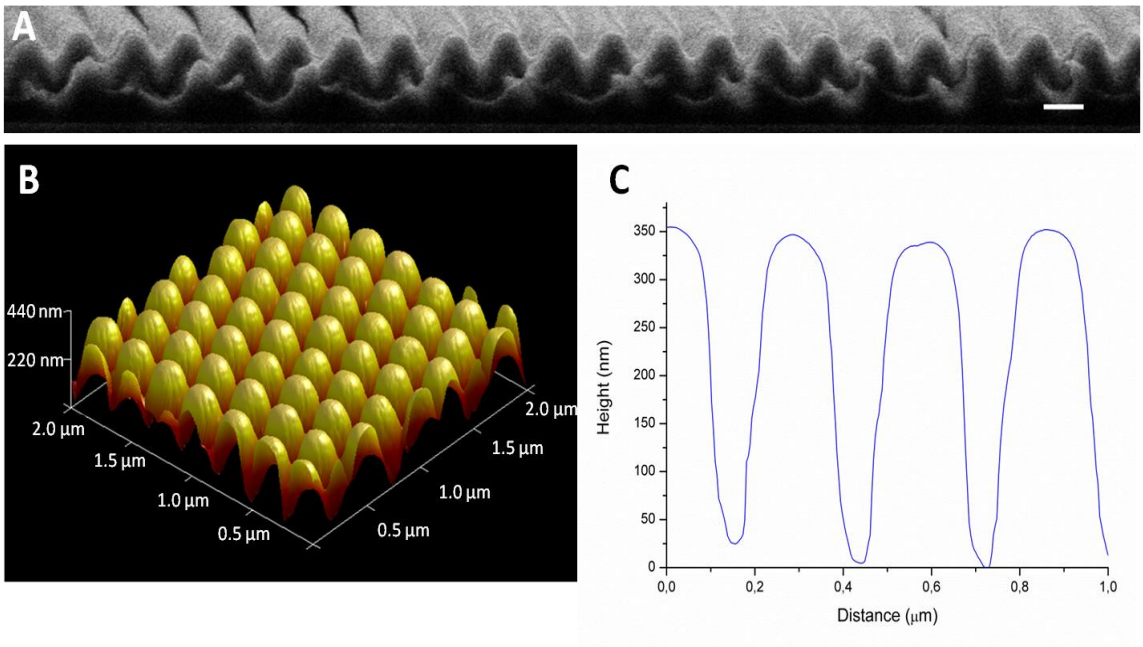


*Figure 9. Moth-eye mimetic topography imaging and geometrical characterization by A) SEM, B) AFM three-dimensional image and C) AFM cross sectional profile. Scale bar 200 nm.*

### 4.2. Bactericidal effect of the moth-eye topography

The bactericidal properties of the moth-eye topography were assessed through viability tests of cultured *E. coli*, *P*. *aeruiginosa* and *S. aureus* as model of Gram negative and Gram positive bacteria respectively. For this, bacteria were seeded on the imprinted substrates and smooth substrates as control and incubated during specific periods of time. After the culture period, the live and dead attached bacteria were counted from fluorescent microscopy images on the smooth and imprinted PMMA substrates. Figure 10 shows representative fluorescence microscopy images of the live-dead bacteria observed on the substrates. As it can be seen on the images, the coverage percentage and total amount of bacteria adhered onto the substrates were similar. However, the viability of the three bacteria tested was found significantly affected by the topography. The percentages of dead bacteria attached on control surfaces

were found to be 5% for *S. aureus* and *P. aeruginosa* and 15% for *E.coli*. In contrast, a significant increase of the dead population of bacteria was seen on the moth-eye topographical substrates. On these substrates, the percentage of non-viable bacteria increased up to 55%, 45%, 30% for *S. aureus*, *E. coli* and *P. aeruginosa* respectively (Fig. 10D). This large increase on the amount of non-viable bacteria provides evidence for the bactericidal effect of the moth-eye topography against Gram positive and Gram negative bacteria compared to the control surfaces. The local interaction and morphology of bacteria cultured on smooth and moth-eye substartes was examined through SEM imaging. For this, bacteria were fixed with PFA before imaging in order to preserve the bacteria morphology unchanged due to the high vacuum inside of the SEM chamber. The SEM images indicate that the bacteria seeded on smooth PMMA after the fixing procedue kept their typical morphology. As Figures 10 A'', 10 B'', 10 C'' show, the *S. aureus* retained the characteristic cocci shape and *E. coli* and *P. aeruginosa* kept their rod-like morphology. Conversely, for the bacteria attached onto the moth-eye topography displayed in Figures 10 A''', 10 B''' and 10 C''' for *S. aureus, E. coli* and *P. aeruginosa* respectively, it can be seen that some of them have lost their typical morphology and have adopted a squashed appearence indicative of the membrane damage or rupture with the release of the inner content. Similar bacterial morphology has been seen on bacteria attached to cicada wing and dragonfly wing inspired topographies.[96, 100, 193, 201, 203] The moth-eye mimetic topography studied in this work, having a geometrical dimensions more similar to those of the dragon fly wing, reveals a comparable bactericidal effect.

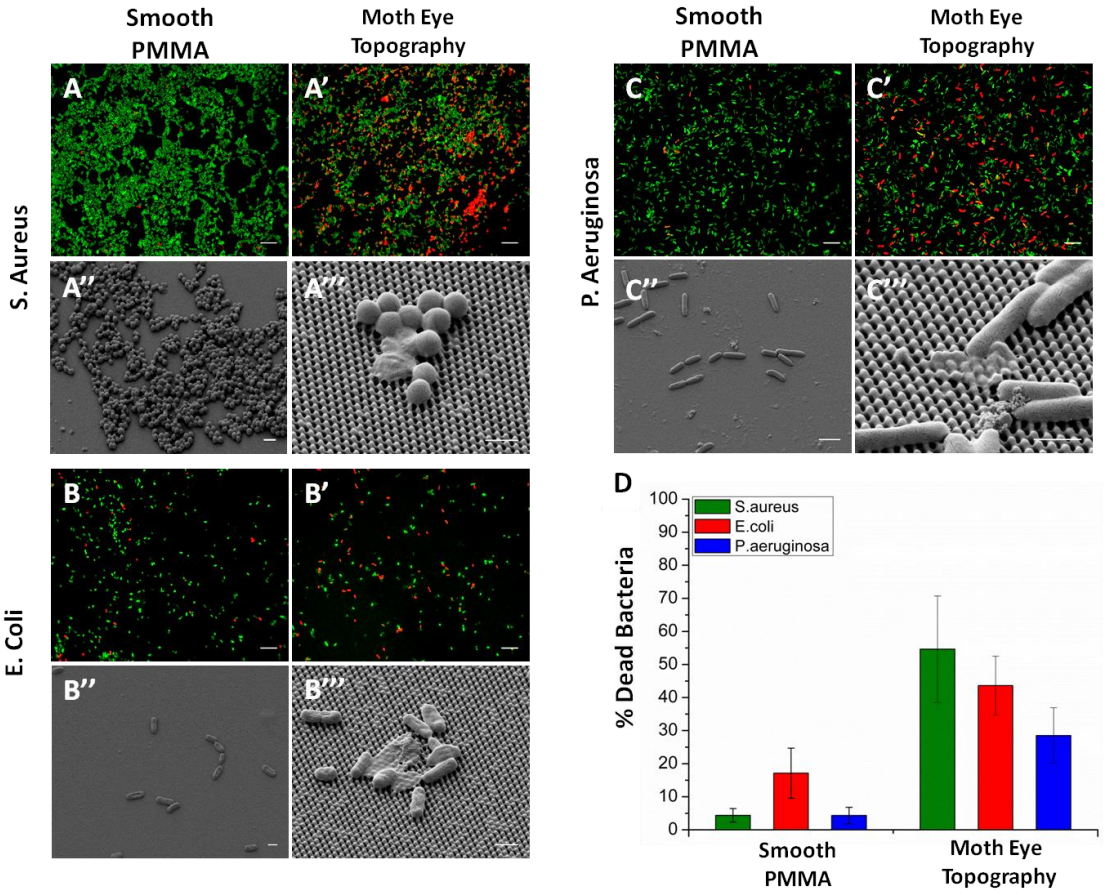


*Figure 10. Bactericidal properties of the moth-eye mimetic topography. Comparative flourescence imaging of live-dead S.aureus (A,A'), E.coli (B,B') and P.aeruginosa (C,C') incubated on pristine PMMA and moth-eye topography. Scale bar 5 µm. Comparative SEM imaging of the bacteria-topography interaction of S.aureus (A'',A'''), E.coli (B'',B''') and P.aeruginosa (C'',C''') attached onto pristine PMMA and moth-eye topography. Scale bar 1 µm. Bactericidal effectiveness plotting of smooth PMMA and moth-eye topography against S. aureus, E.coli and P.aeruginosa. Error bars correspond to the standard deviation.*

### 4.3. Bacteria-surface interaction: Bactericidal mechanism

The bactericidal effect of bioinspired patterned surfaces has been attributed solely to a mechanical topographical effect on the surface adhered bacteria. The bactericidal mechanism has been described by physical models based on a severe increase in contact adhesion area upon bacterial attachmnet that

leads to fatal membrane stretching followed by bacterial death.[96, 214, 215] Referring to the simulations performed by Li,[214] the moth-eye topography here described with a diameter of 80 nm and a height of 350 nm, it is predicted to have optimal dimensions to induce a high stretching degree hence, strong bactericidal effect.

Topographical surfaces with high density of nanostructures with feature size smaller than that of bacteria, initially offer an effective decrease in the contact area available for adhesion. In the case of the moth-eye topography, the contact area fraction corresponding to the top cone surface is approximately 0.2. Hence, upon initial attachment, bacteria will try to increase the area of contact with the surface pursuing an optimal interaction, which will lead to a bacterial membrane deformation around the nanocones. This deformation will bring closer molecules from the bacteria membrane to moth-eye surface[76] mimicking a zipper's mechanism and increasing the adhesion points as a result the adhesion force. Concomitantly with membrane deformation, due to the increase in contact area between the bacteria and the nanocones, stretching forces would appear on the suspended part of the membrane between nanocones. When the stretching force reaches the critical breaking value beyond the membrane stretching modulus, the bacteria membrane will rupture and would lead to the bacterial death. This process is represented in Figure 11.[215, 216]

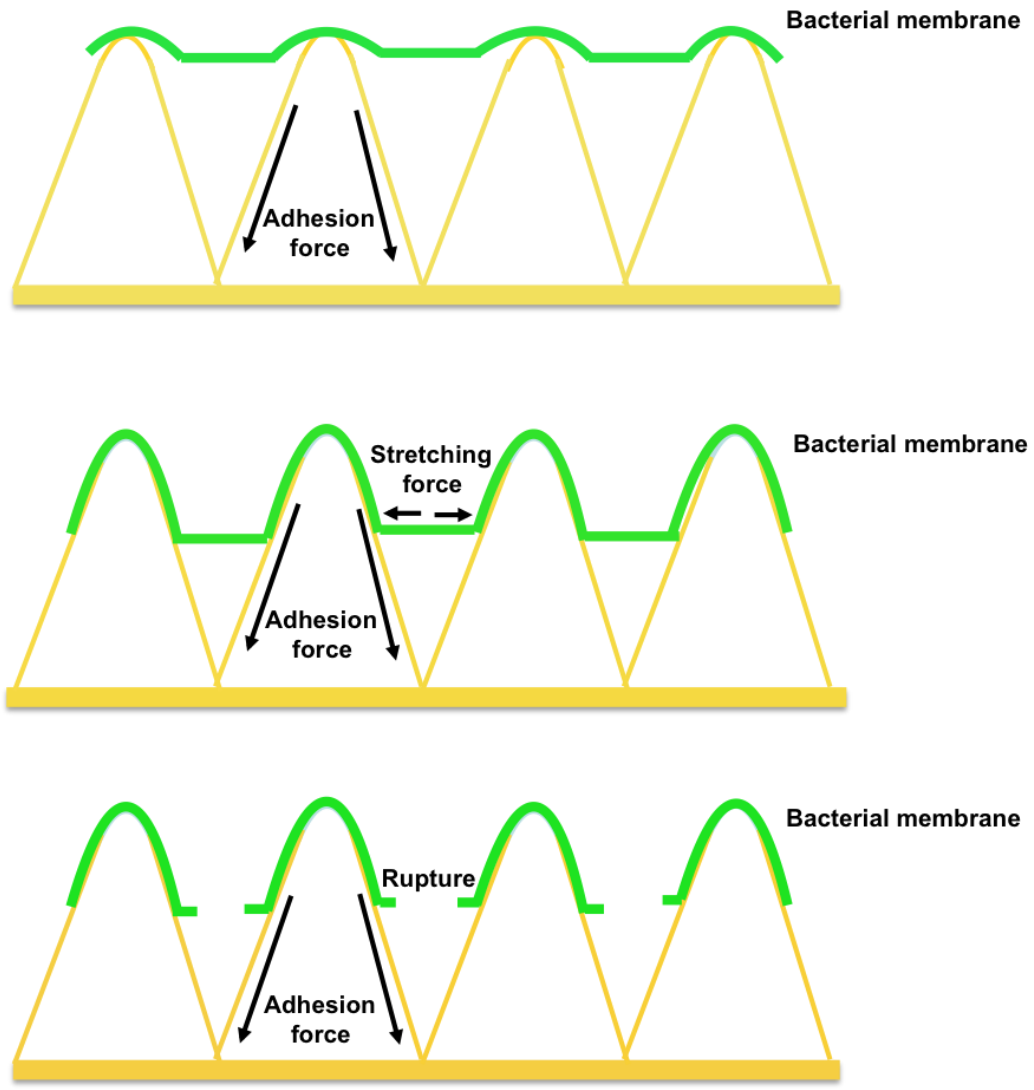


*Figure 11. Schematic of the bactericidal mechanism proposed for the moth-eye mimetic topography. During the initial attachment the interaction between bacteria and surface is reversible, once bacteria-surface interaction becomes irreversible bacteria increase the contact area to reach the optimal adhesion, the presence of moth-eye mimetic topography causes membrane deformation that leads to bacterial death.*

### 4.4. Biocompatible properties of moth-eye mimetic topography

Despite the interest on antibacterial topographies for medical implants and tissue regeneration, only few works have determined the impact of bactericidal topographies on eukaryotic cell response.[100, 200, 202, 203, 217] On the other hand, it is widely recognized that the substrate topographic features can elicit specific cell functions and ultimately influence the cell response.[35, 44, 48, 217, 218] Titanium nanowires inspired on the cicada wing topography have shown to be antibacterial substrates that support human osteoblast cells proliferation.[100] Dragonfly wing titanium inspired bactericidal nanostructures have also proven to be suitable surfaces for fibroblast proliferation.[203] Black silicon has been shown recently to support fibroblast spreading and at the same time had a reduced inflammatory response when implanted in mice.[202] Keratinocytes have a key role on skin formation and particularly HaCaT cells have been reported to have a high sensitivity towards non biological surfaces.[108, 196] Only few works on polymer nanofibers scaffolds have been described to be suitable for HaCaT adhesion and normal cell functions.[107, 208, 219, 220] Here, the biocompatible properties of moth-eye mimetic topography towards HaCaT cells were evaluated to address their potential application in biomedical devices.

Initially, the HaCaT cell proliferation and morphology on smooth PMMA and moth-eye topography were characterized. HaCaT cells were cultured on moth-eye patterned and smooth PMMA films and on smooth polystyrene as control surface because it is the material widely employed cell culture. The cell proliferation monitored during 15 days is plotted in Figure 12A. Cells entered into the logarithmic phase on the 9$^{th}$ day, the maximum growth level was reached in the 13$^{th}$ day and there was a reduction of the cell viability in the 15$^{th}$

day by overcrowding and exhaustion of the medium. The three different substrates exhibited the same growth profile as depicted in Figure 12A, indicating that moth-eye mimetic topography did not produce any apparent detrimental effect on the viability of HaCaT cells.

The influence of moth-eye topography on HaCaT cells´ morphology was also evaluated comparatively to the smooth PMMA by fluorescence microscopy imaging (Fig. 12B, 12B'). The HaCaT cells were collected at the beginning of log phase where the cell spreading and cell elongation were obtained. The HaCaT cells exhibited an extended morphology on the smooth PMMA substrates and moth-eye mimetic topography. Cell spreading (Fig. 12C) and elongation (Fig. 12D) mean values did not reveal significant changes, indicating that the nanostructured surface did not significantly influence the HaCaT cell response.

SEM imaging was used to study the influence of the surface on cell morphology and cell-topography interaction. Figure 12B'', 12B''' shows the morphology of HaCaT cells cultured on smooth PMMA and on the moth-eye topography. HaCaT cells appear forming small colonies attached to smooth PMMA and on to the moth-eye topography, and no significant morphologycal changes were observed on the SEM images what is consistent with the images obatined by fluorescence microscopy.

These results indicate that the nanometrical dimensions of the moth-eye mimetic topography do not impact HaCaT cell adhesion, proliferation or morphology appearing as a suitable surface to support cell development. Hence, the moth-eye mimetic topography appears to be a promising bactericidal topography with biocompatible properties which can potentially

facilitate the hot tissue integration process of implantable devices or resorbable scaffolds for tissue renegeration.

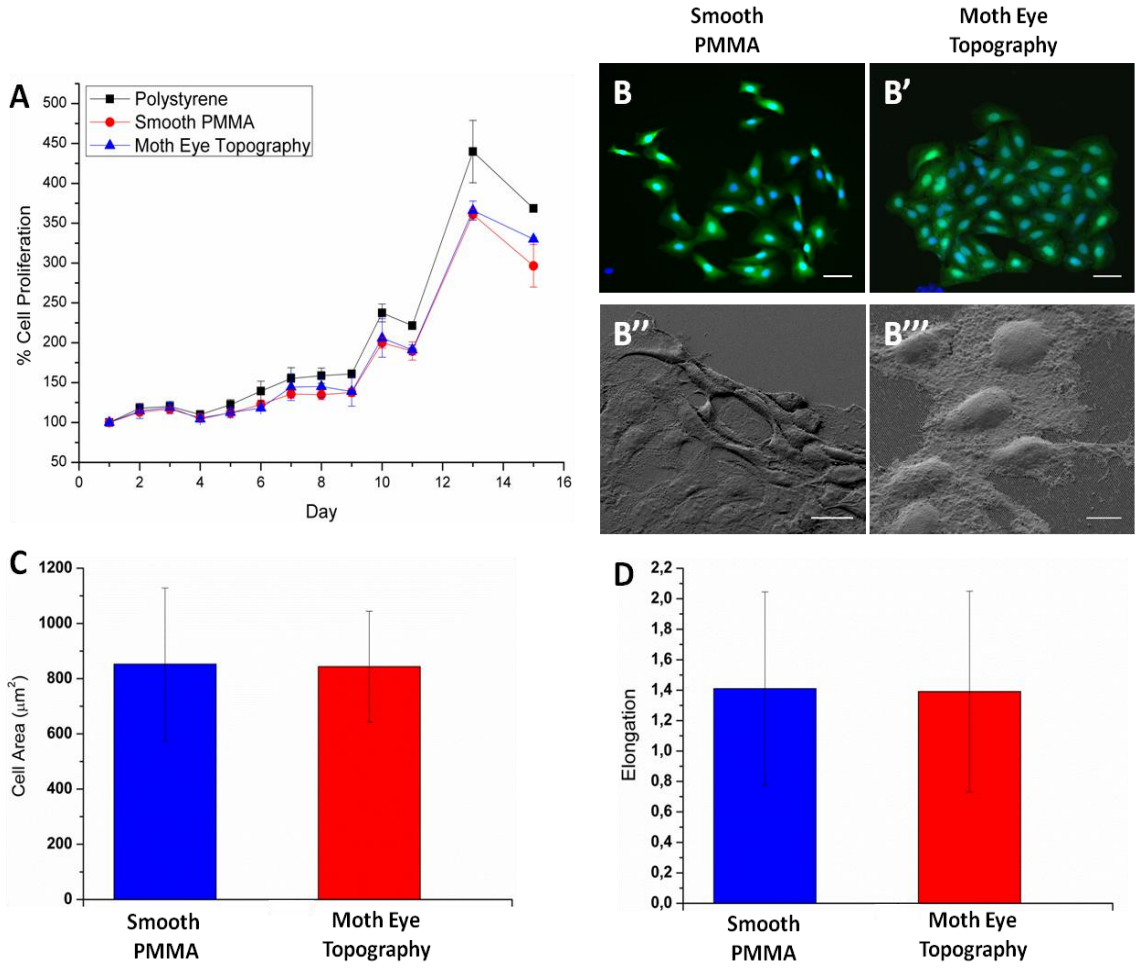


*Figure 12. Biocompatible properties of moth-eye mimetic topography. (A) HaCaT cell proliferation profile on polysterene, smooth PMMA and on the moth-eye topography. (B) Fluorescence Imaging (B,B', Scale bar 50 µm) and SEM imaging (B'' Scale bar 20 µm ,B''' Scale bar 2 µm) of HaCaT cells seeded on smooth PMMA and on the moth-eye topography. (C) Cell spreading and (D) cell elongation of HaCaT cells seeded on smooth PMMA and on the moth-eye topography. Error bars represent standard deviation.*

## 5. Conclusion

Bioinspired bactericidal polymer topography mimicking the nanostructures present on the moth-eye has been fabricated on polymer using thermal nanoimprinting. This surface has been proven to be an effective bactericidal topography against Gram positive and Gram negative bacteria.

Mechanistically, the results support the theoretical models proposed before where the mechanical rupture of bacteria by the nanocone of the surfaces is the result of the stretching force on the membrane of bacteria pursuing a stable attachment leading to the bacterial death.

Moreover, the biocompatibility of the moth-eye mimetic topography towards human keratinocytes has been demonstrated. The topography did not induce dramatically changes in cell morphology or the general biological response.

In summary, this study indicates that moth-eye mimetic polymer topography is a broad spectrum non-resistant causing bactericidal surface that at the same time supports mammalian cell growth and proliferation. This study serves to support a technology that may launch a new and innovative direction on the design of biomaterials with capacity to reduce the risk of medical device-associated infections while enhancing host tissue integration making these surfaces valuable for regenerative medicine and bio-implant applications.

# Chapter 5

# Bactericidal Moth-eye mimetic nanopatterned nanocomposites

## 1. Introduction

Since the ancient times, Egyptians, Greeks and Romans used metals such as silver, copper, zinc or mercury to contain and preserve water and food supplies. Silver has been employed in wound dressing to treat infections from burn injuries and wounds.[221-223] However till today, the bactericidal mechanism remains unclear. There are two main accepted mechanisms to explain bactericidal effect of metallic materials. The first mechanism is the releasing of positively charged metallic ions into the media. The positive ions could screen and destabilize the negative charge of the bacterial membrane.[224] The second mechanism could be that the dissolved metal ions could react with bacterial membrane proteins altering membrane integrity.[222] For instance, silver as the most used antibacterial metal has been widely study and it is accepted that its bactericidal activity is primarily due to the reaction of silver ions with disulfide or sulfhydryl groups of the cysteines' side chains. This reaction induces conformational changes in the proteins causing the loss of their function. Once the membrane permeability is compromised, silver ions can enter into the cell targeting DNA, ribosomes and intracellular proteins causing irreversible damage on bacteria.[225]

Other alternative mechanism is based on the capacity of metals to participate in redox reactions. Redox-active metals can generate or catalyze reactive oxygen species (ROS). ROS create an oxidative stress that can induce damage of cell proteins, lipids and DNA,[226, 227] if they exceed the antioxidant capacity of the cell.[224]

Today metal oxides, such as $TiO_2$ and ZnO, have emerged as very attractive antibacterial agents because of their stability, low cost, low toxicity and their photocatalytical properties.[228]

A photocatalyst is defined as a material that can absorb light generating electron-hole pairs that enable the chemical transformation of reaction participants and it is self-regenerated after each cycle.[228]

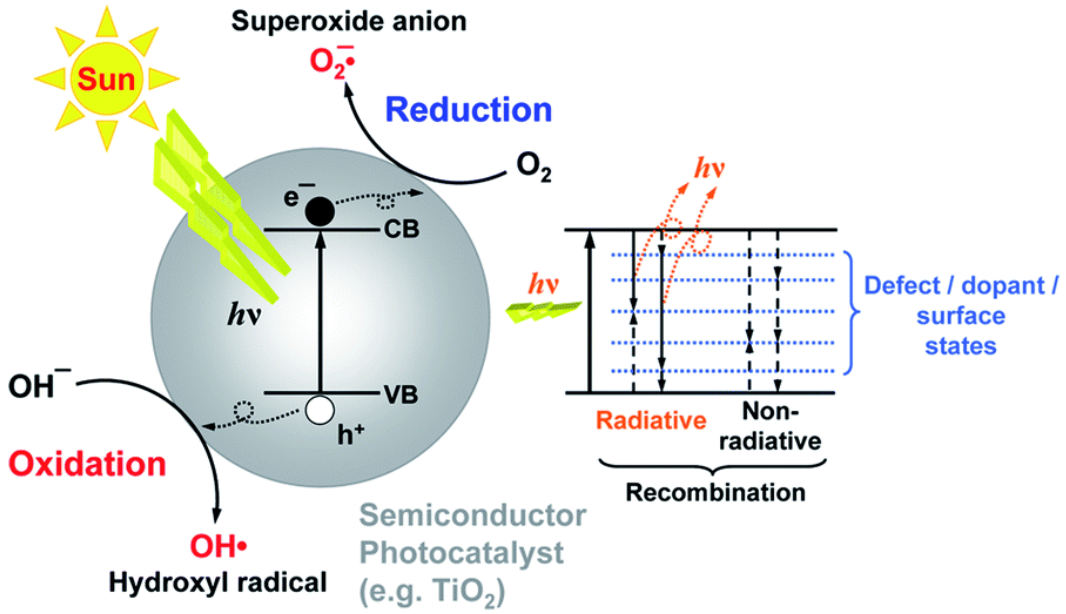


*Figure 1. Schematic representation of the principle of photocatalytical process. Reproduced with permission from Ref.*[229]

Semiconductor metal oxide photocatalyst (e.g. $TiO_2$ or ZnO), absorb light creating electron-holes pairs that can be transferred to other molecules present on the surface of the photocatalyst. Typically, the electron is transferred to an acceptor molecule if the redox potential is lower than the conduction band (CB) of the photocatalyst, whereas a hole can be transferred to a donor molecule if its redox potential is higher than the valence band (VB) of the photocatalyst. (Fig 1).[229]

In aqueous solution, semiconductor materials under UV or visible light exposure can produce ROS. The interaction between water molecules and the photogenerated electron holes produces $^{\bullet}OH$ and $H^+$. In addition the electron can reduce $O_2$ molecules present in water and yield the superoxide anion ($^{\bullet}O_2^-$), which can be transformed into singlet oxygen ($^1O_2$). These species can react and combine between them (Fig 2) yielding different ROS that are pernicious to bacteria.[230]

$$ZnO + h\nu \rightarrow e^- + h^+, \quad (1)$$

$$h^+ + H_2O \rightarrow {}^{\bullet}OH + H^+, \quad (2)$$

$$e^- + O_2 \rightarrow {}^{\bullet}O_2^-, \quad (3)$$

$${}^{\bullet}O_2 + H^+ \rightarrow HO_2^{\bullet}, \quad (4)$$

$$HO_2^{\bullet} + H^+ + e^- \rightarrow H_2O_2. \quad (5)$$

*Figure 2. Generation of reactive oxygen species and formation of additional active molecules. Image modified with permission from Ref.[230]*

The ROS generated exhibit different bactericidal action. For instance, superoxide and hydroxyl radicals cannot penetrate the membrane due to their negative charges. Therefore, it is common to find these species in the outer surface of bacterial membrane causing peroxidation of unsaturated phospholipids damaging membrane architecture (Fig. 3). ROS action on bacterial membrane can cause conformational changes of membrane proteins, altering fluidity and integrity, which ultimately finishes with an ionic imbalance that leads to bacterial death.[231]

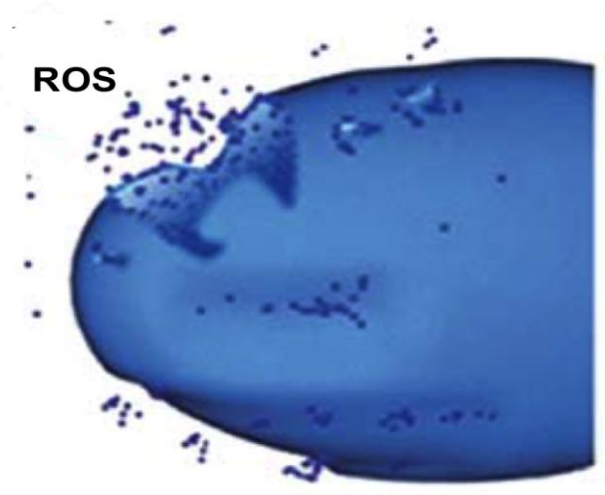


*Figure 3. Membrane damage produced by the oxidative action of ROS. Image reproduced with permission from Ref.*[230]

In contrast, hydrogen peroxide molecules are able to pass through the bacterial membrane causing internal cell damage by damaging the respiratory enzymes, decreasing the ATP production, or DNA and proteins causing bacterial death.[230]

Thus, the increase of ROS production by photocatalyst materials induces damage of phospholipids, lipoproteins and nucleic acids, which finally causes the death of bacteria.

### 1.1. Metal and metal oxide nanoparticles as effective antibacterial materials.

Recently, the advances in nanotechnology in the synthesis of nanoparticles (NP) have provided a new route to formulate effective antibacterial materials.[232] The large surface to volume ratio provides NPs with and enhanced mechanical, chemical, electrical, optical and magnetic properties compared to the bulk material and have been extensively used for biological and biomedical research.[233, 234] Thus, metal and metal oxide nanoparticles

have emerged as an effective antibacterial treatment against infectious disease including the antibiotic-resistance ones.[175, 235]

Chemical synthesis routes to obtain different size and shaped nanoparticles have been intense subject of research and many works have addressed the bactericidal mechanism and the influence of the morphological parameters of the nanoparticles on their antibacterial effect. The bactericidal effect of metal and metal oxide nanoparticles has been previously evaluated. Ag, Cu, CuO, ZnO, $TiO_2$, Au, are the most common nanoparticles used as antibacterial materials. Ag nanoparticles have been the most extensively employed inorganic nanoparticles as antimicrobial materials as they have been found to be effective bactericidal material against Gram positive[236] and Gram negative[237] bacteria. The influence of size and morphology on bactericidal properties has been evaluated,[238] as well as the bactericidal effectiveness of $Ag_2O$ nanoparticles. Ag-Au alloys have been shown as interesting alternative to developed effective non-resistance antibacterial materials.[239]

Analogous to the bulk metals, the antibacterial mechanism of nanoparticles remains unclear. The most accepted mechanism is related to the metal ion release and photocatalytic activity.[240] Moreover, the positive surface charge of metal nanoparticles facilitates the interaction with the negatively charged bacterial membrane resulting in an enhancement of the antibacterial properties.[175, 241] For instance, Ag nanoparticles have been reported to act mainly by ion releasing, silver ions can target membrane proteins and interfere metabolic processes and DNA replication.[238, 242] Bactericidal action of $TiO_2$ nanoparticles is based in the photocatalytical properties of this material as explained before. Under UV light $TiO_2$ produce ROS generating oxidative stress

that leads to bacterial death.[243, 244] The specific bactericidal mechanism of ZnO nanoparticles is not fully known, but it is acepted that this nanoparticles can act through photocatalysis, ion releasing, and membrane disruption through direct contact or by internalization into the cell.[245, 246] CuO nanoparticles act through direct interaction with bacterial membrane and damaging vital bacterial enzymes.[247, 248]

However, in spite of the low toxicity exhibited by metal oxide nanoparticles, the widespread use of these nanomaterials and possible accumulation in the environment is a reason of concern due to ecotoxicity to other organisms including earth autochthonous micro flora (bacteria, fungi, algae) and non-target organisms such as aquatic species [20-21].[175, 235] Accordingly, until the toxicity mechanisms of the metal oxide NP are completely elucidated, there is a need to reduce the use of NPs.

To this end, the binding of nanoparticles into polymer matrices appears to be an interesting approach to reduce the environmental impact.[249]

### 1.2. Polymer nancomposites.

A nanocomposite is a matrix to which nanoparticles have been added to improve a particular property of the material. Due to the addition of nanoparticles, general properties such as mechanical strength or toughness improve significantly. Other properties, depending on the nature of the nanoparticles such as electrical or thermal conductivity can be improved as well.[250, 251] Antibacterial properties have been also achieved with nanocomposites, by incorporation of nanoparticles such as copper and mostly silver,[14, 181] and the oxides like ZnO and $TiO_2$.[109, 252]

Nanocomposite manufacturing is generally performed by dispersion of the nanoparticle fillers within the polymer matrix. The methods employed to fabricate nanocomposites include: intercalation method, in situ polymerization, sol gel method and direct mixing of polymer and nanofillers.

The common method employed for the fabrication of nanocomposites using thermoplastic polymers as matrix, is direct mixing or blending. This requires to bring the polymer to the molten temperature where the nanoparticles are dispersed by mechanical shear (Fig. 4).[224] The uniform and homogeneous dispersion of nanoparticles in the polymer matrix is one of the main challenges faced during polymer nanocomposite fabrication because the nanofillers have a tendency to form aggregates. These aggregates degrade the properties of nanocomposites. An additional challenge in the melt blending process is the excess of temperature produced due to shear resulting in the degradation of the polymer.[253]

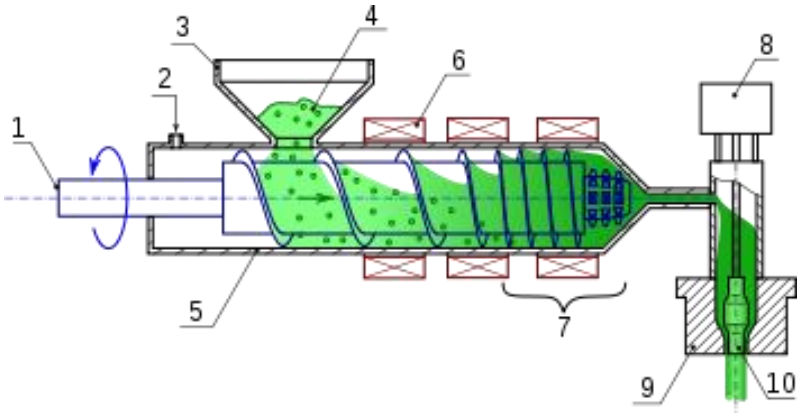


*Figure 4*. Extrusion-blow moulding of polymer s:1, reciprocating screw, 2. compressed air; 3. hopper;4. granules;5. barrel; 6. heaters;7.grinding, mixing;8.actuator's hydraulic generator; 9. draw plate;10. core/punch. *Image reproduced from https://commons.wikimedia.org/wiki/*

## 2. Antibacterial and Cytotoxic action of Nanocomposites

The antibacterial action of several nanocomposites has been reported before.[254] Metal oxide particles such as $TiO_2$, ZnO and to a lesser extent CuO are growing interest as fillers due to lower toxicological concerns. Synthetic polymers such as PMMA, polyester or acrylics combined with $TiO_2$ and ZnO have been shown to be effective antibacterial nanocomposites against Gram positive and Gram negative bacteria.[109, 252, 255, 256] Biological polymers such as chitosan or cellulose have been combined with CuO and $TiO_2$ nanoparticles to effectively reduce bacterial proliferation.[257-259] These results prove that despite of being embedded on a polymer matrix, the bactericidal properties of the nanoparticles are retained.

The cyto-toxicity of metal oxide nanocomposites has also been investigated in few studies; Schwartz and coworkers[260] found that ZnO polymer composites are non-cytotoxic towards a mammalian cell line at bactericidal loadings. Wu *et al*., also found a negligible cyto-toxicity for the nanocomposites containing poly lactic glycolic acid (PLGA) and $TiO_2$ NPs with concentrations up to 10%.[255]

Nonetheless, there are still concerns on their safety for humans particularly on the free NPs form because the mechanisms of action still are not fully known.[245] On the other hand, as mentioned above, free nanoparticles in the environment pose an ecological risk for other organisms including earth autochthonous micro flora and aquatic species.[247, 248] Consequently, until the toxicity mechanisms of the metal oxide NPs are completely unraveled, there is a need reduce the amount of nanoparticle used and to design products with contained toxicity and with reduced environmental impact; products that enable the safe disposal or recovery for recycle of the nanoparticle.

Given these premises, this thesis reports a practical processing method based on nanoimprinting replication to fabricate a moth-eye mimetic antibacterial nanocomposite surface with enhanced bactericidal efficacy. The method allows an efficient nanoparticle-matrix dispersion and topography imprinting in a single step. Accordingly, the method permits decreasing the NP load employed, which is limited and contained within the effective surface.

The nanoparticles in synergy with the topography conferred antibacterial action versus Gram positive and Gram negative bacteria in the presence UV light for $TiO_2$ NPs and in its absence in the case of ZnO. Bacterial inhibition ranges from 60-90%. The biocompatibility of the PMMA-ZnO bio-inspired bactericidal nanocomposite towards human keratinocytes is also studied and demonstrated.

Overall, this work aims at providing a safe by design moth-eye patterned nanocomposites with a synergic bactericidal activity as new emerging, non-resistance causing efficient antibacterial materials with no cytotoxicity.

## 3. Experimental section

**3.1 Synthesis of $TiO_2$ nanoparticles** $TiO_2$ nanoparticles were synthesized by the hydrothermal method described before by Burnside *et al*.[261] For this, 20 ml of Titanium isopropoxide (IV) (Acros organics) was added to 36 ml of deionized water and the mixture was stirred for one hour. The resultant product was filtered and washed for three times using deionized water. The solid obtained after filtration was placed into a Teflon-lined titanium autoclave and mixed with 3.9 ml of 0.6 M tetramethylammonium hydroxide (Sigma Aldrich). The reactants were placed in an oven at 120°C for 14 hours. The resultant colloid was centrifuged two times at 10.000 rpm for 10 min to remove aggregates. The

obtained aqueous solution contained a 24 *% wt* of nanoparticles, with a diameter of 24 nm as measured by dynamic light scattering (Malvern Zetasizer). For the fabrication of nanocomposite films, the TiO2 nanoparticles were further dispersed in methanol (0.5 *% wt*.) by ultrasonication.

**3.2 Modification of ZnO nanoparticles.** ZnO nanoparticles with an average diameter of 20 nm (Nanoamor) were silanized to improve their dispersion. For this, 1 gr of ZnO nanoparticles was dispersed in 100 ml of deioneized water by ultrasonication for 10 min. To this, 1 ml of the silane agent 3-aminopropyltriethoxysilane (APTMS, Sigma-Aldrich) was added in the dispersion. The mixture was stirred for 24 hours at 95 $^{0}$C. Then the dispersed nanoparticles were separated from the solvent by centrifugation at 10000 rpm 10 min, followed by washing with methanol to remove the excess of silane. The modified particles were then dried in an oven at 100 $^{o}$C for 24 h in vacuum. For the fabrication of nanocomposites a modified ZnO nanoparticle dispersion was prepared in methanol (0.5 % wt.) by ultrasonication.

**3.3 Fabrication of PMMA bioinspired nanocomposites**. The bioinspired nanocomposites were fabricated on (PMMA). First, PMMA thin films were produced on glass cover slips (18 mm in diameter). The glass cover slips surfaces initially were activated with oxygen plasma (Tepla 600) at 300 W for 5 min to improve the adhesion then, a solution of PMMA (Mw 120.000, Sigma Aldrich) on toluene (7.5 wt %) was spin coated at 1000 rpm for 1 min and formed films annealed at 100 °C. Subsequently, the films were activated with oxygen plasma (Tepla 600) at 50 W for 1 min. Next, $TiO_2$ or ZnO nanoparticle dispersions were spin coated on the surface of the PMMA film. The moth's eye nanostructures from a Ni nickel mold (HT-AR-02, Holotools) were replicated on

PDMS and the replica mold was used for the nanoimprinting processes. On the PMMA-NP film, the moth-eye nanocomposite structures were nanoimprinted at 170 $^{o}$C and 45 bars for 5 min using an Eitre 3 system (Obducat). Smooth nanocomposites for the control experiments where fabricated using a flat slab of PDMS. The nanocomposite substrates were imaged by SEM using an Auriga FIB-SEM system (Zeiss) and AFM using a Multimode 8 system (Bruker).

**3.4 NPs and free Zn and Ti ions released from the nanocomposites determination**.

Nanocomposite imprinted films with a surface of 0.25 cm$^2$were immersed on 2ml of PBS 1X for 7 h. On the solutions, dynamic light scattering and absorbance measurements were performed to detect free NPs released. The concentration of free ions was determined form Inductively couple plasma-mass spectroscopy (ICP-MS) measurements

**3.5 Detection of ROS production**

To verify the production of hydroxyl radicals from the ZnO composite films in the dark fluorescence spectroscopy using terephthalic acid (TA) as the trap agent was employed. TA reacts with •OH and forms 2-hydroxy-terephthalate which fluorescence emission correlates to the hydroxyl radical concentration. In a typical procedure, nanocomposite imprinted films with a surface of 3 cm$^2$ are immersed on 3 ml of TA solution (2mM) and stirred in the dark. At intervals of 1 hour, the fluorescence emission of the solution at excitation wavelength of 312 nm is read at 425 nm

**3.6 Bacteria Culture and Live/Dead Viability assays.** *Escherichia coli* (CECT 516), *Pseudomona aeruginosa* (CECT 4628) (Colección Española de Cultivos

Tipo, Universidad de Valencia), and *Staphylococcus aureus* (RN 4220) were used to assess the antibacterial properties of the topography. The glycerol stocks of bacteria were incubated at 37 °C in 50 ml of Luria-Bertani media (LB) overnight (pH= 7.6). The obtained bacterial suspension was diluted to $OD_{600}$= 0.2. The imprinted PMMA nanocomposites and flat ones for control were placed in 12 well-plates and incubated in static conditions in dark conditions with 2 ml of bacterial suspension for 7 hours for *E.coli* and *S. aureus* and 5 hours for *P. aeruginosa*. After the incubation period, the $TiO_2$ nanocomposites were exposed to UV light with a maximum intensity at 356 nm, i.e. in the UV-A region nonhazardous to bacteria ((UVASPOT 400/T, Honle) providing 80 $mW/cm^2$ of light intensity for 2 min. Then, PMMA substrates were gently rinsed using PBS 1X (Fisher Scientific) and stained (0.13 µl of stain diluted in 1 ml Tris-HCl) using Live/Dead® Baclight$^{TM}$ Viability Kit (Molecular Probes) for 15 min in the dark at room temperature. Lastly, the PMMA substrates were rinsed with PBS 1X and mounted with *Bac*Light mounting oil. The substrates were imaged using a fluorescent microscope (Leica). Live and dead bacteria were counted using the Image J image analysis software by NIH. Four independent trials were run with three replicates of each substrate.

**3.7 Bioinspired nanocomposites-bacteria interaction**. SEM was used to imaging the interaction between bacteria and moth-eye inspired nanocomposites. Prior imaging, all substrates were rinsed with PBS 1X and then fixed with 4% paraformaldehyde (PFA) (Sigma-Aldrich) for 15 min. Subsequently, the substrates were rinsed in increasing gradients of 0, 50, 75, 100% ethanol for 5 min each. These substrates were air dried and sputter-

coated with a thin layer of gold and imaging on an Auriga FIB-SEM system (Zeiss).

**3.8 Cell proliferation assay**. Human keratinocytes (HaCaT) expressing green fluorescent protein (GFP) were cultured in Dulbecco's modified Eagle's medium (DMEM, Biowest) supplemented with 10% fetal bovine serum (Gibco), 1% L-Glutamine (Biowest) and 1% penicillin–streptomycin (Biowest) at 37 °C and 5% $CO_2$ atmosphere.

The growth and proliferation of the HaCaT cells was monitored on Polystyrene (PS) films, smooth and nanostructured PMMA and on smooth and moth-eye patterned nanocomposites. Three independent trials with three replicates of each substrate were run. HaCaT cells were seeded at concentration of 20.000 cells per ml. Cell proliferation was evaluated by a colorimetric method based on the reduction of Resazurin (blue) by the cell metabolic products to resofurin (pink). The solution of Resazurin salt (Alfa Aesar) was prepared at a concentration of 10 µg/ml. Absorbance measurements were taken over a period of 15 days at 570 and 600 nm using a H4 hybrid micro plate reader (BioTek).

**3.9 Cell morphology imaging.** HaCaT cells were seeded and cultured on the different substrates, and collected after 9 days corresponding with the beginning of the log growth phase and on the $15^{th}$ day after the maximum growth level. The cells nuclei were stained using Dapi (Molecular Probes) and the expressed GFP was used for cytoplasm visualization. Prior imaging, the substrates were rinsed with PBS 1X and mounted on FluorSave reagent media (CalBiochem). Images were obtained using a fluorescent microscope (Leica).

Cell morphology was analyzed using the Image J image analysis software by NIH

## 4. Results and Discussion

### 4.1. Moth-eye mimetic nanocomposites film fabrication and characterization

PMMA is a polymer accepted by the United States Food and Drug Administration as biomaterial and it is commonly employed in ocular implants. It is also a commodity plastic used in a wide range of applications. PMMA as thermoplastic, it is readily processable by thermal nanoimprinting, for the fabrication of the antibacterial moth-eye patterned nanocomposites. A new practical process was developed that allowed to create nanocomposites and moth-eye patterns in a single processing step. The fabrication starts by layering a PMMA solution onto a glass substrate by spin coating. Subsequently, a methanol dispersion of the NP (*0.5 %wt*) is spin-coated onto the PMMA film. In the next step, the films are imprinted by a thermal process using a PDMS replica mold patterned with the moth-eye topography. After cooling, the films are de-molded obtaining the polymer moth-eye structures filled with dispersed nanoparticles.

This method allows material saving due to the presence of NPs only in the effective area at the same time that we obtained multifunctionality is obtained derived from the topographical elements that provide superhydrophobic, antireflective or antibacterial properties, and the nanoparticles, which enhance this functionalities and provide new ones as photocalytical effect at the same

time that improve the mechanical resistance of the polymer.[262] The fabrication process is depicted in Figure 4.

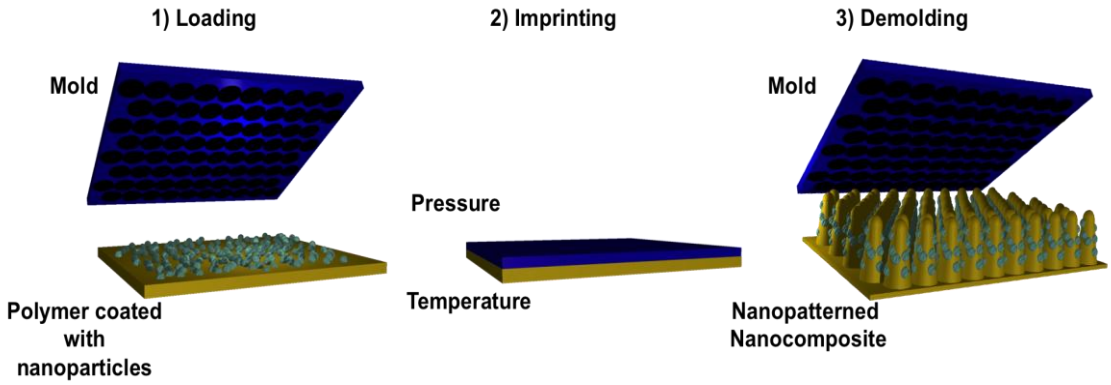


*Figure 4. Fabrication process of nanocomposites by nanoimprinting replication*

The quality of the replication was assessed by SEM and AFM imaging. As displayed in Figure 5A and 5B the SEM and AFM images of the nanoimprinted substrates revealed a topography formed by well-defined nanocones disposed on hexagonal arrangement with the NPs homogeneously distributed and embedded into the nanocones´ matrix. The absence of pronounced agglomerates is indication of a strong interfacial interaction between the organic functional groups of the grafted particles and the matrix leading to intimate filler/matrix contact.

From the AFM images, the height of the topography was determined to have a mean height of 310 nm and a feature width on the cap of 60-80 nm with an aspect ratio of 3.8 and a pitch of 250 nm (Fig 5C). These dimensions are in good agreement with those of the original mold and as such, we can corroborate the good pattern fidelity of the nanocomposite imprinting process.

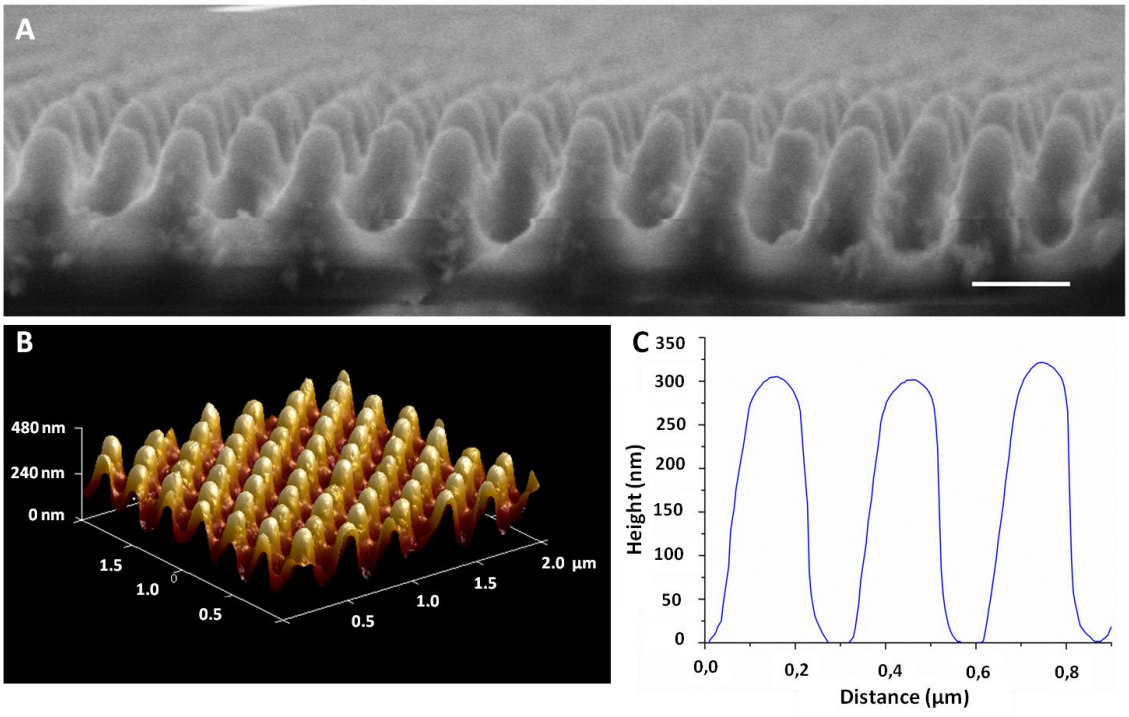


*Figure 5. Moth-eye mimetic nanopatterned nanocomposite images and geometrical characterization by A) SEM, B) three-dimensional AFM imaging and C) AFM cross sectional profile of moth-eye mimetic nanostructures. Scale bar 200 nm.*

### 4.2. Antibacterial effect of moth-eye inspired nanocomposites.

#### 4.2.1. Antibacterial properties of ZnO-PMMA nanocomposites

To determine the bactericidal activity of the ZnO-PMMA films, the viability of *E. coli*, *P. aeruginosa* and *S. aureus* was assessed as model of Gram negative and Gram positive bacteria. After the defined incubation periods of the bacteria suspensions on the substrates, the live and dead bacteria attached on to the surfaces were fluorescently stained and counted from fluorescent microscopy images. Figure 6 shows representative fluorescence microscopy images of the different live-dead bacteria populations observed on the PMMA-ZnO moth-eye imprinted and smooth nanocomposites and smooth and imprinted PMMA used as controls. The results reveal a bactericidal efficiency around 50% for *S.aureus* and *E.coli* and 30% for *P.aeruginosa* of the smooth PMMA-ZnO nanocomposite

surfaces and similar for the case of the moth-eye mimetic topography. However, the population of dead bacteria increased up to 80% percent for *S.aureus* and *E.coli* and 60% for *P.aeruginosa* when bacteria are cultured onto ZnO-nanocomposites moth-eye imprinted topography (Fig 6), underlying the synergistic bactericidal effect of topography and ZnO.

Similar bactericidal efficacy have been reported before for nanocomposites of ZnO NPs and biopolymers[195, 263] and biocompatible polymers such as PMMA[109] and poly lactic acid (PLA).[207]

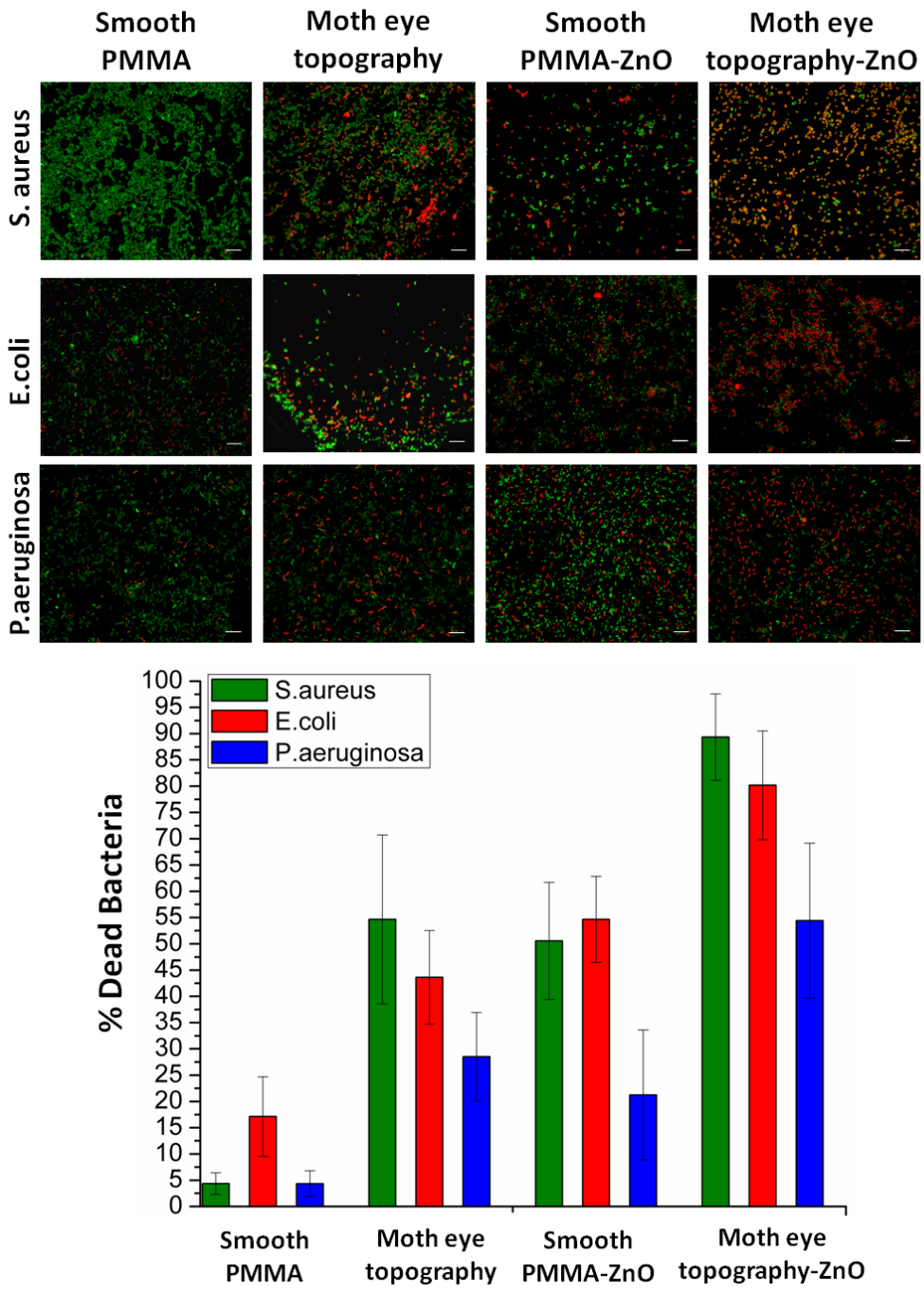


*Figure 6. Bactericidal efficiencies of moth-eye mimetic ZnO nanocomposite topography. Comparative flourescence imaging of live-dead S.aureus, E.coli and P.aeruginosa incubated on smooth PMMA and ZnO-PMMA nanocomposites and on PMMA and ZnO nanocomposite moth-eye topographies. Scale bar 5 µm. Error bars represent standard deviation.*

### 4.2.2 Antibacterial efficacy of the $TiO_2$-PMMA nanocomposite

Similar methodology was employed for the study of the bactericidal efficacy of smooth and moth-eye patterned PMMA-$TiO_2$ nanocomposites. Initially, bacteria cultured onto smooth PMMA and onto the moth-eye mimetic substrates were exposed to UV light for 2 min to account for any bactericidal effect due to the radiation in the absence of $TiO_2$ NPs (Fig. 7)

Likewise, as control, the bactericidal effect of the smooth PMMA-$TiO_2$ composite comparatively to the neat PMMA and in absence of UV light was examined and no evidence of bactericidal action was found (Fig. 8)

Hence, for the case of PMMA-$TiO_2$ composites a UV exposure was performed to induce the photocatalytic bactericidal effect of the NPs.

Figure 7 shows representative fluorescence microscopy images of the different live-dead bacteria populations observed on the PMMA-$TiO_2$ moth-eye imprinted and smooth nanocomposites and smooth and imprinted PMMA substrates used as controls. The results revealed a reduction of the bacterial load about 50% for both of the moth-eye PMMA topography and the smooth PMMA-$TiO_2$ nanocomposite upon UV illumination. However, this percentage increased up to 90% for the three bacterial strains (Fig. 7) for the moth-eye PMMA $TiO_2$ patterned nanocomposite.

These results are in good agreement with previous observations where $TiO_2$ polymer nanocomposites have been shown as effective bactericidal materials.[258, 264, 265] The bactericidal mechanism of $TiO_2$ nanoparticles due to photocatalytic reactions and resulting formation of ROS is well accepted. Exogenous ROS at high concentration can produce lipid peroxidation and protein damage causing destruction of the bacteria membrane that would lead

to the bacterial death.[235] Recent studies have provided further evidence of the mechanism of ROS mediated alteration of gene expression related to regulatory, signaling and growth process photoinduced by TiO2 that ultimately lead bacteria death.[266]

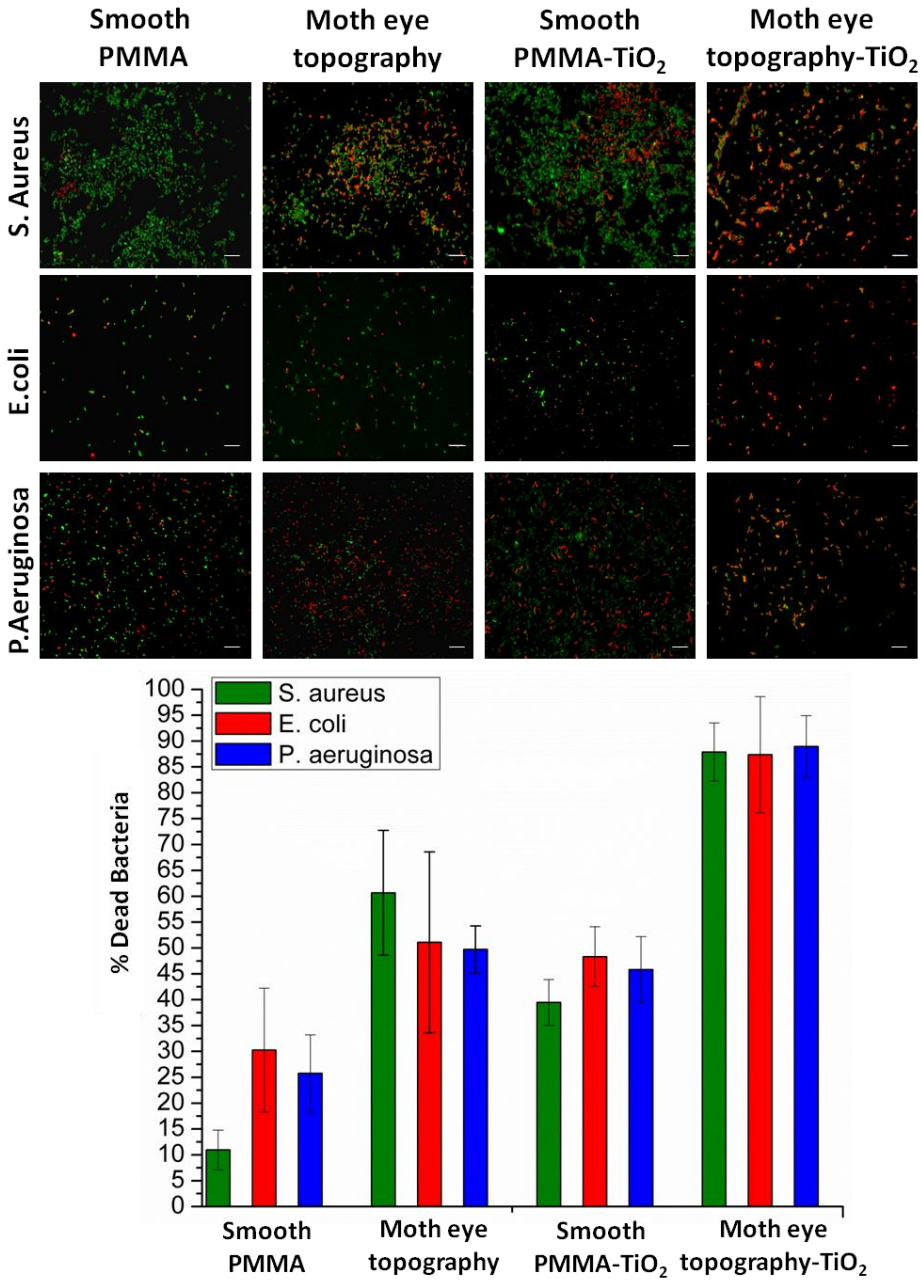


*Figure 7. Bactericidal efficiencies of moth-eye mimetic $TiO_2$ nanocomposite topography. Comparative flourescence imaging of live-dead S.aureus, E.coli and P.aeruginosa incubated on smooth PMMA and nanocomposites and moth-eye mimetic PMMA and $TiO_2$ nanocomposites topography. Scale bar 5 µm. Error bars represent standard deviation.*

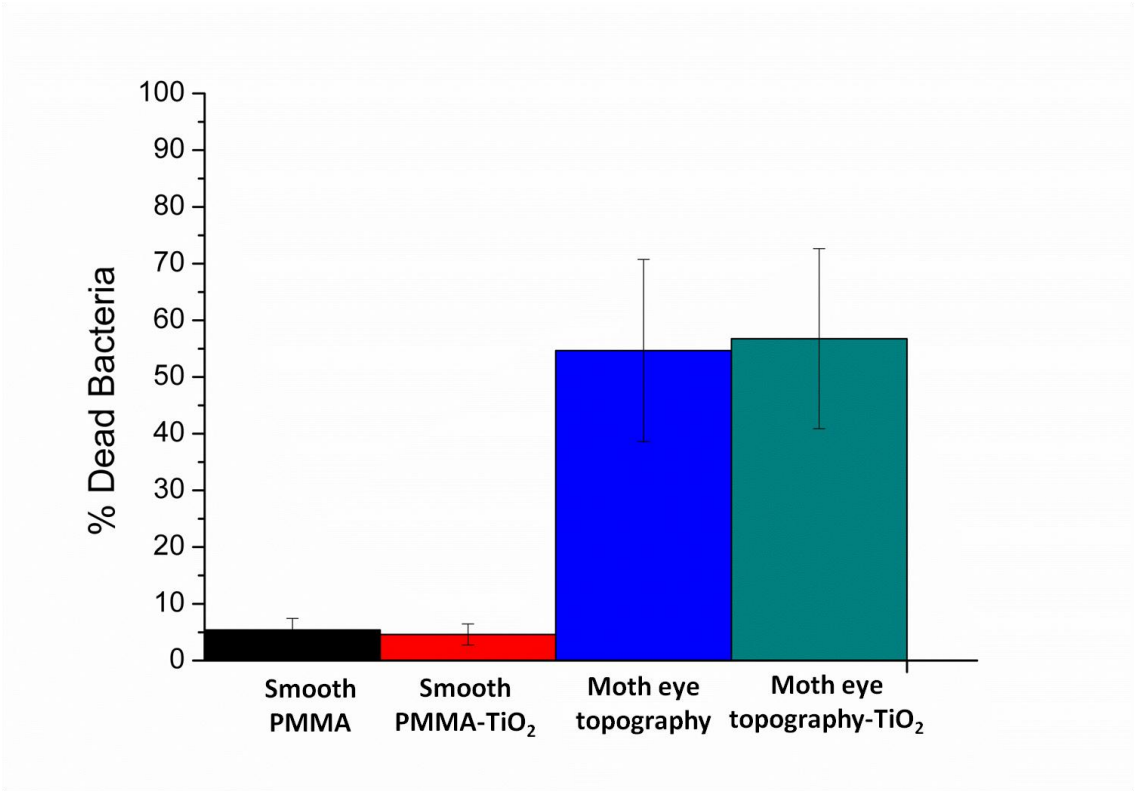


*Figure 8. Bactericidal action against S.aureus of smooth and nanopatterned $TiO_2$ in the absence of UV light exposure.*

### 4.3. Bacteria-surface interaction: Bactericidal mechanism

The morphological observation by SEM imaging of the bacteria attached to the surfaces of smooth and moth-eye patterned nanocomposites in Figure 9 reveals distinct morphological changes as well as membrane damage (red arrows) on the bacteria grown onto the nanocomposite surfaces. In Figure 9E (blue arrow) can also be appreciated the presence of EPS secretion indicating a compromised bacterial membrane integrity caused by the bacteria attachment.[213] On nanopatterned nanocomposites, the dead bacteria showed predominantly a significant loss of morphology, exhibiting the broad and elongated (Fig. 9D) morphology seen before on bactericidal natural or biomimetic topographies.[95, 96] But in this case, some bacteria exhibited in addition rough surface and cavities on their membrane (Fig. 9L) (Fig. 9F), which

are distinctive features of oxidative damage.[264, 267, 268] Thus, from the fluorescence and SEM images, a synergistic action of moth-eye mimetic topography and nanoparticles can be recognized.

The bactericidal effect of polymer nanocomposites have been ascribed to the presence of nanoparticles, and the polymer has been considered as the non-active part.

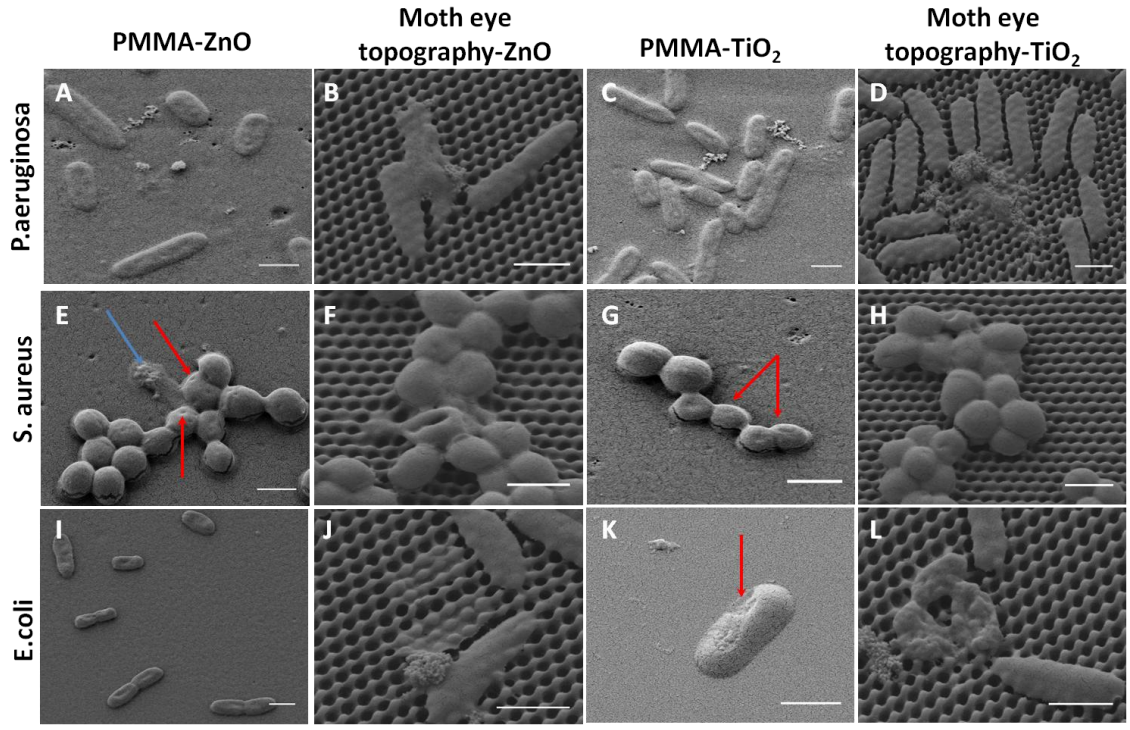


*Figure 9. Comparative SEM imaging of the bacteria-topography interaction of S.aureus, E.coli, and P.aeruginosa attached onto smooth PMMA nanocomposites and moth-eye mimetic nanopatterned nanocomposites. Scale bar 1 µm.*

In the case of ZnO containing materials, a myriad studies have investigated the basis of the antibacterial mechanisms involved including the generation of ROS, the release of zinc ions from ZnO and the penetration and disorganization of the bacterial membrane upon contact with ZnO nanoparticles.[269] However, the bactericidal mechanisms remain till today unclear and still under debate.

In order to get further insight into the dominant biocidal activity that possibly applies in the case of the ZnO patterned nanocomposites of the current study, control experiments were carried out. To exclude a possible bactericidal action from free NPs, release experiments of NPs from the nanocomposite surface to the aqueous media were performed. At the detection limit, no NPs were detected in both ZnO and $TiO_2$ composite imprinted films.

Free $Zn^{2+}$ ions have been postulated to be toxic for bacteria because the interaction between $Zn^{2+}$ ions and bacteria can destroy the membrane charge balance, leading to membrane deformation and ultimately bacteriolysis.

Hereby, the concentration of $Zn^{2+}$ ions dissolved from the ZnO composite imprinted films were determined by ICP-MS. The concentrations of $Zn^{2+}$ ions released from ZnO films were less than 0,5 mg/L (Table 1). This concentration is indeed higher than expected, and possibly comes from partial dissolution of the NPs that are not fully covered by the polymer matrix in the composite. As noted by *Joe et al.,*[270] the solubility of ZnO increases in PBS buffer since the anionic components promote the dissolution. Nonetheless, this concentration is much lower than the concentration reported in previous works where the concentration above 1 mg/L in control experiment did not give rise to any inhibition effects.[231, 271, 272] Therefore, it is believed that there was no significant direct relationship between released $Zn^{2+}$ and the antimicrobial activity of the ZnO nanocomposites.

| Nanocomposite | $Zn^{2+}$ (mg/l) | $Ti^{4+}$ (mg/l) |
|---|---|---|
| Control | 0.01 | 0 |
| Moth eye ZnO nanocomposite | **≤0.5** | 0 |
| Moth eye $TiO_2$ nanocomposite | 0.01 | **0.01** |

*Table 1. Concentration of metal ions released by ZnO and $TiO_2$ in PBS.*

Next, the bactericidal effect due to production of ROS in the dark was examined. Since several authors have demonstrated the production of ROS by ZnO materials in light conditions. *Prasanna et al.,*[273] have put forward the mechanism for ROS generation in the dark. The authors proposed that oxygen present reacts with an electron from the ZnO surface to form a superoxide anion radical ($^{\bullet}O_2^-$). A superoxide in water solvates to form a hydroperoxyl radical ($^{\bullet}HO_2$), and the latter can recombine to form $H_2O_2$. $H_2O_2$ can react with a superoxide anion radical to form a hydroxyl radical ($^{\bullet}OH$) and a hydroxyl ion ($OH^-$). However they indicated that the generation of singlet oxygen ($^1O_2$). is not possible in the dark.[273]

As such, hydrogen peroxide ($H_2O_2$) and hydroxyl radicals ($^{\bullet}OH$) would be the reactive species responsible primarily for the antimicrobial activity of ZnO.

Hence, the production of hydroxyl radicals ($^{\bullet}OH$) in the dark by the ZnO moth-eye patterned nanocomposites was investigated through fluorescence spectroscopy. Figure 10 shows the emission spectra the hydroxyl terephtalic acid formed in the dark. It can be noted that the fluorescence emission increased in small amount but sufficient for detection upon exposure of the films over a period of 7h. Plotting the hydroxyl terephtalic generation kinetics in

Figure 10C, it can be seen that the emission intensity increased linearly, indicating that hydroxyl radicals are produced with time.

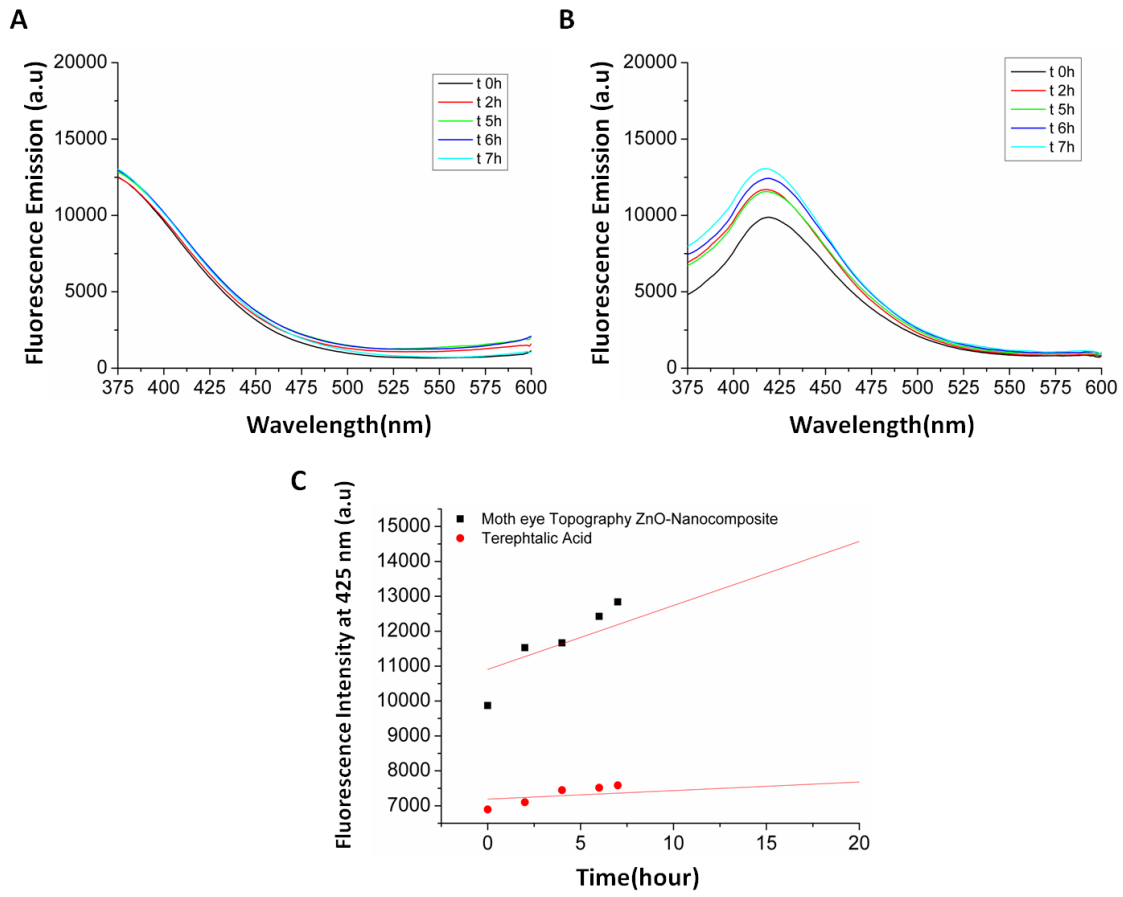


*Figure 10. Detection of ZnO-Moth eye nanocomposites ROS production in dark conditions. Fluorescent spectra of terephtalic acid in the absence (A) and in the presence of ZnO Moth eye nanocomposites (B). Fluorescent intensity of hydroxyl terephtalic acid at 425 nm (C)*

As mentioned above, $TiO_2$ nanocomposites exerted a bactericidal activity only under UV light exposure through the generation of ROS. As reported before,[264, 266] $TiO_2$-polymer composites induce lipid oxidation increasing the membrane fluidity and disruption leading to bacterial death. In the present work, it was found that with only a small amount of $TiO_2$ NPs and 2 min UV exposure, the patterned $TiO_2$ nanocomposites provoked an intensive bactericidal action.

The bactericidal effect of natural and biomimetic surfaces such as cicada wing,[95] dragonfly wing,[96] or gecko skin[99] has been ascribed to mechanical rupture of the bacteria membrane by the nanocone topography as a result of the stretching force exerted onto the membrane of bacteria pursuing a stable attachment.

Hence, as a hypothetical bactericidal mechanism for the moth-eye patterned nanocomposites, it can be postulated that when bacteria attach to these surfaces suffer local stresses due to membrane deformation. And this mechanical local stress produced, increases the susceptibility of the membrane to oxidative damage.

Within this hypothetical context, it can be asserted that the nanopatterned nanocomposites produce a collaborative bactericidal effect, in which the polymer topography plays an active role by compromising the bacterial membrane aiding to the bactericidal action of nanoparticles.

### 4.4. Cellular toxicity of moth-eye patterned ZnO-nanocomposite

An important requirement for antibacterial materials for use in the biomedical field is to be cytocompatible and additionally, promote the host tissue integration. Hence, antibacterial materials should inhibit the bacterial growth without impacting the viability and growth of eukaryotic cells.[274] Alongside with the bactericidal activity, the cytotoxicity towards HaCaT cells of the patterned nanocomposites was assayed. Keratinocytes constitute 90% of the epidermis layer and their proliferation and spread as well as their sensitivity to direct contact with surfaces,[108, 196] make these cells good models to test

cytocompatibility. HaCat cells have been employed before to test the biocompatibility of films[275] and scaffolds.[209, 210]

The attachment and proliferation of HaCaT cell was investigated on of the moth-eye patterned ZnO-nanocomposite surfaces. For this, the cells´ proliferation was monitored during 15 days on smooth and patterned nanocomposites using as controls the smooth and patterned neat PMMA together with polystyrene because of its extensive use for *in vitro* cell culture. The cell growth profile obtained is depicted in Figure 11A, exhibited a typical cell proliferation curve in which cells entered in the log phase on the 9$^{th}$ day and reached the maximum growth level at the 13$^{th}$ day. The cells´ morphology was analyzed from fluorescence images. For this, cells were collected and labeled fluorescent on the 10$^{th}$ and 13$^{th}$ days of growth. Figure 11B shows the results. As can it be appreciated, cells on the 10$^{th}$ day appear forming small colonies typical of the HaCaT cell line, and in the 13$^{th}$ day, it can be observed that cells have reached a confluent state in which the substrates appear completely covered by keratinocytes. Calculation of the cell spread area revealed no obvious differences in spreading for any of the substrates as plotted in Figure 11C. Thus, it appears reasonable to assert that there is no toxic influence derived from nanoparticles or topography on keratinocytes and as such, the nanopatterned ZnO-nanocomposites should be suitable to support cell development.

Hence, the moth eye patterned ZnO-nanocomposite appears to be a promising bactericidal material without cytotoxic effects, which can potentially facilitate the host-tissue integration process of implantable devices or re-absorbable scaffolds for tissue regeneration.

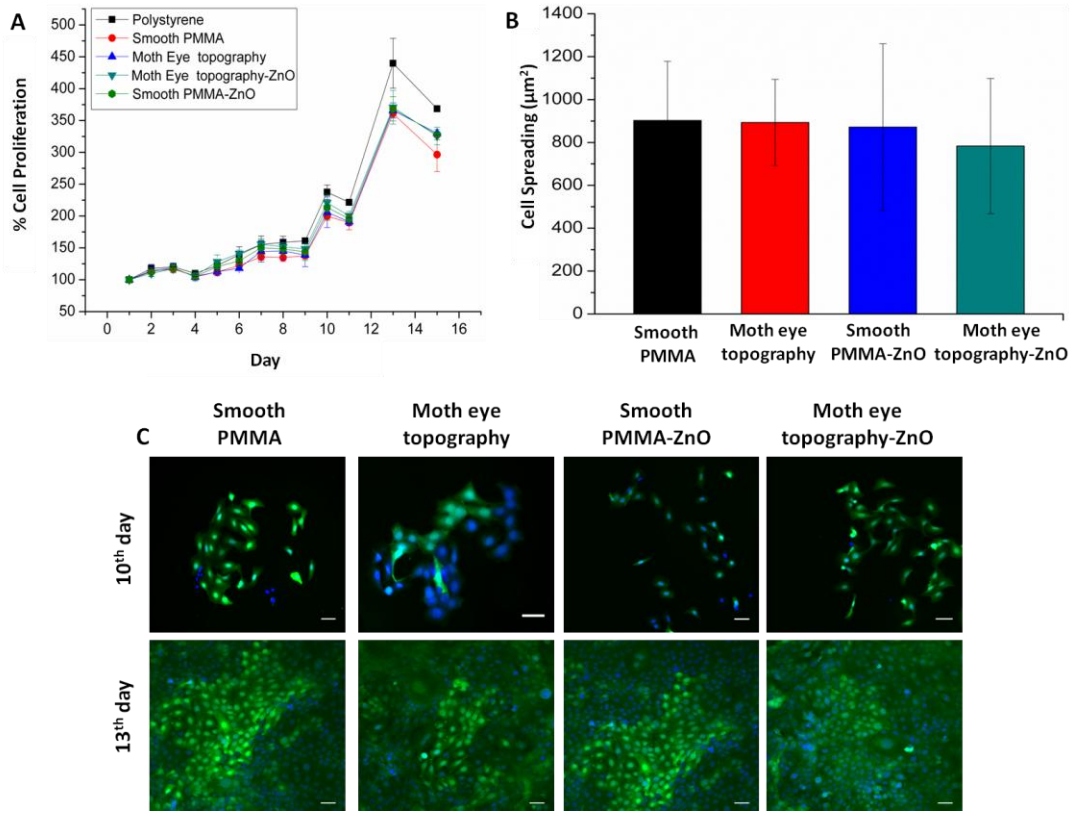


*Figure 11. Biocompatible properties of moth-eye nanocomposite topography. HaCaT proliferation profile on polysterene, smooth PMMA and Moth-eye mimetic nanopatterned nanocomposites (A). Comparison of cellular morphology of HaCaT cells seeded on smooth PMMA and Moth-eye Inspired Topography and smooth and Moth-eye mimetic nanopatterned ZnO nanocomposites. Cell spreading Error bars represent standard deviation(B).Fluorescence Imaging of HaCaT cells after 10$^{th}$ and 13$^{th}$ day of incubation on smooth PMMA, Moth-eye mimetic topography and smooth PMMA and Moth-eye mimetic nanopatterned ZnO nanocomposites. Scale bar 50 µm*

## 5. Conclusion

The development of a new class of bactericidal material based on bioinspired nanopatterned nanocomposites fabricated in one step by a new and practical nanoimprinting process has been presented. The moth-eye patterned nanocomposites demonstrated to be highly efficient bactericidal materials against Gram positive and Gram negative bacteria. The enhanced bactericidal action derived from the synergistic action of mechanical stretching induced by moth-eye nanotopography and the oxidative stress from ROS active ZnO and $TiO_2$ nanoparticles.

The nanopatterned ZnO-PMMA nanocomposites showed in addition good cytocompatibility, with no significant effect on keratinocytes proliferation or morphology.

Thus, this study presents an industry-relevant, scalable technology that may power a new trend for safer-by-design bactericidal products with minimized risks to the environment and human health and with wide potential fields of application not only to the biomedical field but also to consumer care, food packing, furnishing or construction industries.

# Conclusions

This thesis presented examples of micro and nano polymer topographies as effective tools for bacterial and stem cell manipulation. For the fabrication of well-defined micro and nanotopographies advanced nanofabrication techniques were employed largely based on nanoimprinting. This technique provides sub-100 nm resolution with high control of the geometrical and dimensional parameters of the topographical features. Among the nanofabrication techniques, nanoimprinting replication is the most suitable technique providing both high resolution and high throughput polymer nanopatterning. This enables to fabricate at low cost a large number of devices for systematic biological studies of bacterial and cellular behaviors. Moreover, nanoimprinting offers great material processing versatility which allowed for a new processing method to create nanoimprinted nanocomposites surfaces with enhanced bactericidal efficiency.

The results obtained in this thesis lead to the following conclusions:

- Nanoimprinting is a highly practical technique for high throughput and high reproducibility of functional polymer topographies for systematic studies of cell-topography interactions.

- High-aspect-ratio micro and nanopillared topographies fabricated by nanoimprinting are effective tools for in vitro cell function manipulation to probe cellular and nuclear mechanics without the influence of the underlying substrate. HAR polymer topographies can be used to control cellular proliferation, as well as to determine cell morphology and

migration. Moreover HAR micro and nanopillared topographies can be useful tools to study the influence of cell confinement on nuclear mechanics.

- Topographies with size smaller than that of bacteria cells such as the moth-eye mimetic topography are effective bactericidal surfaces against Gram positive and Gram negative bacteria. The bactericidal effect arises from the interaction and adhesion of bacteria to the nanocone like surface resulting on the stretching of the bacterial membrane that eventually leads to the mechanical rupture, release of the intracellular content and bacteria death. Conversely, the moth eye mimetic polymer topography appeared biocompatible towards eukaryotic cells as supported the attachment and proliferation of human keratinocytes. Hence, the moth-eye mimetic topography offers a new bactericidal alternative to antibiotics without causing bacterial resistance while exhibit good properties for host tissue integration. Accordingly, the technology is well poised to be utilized in medical implants.

- Additional functionalities derived by the nature of the nano-fillers employed can be obtained by nanoimprinting on nanocomposites. The incorporation of $TiO_2$ and ZnO nanoparticles onto the moth eye mimetic topography significantly improved the bactericidal properties of the surfaces by a synergistic effect of the moth-eye topography and the photocatalytic nanoparticles, increasing the bactericidal effectiveness up to 90%. At the same time, the moth eye mimetic nanopatterned nanocomposites remained biocompatible towards human keratinocytes.

Hence, bioinspired nanopatterned nanocomposites emerge as a promising technology that provides enhanced synergistic properties with extensive applicability in the biomedical field, food packaging or construction.

# Conclusiones

En esta tesis, se presentan diferentes ejemplos de micro y nanotopografías poliméricas como herramientas para una manipulación eficaz de las funciones biológicas de células madre y bacterias. La fabricación de micro y nanotopografías con estructuras bien definidas requiere el uso de técnicas avanzadas de nanofabricación, que proporcionan un resolución nanométrica y alto control sobre la geometría y dimensiones de los elemento topográficos. De entre todas las técnicas disponibles, la nanoimpresión es la única técnica de alta resolución que permite la fabricación de superficies poliméricas micro y nanoestructuradas a bajo coste. Además, en esta tesis la técnica de nanoimpresión ha sido utilizada para desarrollar un nuevo método de fabricación de nanocompuestos nanoestructurados, consiguiendo nuevos materiales multifuncionales.

Los resultados presentados en esta tesis llevan a las siguientes conclusiones:

- La técnica de nanoimpresión permite la fabricación de superficies poliméricas nanoestructuradas reproducibles, para un estudio sistemático de la interacción célula-superficie.

- Las superficies poliméricas con micro y nanopilares de alta relación de aspecto son herramientas eficaces para la manipulación in vitro de la respuesta nuclear y celular. Estas superficies pueden ser usadas para el control de la proliferación celular, morfología o migración, así como para estudiar la influencia del confinamiento celular sobre el núcleo celular.

- Topografías con un dimensiones inferiores a las de una bacteria, como es el caso de la topografía inspirada en el ojo de la polilla, son superficies bactericidas eficaces contra bacterias Gram positivas y Gram negativas. Su poder bactericida deriva de la interacción de los nanoconos de la superficie con la bacteria cuando esta se adhiere. Esta interacción produce un estrés mecánico sobre la pared bacteriana que provoca la rotura de esta, la liberación del contenido intracelular y la muerte bacteriana. Las propiedades biocompatibles de esta superficie polimérica inspirada en el ojo de la polilla han quedado demostradas mediante el estudio de la proliferación de queratinocitos. Estas superficies aparecen como una alternativa interesante para su uso como materiales antibacterianos para la fabricación de implantes médicos.

- La nanoimpresión se ha presentado como un nuevo método para la fabricación de nanocompuestos nanoestructurados para obtener nuevos materiales multifuncionales. La inclusión de nanopartículas de $TiO_2$ y ZnO dentro de las nanoestructuras del ojo de la polilla aumentan el potencial bactericida de estas superficies debido a la acción sinérgica de la topografía y las nanopartículas que aumentan el porcentaje de muerte bacteriana hasta el 90%. Por otra parte, se ha demostrado que estos materiales mantienen su biocompatibilidad mediante el estudio de la proliferación y morfología de los queratinocitos. Estos nanocompuestos nanoestructurados aparecen como interesantes alternativas para su uso como materiales antibacterianos con aplicación en gran variedad de industrias como la biomédica, en construcción o envasado.

# Bibliography


[1] F. Badique, D. R. Stamov, P. M. Davidson, M. Veuillet, G. Reiter, J.-N. Freund, C. M. Franz, K. Anselme,*Directing nuclear deformation on micropillared surfaces by substrate geometry and cytoskeleton organization*, *Biomaterials* **2013**, 34, 2991.

[2] W. T. Su, Y. F. Liao, C. Y. Lin, L. T. Li,*Micropillar substrate influences the cellular attachment and laminin expression*, *Journal of biomedical materials research Part A* **2010**, 93, 1463.

[3] D. Y. Fozdar, J. Y. Lee, C. E. Schmidt, S. Chen,*Hippocampal neurons respond uniquely to topographies of various sizes and shapes*, *Biofabrication* **2010**, 2, 035005.

[4] S. Bonde, N. Buch-Månson, K. R. Rostgaard, T. K. Andersen, T. Berthing, K. L. Martinez,*Exploring arrays of vertical one-dimensional nanostructures for cellular investigations*, *Nanot* **2014**, 25, 362001.

[5] V. Vogel,*Mechanotransduction involving multimodular proteins: converting force into biochemical signals*, *Annu. Rev. Biophys. Biomol. Struct.* **2006**, 35, 459.

[6] V. Vogel, M. Sheetz,*Local force and geometry sensing regulate cell functions*, *Nat. Rev. Mol. Cell Biol.* **2006**, 7, 265.

[7] S.-Y. Tee, A. R. Bausch, P. A. Janmey,*The mechanical cell*, *Curr. Biol.* **2009**, 19, R745.

[8] Y. Shao, J. Fu,*Integrated micro/nanoengineered functional biomaterials for cell mechanics and mechanobiology: a materials perspective*, *Adv. Mater.* **2014**, 26, 1494.

[9] F. Lautenschläger, M. Piel,*Microfabricated devices for cell biology: all for one and one for all*, *Curr. Opin. Cell Biol.* **2013**, 25, 116.

[10] J. Castillo, M. Dimaki, W. E. Svendsen,*Manipulation of biological samples using micro and nano techniques*, *Integrative Biology* **2009**, 1, 30.

[11] M. Ochsner, M. R. Dusseiller, H. M. Grandin, S. Luna-Morris, M. Textor, V. Vogel, M. L. Smith,*Micro-well arrays for 3D shape control and high resolution analysis of single cells*, *LChip* **2007**, 7, 1074.

[12] M. Ochsner, M. Textor, V. Vogel, M. L. Smith,*Dimensionality controls cytoskeleton assembly and metabolism of fibroblast cells in response to rigidity and shape*, *PLoS One* **2010**, 5, e9445.

[13] J. Albuschies, V. Vogel,*The role of filopodia in the recognition of nanotopographies*, *Sci. Rep.* **2013**, 3.

[14] L. Rizzello, R. Cingolani, P. P. Pompa,*Nanotechnology tools for antibacterial materials*, *Nanomedicine* **2013**, 8, 807.

[15] J. Hu, A. A. Gondarenko, A. P. Dang, K. T. Bashour, R. S. O'Connor, S. Lee, A. Liapis, S. Ghassemi, M. C. Milone, M. P. Sheetz,*High-Throughput Mechanobiology Screening Platform Using Micro-and Nanotopography*, *Nano Lett.* **2016**, 16, 2198.

[16] D. H. Stones, A. M. Krachler,*Against the tide: the role of bacterial adhesion in host colonization*, *Biochem. Soc. Trans.* **2016**, 44, 1571.

[17] W. A. El-Said, T.-H. Kim, K.-B. Lee, J.-W. Choi,*Nanopatterned Surfaces for Stem-Cell Engineering*, *Stem Cell Nanoengineering* **2014**, 99.

[18] B. Geiger, A. Bershadsky, R. Pankov, K. M. Yamada,*Transmembrane crosstalk between the extracellular matrix and the cytoskeleton*, *Nature reviews Molecular cell biology* **2001**, 2, 793.
[19] G. R. Fedorchak, A. Kaminski, J. Lammerding,*Cellular mechanosensing: getting to the nucleus of it all*, *PBMB* **2014**, 115, 76.
[20] M. A. Wozniak, C. S. Chen,*Mechanotransduction in development: a growing role for contractility*, *Nature reviews Molecular cell biology* **2009**, 10, 34.
[21] D. E. Jaalouk, J. Lammerding,*Mechanotransduction gone awry*, *Nature reviews Molecular cell biology* **2009**, 10, 63.
[22] W. L. Murphy, T. C. McDevitt, A. J. Engler,*Materials as stem cell regulators*, *Nature materials* **2014**, 13, 547.
[23] C. Bettinger, J. T. Borenstein, S. L. Tao, *Microfluidic cell culture systems*, William Andrew, **2012**.
[24] P. Russell, J. Z. Gasiorowski, P. F. Nealy, C. J. Murphy,*Response of human trabecular meshwork cells to topographic cues on the nanoscale level*, *Invest. Ophthalmol. Vis. Sci.* **2008**, 49, 629.
[25] N. W. Karuri, S. Liliensiek, A. I. Teixeira, G. Abrams, S. Campbell, P. F. Nealey, C. J. Murphy,*Biological length scale topography enhances cell-substratum adhesion of human corneal epithelial cells*, *J. Cell Sci.* **2004**, 117, 3153.
[26] A. I. Teixeira, G. A. McKie, J. D. Foley, P. J. Bertics, P. F. Nealey, C. J. Murphy,*The effect of environmental factors on the response of human corneal epithelial cells to nanoscale substrate topography*, *Biomaterials* **2006**, 27, 3945.
[27] S. Ankam, M. Suryana, L. Y. Chan, A. A. K. Moe, B. K. K. Teo, J. B. K. Law, M. P. Sheetz, H. Y. Low, E. K. F. Yim,*Substrate topography and size determine the fate of human embryonic stem cells to neuronal or glial lineage*, *Acta Biomater.* **2013**, 9, 4535.
[28] S. J. Liliensiek, S. Campbell, P. F. Nealey, C. J. Murphy,*The scale of substratum topographic features modulates proliferation of corneal epithelial cells and corneal fibroblasts*, *Journal of biomedical materials research Part A* **2006**, 79, 185.
[29] C. Le Clainche, M.-F. Carlier,*Regulation of actin assembly associated with protrusion and adhesion in cell migration*, *Physiol. Rev.* **2008**, 88, 489.
[30] G. Giannone, R.-M. Mège, O. Thoumine,*Multi-level molecular clutches in motile cell processes*, *Trends Cell Biol.* **2009**, 19, 475.
[31] G. Jiang, G. Giannone, D. R. Critchley, E. Fukumoto, M. P. Sheetz,*Two-piconewton slip bond between fibronectin and the cytoskeleton depends on talin*, *Nature* **2003**, 424, 334.
[32] B. Geiger, J. P. Spatz, A. D. Bershadsky,*Environmental sensing through focal adhesions*, *Nature reviews Molecular cell biology* **2009**, 10, 21.
[33] J. Fu, Y.-K. Wang, M. T. Yang, R. A. Desai, X. Yu, Z. Liu, C. S. Chen,*Mechanical regulation of cell function with geometrically modulated elastomeric substrates*, *Nat. Methods* **2010**, 7, 733.
[34] M. Ghibaudo, J.-M. Di Meglio, P. Hersen, B. Ladoux,*Mechanics of cell spreading within 3D-micropatterned environments*, *LChip* **2011**, 11, 805.
[35] Z. Jahed, S. Molladavoodi, B. B. Seo, M. Gorbet, T. Y. Tsui, M. R. Mofrad,*Cell responses to metallic nanostructure arrays with complex geometries*, *Biomaterials* **2014**, 35, 9363.

[36] J. Lee, B. S. Kang, B. Hicks, T. F. Chancellor, B. H. Chu, H.-T. Wang, B. G. Keselowsky, F. Ren, T. P. Lele,*The control of cell adhesion and viability by zinc oxide nanorods*, *Biomaterials* **2008**, 29, 3743.
[37] E. Luong-Van, I. Rodriguez, H. Y. Low, N. Elmouelhi, B. Lowenhaupt, S. Natarajan, C. T. Lim, R. Prajapati, M. Vyakarnam, K. Cooper,*Review: Micro- and nanostructured surface engineering for biomedical applications*, *JMatR* **2013**, 28, 165.
[38] L. Hanson, Z. C. Lin, C. Xie, Y. Cui, B. Cui,*Characterization of the cell–nanopillar interface by transmission electron microscopy*, *Nano Lett.* **2012**, 12, 5815.
[39] W. Chen, L. G. Villa-Diaz, Y. Sun, S. Weng, J. K. Kim, R. H. W. Lam, L. Han, R. Fan, P. H. Krebsbach, J. Fu,*Nanotopography Influences Adhesion, Spreading, and Self-Renewal of Human Embryonic Stem Cells*, *ACS Nano* **2012**, 6, 4094.
[40] M. A. Kafi, W. A. El-Said, T.-H. Kim, J.-W. Choi,*Cell adhesion, spreading, and proliferation on surface functionalized with RGD nanopillar arrays*, *Biomaterials* **2012**, 33, 731.
[41] S. Bonde, T. Berthing, M. H. Madsen, T. K. Andersen, N. Buch-Månson, L. Guo, X. Li, F. Badique, K. Anselme, J. Nygård,*Tuning InAs Nanowire Density for HEK293 Cell Viability, Adhesion, and Morphology: Perspectives for Nanowire-Based Biosensors*, *ACS applied materials & interfaces* **2013**, 5, 10510.
[42] M. A. Bucaro, Y. Vasquez, B. D. Hatton, J. Aizenberg,*Fine-tuning the degree of stem cell polarization and alignment on ordered arrays of high-aspect-ratio nanopillars*, *ACS nano* **2012**, 6, 6222.
[43] S.-W. Kuo, H.-I. Lin, J. H.-C. Ho, Y.-R. V. Shih, H.-F. Chen, T.-J. Yen, O. K. Lee,*Regulation of the fate of human mesenchymal stem cells by mechanical and stereo-topographical cues provided by silicon nanowires*, *Biomaterials* **2012**, 33, 5013.
[44] J. Padmanabhan, E. R. Kinser, M. A. Stalter, C. Duncan-Lewis, J. L. Balestrini, A. J. Sawyer, J. Schroers, T. R. Kyriakides,*Engineering cellular response using nanopatterned bulk metallic glass*, *ACS nano* **2014**, 8, 4366.
[45] K. S. Beckwith, S. P. Cooil, J. W. Wells, P. Sikorski,*Tunable high aspect ratio polymer nanostructures for cell interfaces*, *Nanoscale* **2015**, 7, 8438.
[46] Z. Pan, C. Yan, R. Peng, Y. Zhao, Y. He, J. Ding,*Control of cell nucleus shapes via micropillar patterns*, *Biomaterials* **2012**, 33, 1730.
[47] T. J. Kirby, J. Lammerding,*Cell mechanotransduction: Stretch to express*, *Nat Mater* **2016**, 15, 1227.
[48] P. M. Davidson, H. Özçelik, V. Hasirci, G. Reiter, K. Anselme,*Microstructured Surfaces Cause Severe but Non ‐ Detrimental Deformation of the Cell Nucleus*, *Adv. Mater.* **2009**, 21, 3586.
[49] C. R. Jacobs, H. Huang, R. Y. Kwon, *Introduction to cell mechanics and mechanobiology*, Garland Science, **2012**.
[50] X. Cao, E. Moeendarbary, P. Isermann, P. M. Davidson, X. Wang, M. B. Chen, A. K. Burkart, J. Lammerding, R. D. Kamm, V. B. Shenoy,*A Chemomechanical Model for Nuclear Morphology and Stresses during Cell Transendothelial Migration*, *BpJ* **2016**, 111, 1541.
[51] R. Horwitz, D. Webb,*Cell migration*, *Curr. Biol.* **2003**, 13, R756.
[52] R. J. Petrie, A. D. Doyle, K. M. Yamada,*Random versus directionally persistent cell migration*, *Nature reviews Molecular cell biology* **2009**, 10, 538.

[53] G. Charras, E. Sahai,*Physical influences of the extracellular environment on cell migration*, *Nature Reviews Molecular Cell Biology* **2014**, 15, 813.
[54] M. Ventre, C. F. Natale, C. Rianna, P. A. Netti,*Topographic cell instructive patterns to control cell adhesion, polarization and migration*, *Journal of The Royal Society Interface* **2014**, 11, 20140687.
[55] M. Ventre, P. A. Netti,*Engineering cell instructive materials to control cell fate and functions through material cues and surface patterning*, *ACS applied materials & interfaces* **2016**, 8, 14896.
[56] E. I. Liang, E. J. Mah, A. F. Yee, M. A. Digman,*Correlation of Focal Adhesion Assembly and Disassembly with Cell Migration on Nanotopography*, *Integrative Biology* **2017**.
[57] K. I. Anderson, Y.-L. Wang, J. V. Small,*Coordination of protrusion and translocation of the keratocyte involves rolling of the cell body*, *J. Cell Biol.* **1996**, 134, 1209.
[58] M. T. Yang, J. Fu, Y.-K. Wang, R. A. Desai, C. S. Chen,*Assaying stem cell mechanobiology on microfabricated elastomeric substrates with geometrically modulated rigidity*, *Nat. Protoc.* **2011**, 6, 187.
[59] A. Saez, E. Anon, M. Ghibaudo, O. Du Roure, J. M. Di Meglio, P. Hersen, P. Silberzan, A. Buguin, B. Ladoux,*Traction forces exerted by epithelial cell sheets*, *J. Phys.: Condens. Matter* **2010**, 22, 194119.
[60] O. Du Roure, A. Saez, A. Buguin, R. H. Austin, P. Chavrier, P. Siberzan, B. Ladoux,*Force mapping in epithelial cell migration*, *Proc. Natl. Acad. Sci. U. S. A.* **2005**, 102, 2390.
[61] R. J. Pelham, Y.-l. Wang,*High resolution detection of mechanical forces exerted by locomoting fibroblasts on the substrate*, *Mol. Biol. Cell* **1999**, 10, 935.
[62] U. S. Schwarz, N. Q. Balaban, D. Riveline, A. Bershadsky, B. Geiger, S. A. Safran,*Calculation of forces at focal adhesions from elastic substrate data: the effect of localized force and the need for regularization*, *BpJ* **2002**, 83, 1380.
[63] D. A. Lee, M. M. Knight, J. J. Campbell, D. L. Bader,*Stem cell mechanobiology*, *J. Cell. Biochem.* **2011**, 112, 1.
[64] M. A. Conti, S. Even-Ram, C. Liu, K. M. Yamada, R. S. Adelstein,*Defects in cell adhesion and the visceral endoderm following ablation of nonmuscle myosin heavy chain II-A in mice*, *J. Biol. Chem.* **2004**, 279, 41263.
[65] A. J. Engler, S. Sen, H. L. Sweeney, D. E. Discher,*Matrix elasticity directs stem cell lineage specification*, *Cell* **2006**, 126, 677.
[66] K. Kurpinski, J. Chu, C. Hashi, S. Li,*Anisotropic mechanosensing by mesenchymal stem cells*, *Proceedings of the National Academy of Sciences* **2006**, 103, 16095.
[67] A. Ranga, S. Gobaa, Y. Okawa, K. Mosiewicz, A. Negro, M. P. Lutolf,*3D niche microarrays for systems-level analyses of cell fate*, *Nature communications* **2014**, 5.
[68] C. H. Rasmussen, P. M. Reynolds, D. R. Petersen, M. Hansson, R. M. McMeeking, M. Dufva, N. Gadegaard,*Enhanced Differentiation of Human Embryonic Stem Cells Toward Definitive Endoderm on Ultrahigh Aspect Ratio Nanopillars*, *Adv. Funct. Mater.* **2016**, 26.
[69] M. J. Dalby, N. Gadegaard, R. Tare, A. Andar, M. O. Riehle, P. Herzyk, C. D. Wilkinson, R. O. Oreffo,*The control of human mesenchymal cell*

*differentiation using nanoscale symmetry and disorder*, *Nature materials* **2007**, 6, 997.
[70] R. J. McMurray, N. Gadegaard, P. M. Tsimbouri, K. V. Burgess, L. E. McNamara, R. Tare, K. Murawski, E. Kingham, R. O. Oreffo, M. J. Dalby,*Nanoscale surfaces for the long-term maintenance of mesenchymal stem cell phenotype and multipotency*, *Nature materials* **2011**, 10, 637.
[71] K. A. Kilian, B. Bugarija, B. T. Lahn, M. Mrksich,*Geometric cues for directing the differentiation of mesenchymal stem cells*, *Proceedings of the National Academy of Sciences* **2010**, 107, 4872.
[72] M. C. van Loosdrecht, J. Lyklema, W. Norde, A. Zehnder,*Influence of interfaces on microbial activity*, *Microbiol. Rev.* **1990**, 54, 75.
[73] M. Fletcher,*Bacterial biofilms and biofouling*, *Curr. Opin. Biotechnol.* **1994**, 5, 302.
[74] H. J. Busscher, H. C. van der Mei,*How do bacteria know they are on a surface and regulate their response to an adhering state?*, *PLoS Pathog.* **2012**, 8, e1002440.
[75] A. W. Decho, Multidisciplinary Digital Publishing Institute, 2013.
[76] A. K. Harapanahalli, J. A. Younes, E. Allan, H. C. van der Mei, H. J. Busscher,*Chemical signals and mechanosensing in bacterial responses to their environment*, *PLoS Pathog.* **2015**, 11, e1005057.
[77] K. L. Van Dellen, L. Houot, P. I. Watnick,*Genetic analysis of Vibrio cholerae monolayer formation reveals a key role for ΔΨ in the transition to permanent attachment*, *J. Bacteriol.* **2008**, 190, 8185.
[78] C. J. Gode‐Potratz, R. J. Kustusch, P. J. Breheny, D. S. Weiss, L. L. McCarter,*Surface sensing in Vibrio parahaemolyticus triggers a programme of gene expression that promotes colonization and virulence*, *Mol. Microbiol.* **2011**, 79, 240.
[79] A. K. Harapanahalli, Y. Chen, J. Li, H. J. Busscher, H. C. van der Mei,*Influence of adhesion force on icaA and cidA gene expression and production of matrix components in Staphylococcus aureus biofilms*, *Appl. Environ. Microbiol.* **2015**, 81, 3369.
[80] E. Perozo, A. Kloda, D. M. Cortes, B. Martinac,*Physical principles underlying the transduction of bilayer deformation forces during mechanosensitive channel gating*, *Nat. Struct. Mol. Biol.* **2002**, 9, 696.
[81] A. Persat,*Bacterial mechanotransduction*, *Curr. Opin. Microbiol.* **2017**, 36, 1.
[82] K. Otto, T. J. Silhavy,*Surface sensing and adhesion of Escherichia coli controlled by the Cpx-signaling pathway*, *Proceedings of the National Academy of Sciences* **2002**, 99, 2287.
[83] S. Hou, H. Gu, C. Smith, D. Ren,*Microtopographic patterns affect Escherichia coli biofilm formation on poly (dimethylsiloxane) surfaces*, *Langmuir* **2011**, 27, 2686.
[84] A. Z. Komaromy, S. Li, H. Zhang, D. V. Nicolau, R. I. Boysen, M. T. W. Hearn,*Arrays of nano-structured surfaces to probe the adhesion and viability of bacteria*, *MiEng* **2012**, 91, 39.
[85] A. I. Hochbaum, J. Aizenberg,*Bacteria pattern spontaneously on periodic nanostructure arrays*, *Nano Lett.* **2010**, 10, 3717.
[86] D. P. Bakker, H. J. Busscher, J. van Zanten, J. de Vries, J. W. Klijnstra, H. C. van der Mei,*Multiple linear regression analysis of bacterial deposition to*

*polyurethane coatings after conditioning film formation in the marine environment*, *Microbiology* **2004**, 150, 1779.

[87] A. Epstein, A. Hochbaum, P. Kim, J. Aizenberg,*Control of bacterial biofilm growth on surfaces by nanostructural mechanics and geometry*, *Nanot* **2011**, 22, 494007.

[88] C. Díaz, P. L. Schilardi, R. C. Salvarezza, M. F. L. de Mele,*Have flagella a preferred orientation during early stages of biofilm formation?: AFM study using patterned substrates*, *Colloids Surf. B. Biointerfaces* **2011**, 82, 536.

[89] H. Tang, T. Cao, X. Liang, A. Wang, S. O. Salley, J. McAllister, K. Y. Ng,*Influence of silicone surface roughness and hydrophobicity on adhesion and colonization of Staphylococcus epidermidis*, *Journal of Biomedical Materials Research Part A* **2009**, 88, 454.

[90] C. Sousa, P. Teixeira, R. Oliveira,*Influence of surface properties on the adhesion of Staphylococcus epidermidis to acrylic and silicone*, *International journal of biomaterials* **2009**, 2009.

[91] N. Mitik‐Dineva, J. Wang, R. C. Mocanasu, P. R. Stoddart, R. J. Crawford, E. P. Ivanova,*Impact of nano‐topography on bacterial attachment*, *Biotechnology Journal* **2008**, 3, 536.

[92] N. Mitik-Dineva, J. Wang, V. K. Truong, P. R. Stoddart, F. Malherbe, R. J. Crawford, E. P. Ivanova,*Differences in colonisation of five marine bacteria on two types of glass surfaces*, *Biofouling* **2009**, 25, 621.

[93] V. K. Truong, R. Lapovok, Y. S. Estrin, S. Rundell, J. Y. Wang, C. J. Fluke, R. J. Crawford, E. P. Ivanova,*The influence of nano-scale surface roughness on bacterial adhesion to ultrafine-grained titanium*, *Biomaterials* **2010**, 31, 3674.

[94] E. P. Ivanova, V. K. Truong, H. K. Webb, V. A. Baulin, J. Y. Wang, N. Mohammodi, F. Wang, C. Fluke, R. J. Crawford,*Differential attraction and repulsion of Staphylococcus aureus and Pseudomonas aeruginosa on molecularly smooth titanium films*, *Sci. Rep.* **2011**, 1, 165.

[95] J. Hasan, H. K. Webb, V. K. Truong, S. Pogodin, V. A. Baulin, G. S. Watson, J. A. Watson, R. J. Crawford, E. P. Ivanova,*Selective bactericidal activity of nanopatterned superhydrophobic cicada Psaltoda claripennis wing surfaces*, *Appl. Microbiol. Biotechnol.* **2013**, 97, 9257.

[96] D. E. Mainwaring, S. H. Nguyen, H. Webb, T. Jakubov, M. Tobin, R. N. Lamb, A. H.-F. Wu, R. Marchant, R. J. Crawford, E. P. Ivanova,*The nature of inherent bactericidal activity: insights from the nanotopology of three species of dragonfly*, *Nanoscale* **2016**, 8, 6527.

[97] G. S. Watson, D. W. Green, L. Schwarzkopf, X. Li, B. W. Cribb, S. Myhra, J. A. Watson,*A gecko skin micro/nano structure – A low adhesion, superhydrophobic, anti-wetting, self-cleaning, biocompatible, antibacterial surface*, *Acta Biomater.* **2015**, 21, 109.

[98] R. M. May, C. M. Magin, E. E. Mann, M. C. Drinker, J. C. Fraser, C. A. Siedlecki, A. B. Brennan, S. T. Reddy,*An engineered micropattern to reduce bacterial colonization, platelet adhesion and fibrin sheath formation for improved biocompatibility of central venous catheters*, *Clinical and translational medicine* **2015**, 4, 9.

[99] X. Li, G. Cheung, G. S. Watson, J. A. Watson, S. Lin, L. Schwarzkopf, D. Green,*The nanotipped hairs of gecko skin and biotemplated replicas impair*

*and/or kill pathogenic bacteria with high efficiency*, *Nanoscale* **2016**, 8, 18860.
[100] T. Diu, N. Faruqui, T. Sjöström, B. Lamarre, H. F. Jenkinson, B. Su, M. G. Ryadnov,*Cicada-inspired cell-instructive nanopatterned arrays*, *Sci. Rep.* **2014**, 4.
[101] C. D. Bandara, S. Singh, I. O. Afara, A. Wolff, T. Tesfamichael, K. Ostrikov, A. Oloyede,*Bactericidal Effects of Natural Nanotopography of Dragonfly Wing on Escherichia coli*, *ACS Applied Materials & Interfaces* **2017**, 9, 6746.
[102] E. P. Ivanova, J. Hasan, H. K. Webb, V. K. Truong, G. S. Watson, J. A. Watson, V. A. Baulin, S. Pogodin, J. Y. Wang, M. J. Tobin,*Natural bactericidal surfaces: mechanical rupture of Pseudomonas aeruginosa cells by cicada wings*, *Small* **2012**, 8, 2489.
[103] T. Qian, Y. Wang,*Micro/nano-fabrication technologies for cell biology*, *Med Biol Eng Comput* **2010**, 48, 1023.
[104] W. Zhu, X. Ma, M. Gou, D. Mei, K. Zhang, S. Chen,*3D printing of functional biomaterials for tissue engineering*, *Curr. Opin. Biotechnol.* **2016**, 40, 103.
[105] J. A. Matthews, G. E. Wnek, D. G. Simpson, G. L. Bowlin,*Electrospinning of collagen nanofibers*, *Biomacromolecules* **2002**, 3, 232.
[106] B.-M. Min, G. Lee, S. H. Kim, Y. S. Nam, T. S. Lee, W. H. Park,*Electrospinning of silk fibroin nanofibers and its effect on the adhesion and spreading of normal human keratinocytes and fibroblasts in vitro*, *Biomaterials* **2004**, 25, 1289.
[107] T. Sun, D. Norton, R. J. McKean, J. W. Haycock, A. J. Ryan, S. MacNeil,*Development of a 3D cell culture system for investigating cell interactions with electrospun fibers*, *Biotechnol. Bioeng.* **2007**, 97, 1318.
[108] K. S. Rho, L. Jeong, G. Lee, B.-M. Seo, Y. J. Park, S.-D. Hong, S. Roh, J. J. Cho, W. H. Park, B.-M. Min,*Electrospinning of collagen nanofibers: effects on the behavior of normal human keratinocytes and early-stage wound healing*, *Biomaterials* **2006**, 27, 1452.
[109] S. H. Hwang, J. Song, Y. Jung, O. Y. Kweon, H. Song, J. Jang,*Electrospun ZnO/TiO 2 composite nanofibers as a bactericidal agent*, *ChCom* **2011**, 47, 9164.
[110] C. L. Ventola,*Medical applications for 3D printing: current and projected uses*, *Pt* **2014**, 39, 704.
[111] R. L. Truby, J. A. Lewis,*Printing soft matter in three dimensions*, *Nature* **2016**, 540, 371.
[112] P. E. Petrochenko, J. Torgersen, P. Gruber, L. A. Hicks, J. Zheng, G. Kumar, R. J. Narayan, P. L. Goering, R. Liska, J. Stampfl,*Laser 3D printing with sub‐microscale resolution of porous elastomeric scaffolds for supporting human bone stem cells*, *Advanced healthcare materials* **2015**, 4, 739.
[113] H. N. Chia, B. M. Wu,*Recent advances in 3D printing of biomaterials*, *J. Biol. Eng.* **2015**, 9, 4.
[114] E. Sapountzi, M. Braiek, C. Farre, M. Arab, J.-F. Chateaux, N. Jaffrezic-Renault, F. Lagarde,*One-step fabrication of electrospun photo-cross-linkable polymer nanofibers incorporating multiwall carbon nanotubes and enzyme for biosensing*, *JElS* **2015**, 162, B275.
[115] M. A. McCord, M. J. Rooks, presented at SPIE, Bellingham **2000**.
[116] E. Lääniläinen,*Soft Lithography for Surface Micropatterning*, *MS, Helsinki University of Technology* **2006**.
[117] Y. Xia, G. M. Whitesides,*Soft lithography*, *AnRMS* **1998**, 28, 153.

[118] G. M. Whitesides, E. Ostuni, S. Takayama, X. Jiang, D. E. Ingber,*Soft lithography in biology and biochemistry*, *Annu. Rev. Biomed. Eng.* **2001**, 3, 335.
[119] D. Qin, Y. Xia, G. M. Whitesides,*Soft lithography for micro-and nanoscale patterning*, *Nat. Protoc.* **2010**, 5, 491.
[120] J. Hyun, H. Ma, Z. Zhang, T. P. Beebe Jr, A. Chilkoti,*Universal route to cell micropatterning using an amphiphilic comb polymer*, *Adv. Mater.* **2003**, 15, 576.
[121] H. Ma, J. Hyun, Z. Zhang, T. P. Beebe, A. Chilkoti,*Fabrication of biofunctionalized Quasi‐Three‐Dimensional microstructures of a nonfouling comb polymer using soft lithography*, *Adv. Funct. Mater.* **2005**, 15, 529.
[122] A. Kumar, G. M. Whitesides,*Features of gold having micrometer to centimeter dimensions can be formed through a combination of stamping with an elastomeric stamp and an alkanethiol "ink"followed by chemical etching*, *ApPhL* **1993**, 63, 2002.
[123] T. Kaufmann, B. J. Ravoo,*Stamps, inks and substrates: polymers in microcontact printing*, *Polymer Chemistry* **2010**, 1, 371.
[124] M. Mrksich, G. M. Whitesides,*Patterning self-assembled monolayers using microcontact printing: a new technology for biosensors?*, *Trends Biotechnol.* **1995**, 13, 228.
[125] A. Perl, D. N. Reinhoudt, J. Huskens,*Microcontact printing: limitations and achievements*, *Adv. Mater.* **2009**, 21, 2257.
[126] S. Y. Chou, P. R. Krauss, P. J. Renstrom,*Imprint of sub‐25 nm vias and trenches in polymers*, *ApPhL* **1995**, 67, 3114.
[127] Y. Chen,*Applications of nanoimprint lithography/hot embossing: a review*, *Appl. Phys. A* **2015**, 121, 451.
[128] S. Xie, R. Luttge,*Imprint lithography provides topographical nanocues to guide cell growth in primary cortical cell culture*, *MiEng* **2014**, 124, 30.
[129] M. F. Maitz,*Applications of synthetic polymers in clinical medicine*, *Biosurface and Biotribology* **2015**, 1, 161.
[130] N. Kooy, K. Mohamed, L. T. Pin, O. S. Guan,*A review of roll-to-roll nanoimprint lithography*, *Nanoscale research letters* **2014**, 9, 320.
[131] H. W. Choi, T. Zhou, M. Singh, G. E. Jabbour,*Recent developments and directions in printed nanomaterials*, *Nanoscale* **2015**, 7, 3338.
[132] R. R. Søndergaard, M. Hösel, F. C. Krebs,*Roll‐to‐Roll fabrication of large area functional organic materials*, *J. Polym. Sci., Part B: Polym. Phys.* **2013**, 51, 16.
[133] X. Yao, R. Peng, J. Ding,*Cell–material interactions revealed via material techniques of surface patterning*, *Adv. Mater.* **2013**, 25, 5257.
[134] H. Sadri-Ardekani, A. Atala,*Regenerative Medicine and Cell Therapy: Past, Present, and Future*, *Stem Cell Nanoengineering* **2014**, 47.
[135] B. Ohlstein, T. Kai, E. Decotto, A. Spradling,*The stem cell niche: theme and variations*, *Curr. Opin. Cell Biol.* **2004**, 16, 693.
[136] J. Hao, Y. Zhang, D. Jing, Y. Shen, G. Tang, S. Huang, Z. Zhao,*Mechanobiology of mesenchymal stem cells: perspective into mechanical induction of MSC fate*, *Acta Biomater.* **2015**, 20, 1.
[137] Y. R. V. Shih, K. F. Tseng, H. Y. Lai, C. H. Lin, O. K. Lee,*Matrix stiffness regulation of integrin‐mediated mechanotransduction during osteogenic*

*differentiation of human mesenchymal stem cells*, *J. Bone Miner. Res.* **2011**, 26, 730.
[138] J. M. Curran, R. Chen, J. A. Hunt,*Controlling the phenotype and function of mesenchymal stem cells in vitro by adhesion to silane-modified clean glass surfaces*, *Biomaterials* **2005**, 26, 7057.
[139] D. S. W. Benoit, M. P. Schwartz, A. R. Durney, K. S. Anseth,*Small functional groups for controlled differentiation of hydrogel-encapsulated human mesenchymal stem cells*, *Nature materials* **2008**, 7, 816.
[140] S. Kuddannaya, Y. J. Chuah, M. H. A. Lee, N. V. Menon, Y. Kang, Y. Zhang,*Surface chemical modification of poly (dimethylsiloxane) for the enhanced adhesion and proliferation of mesenchymal stem cells*, *ACS applied materials & interfaces* **2013**, 5, 9777.
[141] F. Berthiaume, T. J. Maguire, M. L. Yarmush,*Tissue engineering and regenerative medicine: history, progress, and challenges*, *Annual review of chemical and biomolecular engineering* **2011**, 2, 403.
[142] H. Sekine, T. Shimizu, K. Sakaguchi, I. Dobashi, M. Wada, M. Yamato, E. Kobayashi, M. Umezu, T. Okano,*In vitro fabrication of functional three-dimensional tissues with perfusable blood vessels*, *Nature communications* **2013**, 4, 1399.
[143] S. Bauer, B. J. Kerr, P. H. Patterson,*The neuropoietic cytokine family in development, plasticity, disease and injury*, *Nature Reviews Neuroscience* **2007**, 8, 221.
[144] F. H. Gage,*Mammalian neural stem cells*, *Sci* **2000**, 287, 1433.
[145] F.-J. Müller, E. Y. Snyder, J. F. Loring,*Gene therapy: can neural stem cells deliver?*, *Nature Reviews Neuroscience* **2006**, 7, 75.
[146] W. Chen, Y. Shao, X. Li, G. Zhao, J. Fu,*Nanotopographical surfaces for stem cell fate control: Engineering mechanobiology from the bottom*, *Nano today* **2014**, 9, 759.
[147] M. K. Driscoll, X. Sun, C. Guven, J. T. Fourkas, W. Losert,*Cellular contact guidance through dynamic sensing of nanotopography*, *ACS nano* **2014**, 8, 3546.
[148] E. Potthoff, D. Franco, V. D'Alessandro, C. Starck, V. Falk, T. Zambelli, J. A. Vorholt, D. Poulikakos, A. Ferrari,*Toward a rational design of surface textures promoting endothelialization*, *Nano Lett.* **2014**, 14, 1069.
[149] K. Kulangara, A. F. Adler, H. Wang, M. Chellappan, E. Hammett, R. Yasuda, K. W. Leong,*The effect of substrate topography on direct reprogramming of fibroblasts to induced neurons*, *Biomaterials* **2014**, 35, 5327.
[150] M. Nikkhah, F. Edalat, S. Manoucheri, A. Khademhosseini,*Engineering microscale topographies to control the cell–substrate interface*, *Biomaterials* **2012**, 33, 5230.
[151] C. N. Prinz,*Interactions between semiconductor nanowires and living cells*, *J. Phys.: Condens. Matter* **2015**, 27, 233103.
[152] L. Hanson, W. Zhao, H.-Y. Lou, Z. C. Lin, S. W. Lee, P. Chowdary, Y. Cui, B. Cui,*Vertical nanopillars for in situ probing of nuclear mechanics in adherent cells*, *Nature nanotechnology* **2015**.
[153] S. Oh, K. S. Brammer, Y. J. Li, D. Teng, A. J. Engler, S. Chien, S. Jin,*Stem cell fate dictated solely by altered nanotube dimension*, *Proceedings of the National Academy of Sciences* **2009**, 106, 2130.

[154] L. B. Koh, I. Rodriguez, S. S. Venkatraman,*The effect of topography of polymer surfaces on platelet adhesion*, *Biomaterials* **2010**, 31, 1533.
[155] P. Friedl, K. Wolf, J. Lammerding,*Nuclear mechanics during cell migration*, *Curr. Opin. Cell Biol.* **2011**, 23, 55.
[156] J. D. Pajerowski, K. N. Dahl, F. L. Zhong, P. J. Sammak, D. E. Discher,*Physical plasticity of the nucleus in stem cell differentiation*, *Proceedings of the National Academy of Sciences* **2007**, 104, 15619.
[157] M. A. Schwartz, A. R. Horwitz,*Integrating adhesion, protrusion, and contraction during cell migration*, *Cell* **2006**, 125, 1223.
[158] K. Ye, X. Wang, L. Cao, S. Li, Z. Li, L. Yu, J. Ding,*Matrix stiffness and nanoscale spatial organization of cell-adhesive ligands direct stem cell fate*, *Nano Lett.* **2015**, 15, 4720.
[159] I. A. Janson, A. J. Putnam,*Extracellular matrix elasticity and topography: Material‐based cues that affect cell function via conserved mechanisms*, *Journal of Biomedical Materials Research Part A* **2015**, 103, 1246.
[160] P. K. Mattila, P. Lappalainen,*Filopodia: molecular architecture and cellular functions*, *Nature reviews Molecular cell biology* **2008**, 9, 446.
[161] L. E. McNamara, T. Sjöström, K. Seunarine, R. D. Meek, B. Su, M. J. Dalby,*Investigation of the limits of nanoscale filopodial interactions*, *Journal of tissue engineering* **2014**, 5, 2041731414536177.
[162] U. Jung, T. Kan, K. Kuwana, K. Matsumoto, I. Shimoyama, presented at Solid-State Sensors, Actuators and Microsystems Conference (TRANSDUCERS), 2011 16th International **2011**.
[163] Z. Li, J. Song, G. Mantini, M.-Y. Lu, H. Fang, C. Falconi, L.-J. Chen, Z. L. Wang,*Quantifying the traction force of a single cell by aligned silicon nanowire array*, *Nano Lett.* **2009**, 9, 3575.
[164] D. Choquet, D. P. Felsenfeld, M. P. Sheetz,*Extracellular matrix rigidity causes strengthening of integrin–cytoskeleton linkages*, *Cell* **1997**, 88, 39.
[165] J. P. Califano, C. A. Reinhart-King,*Substrate stiffness and cell area predict cellular traction stresses in single cells and cells in contact*, *Cellular and molecular bioengineering* **2010**, 3, 68.
[166] S. J. Han, K. S. Bielawski, L. H. Ting, M. L. Rodriguez, N. J. Sniadecki,*Decoupling substrate stiffness, spread area, and micropost density: a close spatial relationship between traction forces and focal adhesions*, *BpJ* **2012**, 103, 640.
[167] N. C. Gauthier, T. A. Masters, M. P. Sheetz,*Mechanical feedback between membrane tension and dynamics*, *Trends Cell Biol.* **2012**, 22, 527.
[168] A. Diz-Muñoz, D. A. Fletcher, O. D. Weiner,*Use the force: membrane tension as an organizer of cell shape and motility*, *Trends Cell Biol.* **2013**, 23, 47.
[169] N. C. Gauthier, O. M. Rossier, A. Mathur, J. C. Hone, M. P. Sheetz,*Plasma membrane area increases with spread area by exocytosis of a GPI-anchored protein compartment*, *Mol. Biol. Cell* **2009**, 20, 3261.
[170] H. K. Webb, R. J. Crawford, E. P. Ivanova, in *Antibacterial Surfaces*, Springer **2015**, p. 1.
[171] S. H. Nguyen, H. K. Webb, R. J. Crawford, E. P. Ivanova, in *Antibacterial Surfaces*, Springer **2015**, p. 9.
[172] T. Heister, K. Kaier, M. Wolkewitz,*Estimating the burden of nosocomial infections: Time dependency and cost clustering should be taken into account*, *Am. J. Infect. Control* **2017**, 45, 94.

[173] E. Y. Furuya, F. D. Lowy,*Antimicrobial-resistant bacteria in the community setting*, *Nature Reviews Microbiology* **2006**, 4, 36.
[174] C. de la Fuente-Núñez, F. Reffuveille, L. Fernández, R. E. W. Hancock,*Bacterial biofilm development as a multicellular adaptation: antibiotic resistance and new therapeutic strategies*, *Curr. Opin. Microbiol.* **2013**, 16, 580.
[175] C. R. Arciola, D. Campoccia, P. Speziale, L. Montanaro, J. W. Costerton,*Biofilm formation in Staphylococcus implant infections. A review of molecular mechanisms and implications for biofilm-resistant materials*, *Biomaterials* **2012**, 33, 5967.
[176] M. Otto,*Staphylococcal infections: mechanisms of biofilm maturation and detachment as critical determinants of pathogenicity*, *Annu. Rev. Med.* **2013**, 64, 175.
[177] W. H. Organization,*Antimicrobial resistance global report on surveillance: 2014 summary*, **2014**.
[178] J. M. Blair, M. A. Webber, A. J. Baylay, D. O. Ogbolu, L. J. Piddock,*Molecular mechanisms of antibiotic resistance*, *Nature Reviews Microbiology* **2015**, 13, 42.
[179] R. Laxminarayan, R. R. Chaudhury,*Antibiotic Resistance in India: Drivers and Opportunities for Action*, *PLoS Med.* **2016**, 13, 1001974.
[180] Grande-Bretagne, *Antimicrobial resistance: tackling a crisis for the health and wealth of nations*, Review on Antimicrobial Resistance, **2014**.
[181] Y. Chen, A. K. Harapanahalli, H. J. Busscher, W. Norde, H. C. van der Mei,*Nanoscale cell wall deformation impacts long-range bacterial adhesion forces on surfaces*, *Appl. Environ. Microbiol.* **2014**, 80, 637.
[182] M. Cloutier, D. Mantovani, F. Rosei,*Antibacterial coatings: challenges, perspectives, and opportunities*, *Trends Biotechnol.* **2015**, 33, 637.
[183] J. Hasan, R. J. Crawford, E. P. Ivanova,*Antibacterial surfaces: the quest for a new generation of biomaterials*, *Trends Biotechnol.* **2013**, 31, 295.
[184] W. Barthlott, C. Neinhuis,*Purity of the sacred lotus, or escape from contamination in biological surfaces*, *Planta* **1997**, 202, 1.
[185] K. Liu, L. Jiang,*Bio-inspired design of multiscale structures for function integration*, *Nano Today* **2011**, 6, 155.
[186] M. Jaggy, P. Zhang, A. M. Greiner, T. J. Autenrieth, V. Nedashkivska, A. N. Efremov, C. Blattner, M. Bastmeyer, P. A. Levkin,*Hierarchical Micro-Nano Surface Topography Promotes Long-Term Maintenance of Undifferentiated Mouse Embryonic Stem Cells*, *Nano Lett.* **2015**, 15, 7146.
[187] M. F. Griffin, P. E. Butler, A. M. Seifalian, D. M. Kalaskar,*Control of stem cell fate by engineering their micro and nanoenvironment*, *World journal of stem cells* **2015**, 7, 37.
[188] M. Li, L. Zhu, D. Lin,*Toxicity of ZnO nanoparticles to Escherichia coli: mechanism and the influence of medium components*, *Environ. Sci. Technol.* **2011**, 45, 1977.
[189] J. N. Matthews,*Low-drag suit propels swimmers*, *PhT* **2008**, 61, 32.
[190] S. Nishimoto, B. Bhushan,*Bioinspired self-cleaning surfaces with superhydrophobicity, superoleophobicity, and superhydrophilicity*, *Rsc Advances* **2013**, 3, 671.

[191] W. Song, J. Zhang, J. Guo, J. Zhang, F. Ding, L. Li, Z. Sun,*Role of the dissolved zinc ion and reactive oxygen species in cytotoxicity of ZnO nanoparticles*, *Toxicol. Lett.* **2010**, 199, 389.
[192] S. Kelleher, O. Habimana, J. Lawler, B. O'Reilly, S. Daniels, E. Casey, A. Cowley,*Cicada Wing Surface Topography: An Investigation into the Bactericidal Properties of Nanostructural Features*, *ACS applied materials & interfaces* **2015**.
[193] E. P. Ivanova, J. Hasan, H. K. Webb, G. Gervinskas, S. Juodkazis, V. K. Truong, A. H. Wu, R. N. Lamb, V. A. Baulin, G. S. Watson,*Bactericidal activity of black silicon*, *Nature communications* **2013**, 4.
[194] S. A. Boden, D. M. Bagnall, in *Encyclopedia of Nanotechnology*, DOI: 10.1007/978-94-007-6178-0_262-2 (Ed: B. Bhushan), Springer Netherlands, Dordrecht **2014**, p. 1.
[195] S. Shankar, X. Teng, G. Li, J.-W. Rhim,*Preparation, characterization, and antimicrobial activity of gelatin/ZnO nanocomposite films*, *Food Hydrocolloids* **2015**, 45, 264.
[196] S. Di Cio, T. M. Boggild, J. Connelly, D. S. Sutherland, J. E. Gautrot,*Differential Integrin Expression Regulates Cell Sensing of the Matrix Nanoscale Geometry*, *Acta Biomater.* **2016**.
[197] C. Berne, A. Ducret, G. G. Hardy, Y. V. Brun,*Adhesins involved in attachment to abiotic surfaces by Gram-Negative bacteria*, *Microbiology spectrum* **2015**, 3.
[198] C. C. Büttner, U. Schulz,*Shark skin inspired riblet coatings for aerodynamically optimized high temperature applications in aeroengines*, *Adv. Eng. Mater.* **2011**, 13, 288.
[199] J. F. Vincent, U. G. Wegst,*Design and mechanical properties of insect cuticle*, *Arthropod structure & development* **2004**, 33, 187.
[200] S. Kim, U. T. Jung, S.-K. Kim, J.-H. Lee, H. S. Choi, C.-S. Kim, M. Y. Jeong,*Nanostructured Multifunctional Surface with Antireflective and Antimicrobial Characteristics*, *ACS applied materials & interfaces* **2015**, 7, 326.
[201] M. N. Dickson, E. I. Liang, L. A. Rodriguez, N. Vollereaux, A. F. Yee,*Nanopatterned polymer surfaces with bactericidal properties*, *Biointerphases* **2015**, 10, 021010.
[202] V. T. Pham, V. K. Truong, A. Orlowska, S. Ghanaati, M. Barbeck, P. Booms, A. J. Fulcher, C. M. Bhadra, R. Buividas, V. Baulin,*"Race for the surface": eukaryotic cells can win*, *ACS applied materials & interfaces* **2016**, 8, 22025.
[203] C. M. Bhadra, V. K. Truong, V. T. Pham, M. Al Kobaisi, G. Seniutinas, J. Y. Wang, S. Juodkazis, R. J. Crawford, E. P. Ivanova,*Antibacterial titanium nano-patterned arrays inspired by dragonfly wings*, *Sci. Rep.* **2015**, 5.
[204] J. F. Schumacher, C. J. Long, M. E. Callow, J. A. Finlay, J. A. Callow, A. B. Brennan,*Engineered Nanoforce Gradients for Inhibition of Settlement (Attachment) of Swimming Algal Spores*, *Langmuir* **2008**, 24, 4931.
[205] M. J. Dalby, N. Gadegaard, R. O. Oreffo,*Harnessing nanotopography and integrin-matrix interactions to influence stem cell fate*, *Nature materials* **2014**, 13, 558.
[206] K. Delgado, R. Quijada, R. Palma, H. Palza,*Polypropylene with embedded copper metal or copper oxide nanoparticles as a novel plastic antimicrobial agent*, *Lett. Appl. Microbiol.* **2011**, 53, 50.

[207] R. T. De Silva, P. Pasbakhsh, S. M. Lee, A. Y. Kit,*ZnO deposited/encapsulated halloysite–poly (lactic acid)(PLA) nanocomposites for high performance packaging films with improved mechanical and antimicrobial properties*, *Applied clay science* **2015**, 111, 10.
[208] T. Lou, M. Leung, X. Wang, J. Y. F. Chang, C. T. Tsao, J. G. C. Sham, D. Edmondson, M. Zhang,*Bi-layer scaffold of chitosan/PCL-nanofibrous mat and PLLA-microporous disc for skin tissue engineering*, *Journal of biomedical nanotechnology* **2014**, 10, 1105.
[209] A. Barui, R. Khare, S. Dhara, P. Banerjee, J. Chatterjee,*Ex vivo bio-compatibility of honey-alginate fibrous matrix for HaCaT and 3T3 with prime molecular expressions*, *JMSMM* **2014**, 25, 2659.
[210] B. Guo, Y. Sun, A. Finne-Wistrand, K. Mustafa, A.-C. Albertsson,*Electroactive porous tubular scaffolds with degradability and non-cytotoxicity for neural tissue regeneration*, *Acta Biomater.* **2012**, 8, 144.
[211] N. Maas-Szabowski, A. Stärker, N. E. Fusenig,*Epidermal tissue regeneration and stromal interaction in HaCaT cells is initiated by TGF-α, J. Cell Sci.* **2003**, 116, 2937.
[212] F. Groeber, M. Holeiter, M. Hampel, S. Hinderer, K. Schenke-Layland,*Skin tissue engineering—in vivo and in vitro applications*, *Adv. Drug Del. Rev.* **2011**, 63, 352.
[213] D. Bozukova, C. Pagnoulle, R. Jérôme, C. Jérôme,*Polymers in modern ophthalmic implants—Historical background and recent advances*, *Materials Science and Engineering: R: Reports* **2010**, 69, 63.
[214] X. Li,*Bactericidal mechanism of nanopatterned surfaces*, *PCCP* **2016**, 18, 1311.
[215] S. Pogodin, J. Hasan, V. A. Baulin, H. K. Webb, V. K. Truong, T. H. P. Nguyen, V. Boshkovikj, C. J. Fluke, G. S. Watson, J. A. Watson,*Biophysical model of bacterial cell interactions with nanopatterned cicada wing surfaces*, *BpJ* **2013**, 104, 835.
[216] X. Li, T. Chen,*Enhancement and suppression effects of a nanopatterned surface on bacterial adhesion*, *PhRvE* **2016**, 93, 052419.
[217] P. M. Tsimbouri, L. Fisher, N. Holloway, T. Sjostrom, A. H. Nobbs, R. D. Meek, B. Su, M. J. Dalby,*Osteogenic and bactericidal surfaces from hydrothermal titania nanowires on titanium substrates*, *Sci. Rep.* **2016**, 6.
[218] F. Viela, D. Granados, A. Ayuso-Sacido, I. Rodríguez,*Biomechanical Cell Regulation by High Aspect Ratio Nanoimprinted Pillars*, *Adv. Funct. Mater.* **2016**, 26, 5599.
[219] G. Ramanathan, S. Singaravelu, M. Raja, N. Nagiah, P. Padmapriya, K. Ruban, K. Kaveri, T. Natarajan, U. T. Sivagnanam, P. T. Perumal,*Fabrication and characterization of a collagen coated electrospun poly (3-hydroxybutyric acid)–gelatin nanofibrous scaffold as a soft bio-mimetic material for skin tissue engineering applications*, *RSC Advances* **2016**, 6, 7914.
[220] I. Liakos, L. Rizzello, H. Hajiali, V. Brunetti, R. Carzino, P. Pompa, A. Athanassiou, E. Mele,*Fibrous wound dressings encapsulating essential oils as natural antimicrobial agents*, *Journal of Materials Chemistry B* **2015**, 3, 1583.
[221] M. Spear,*Silver: An Age‐Old Treatment Modality in Modern Times*, *Plast. Surg. Nurs.* **2010**, 30, 90.
[222] H. Kanematsu, D. M. Barry, *Biofilm and materials science*, Springer, **2015**.

[223] M. L. W. Knetsch, L. H. Koole,*New strategies in the development of antimicrobial coatings: the example of increasing usage of silver and silver nanoparticles*, *Polymers* **2011**, 3, 340.
[224] H. Palza,*Antimicrobial polymers with metal nanoparticles*, *International journal of molecular sciences* **2015**, 16, 2099.
[225] R. Rawashdeh, Y. Haik,*Antibacterial Mechanisms of Metallic Nanoparticles: A Review*, *Dynamic Biochemistry, Process Biotechnology and Molecular Biology* **2009**, 3, 12.
[226] S. Shleev, J. Tkac, A. Christenson, T. Ruzgas, A. I. Yaropolov, J. W. Whittaker, L. Gorton,*Direct electron transfer between copper-containing proteins and electrodes*, *Biosens. Bioelectron.* **2005**, 20, 2517.
[227] S. Prabhu, E. K. Poulose,*Silver nanoparticles: mechanism of antimicrobial action, synthesis, medical applications, and toxicity effects*, *International Nano Letters* **2012**, 2, 32.
[228] M. M. Khan, S. F. Adil, A. Al-Mayouf, Elsevier, 2015.
[229] A. B. Djurišić, Y. H. Leung, A. M. C. Ng,*Strategies for improving the efficiency of semiconductor metal oxide photocatalysis*, *Materials Horizons* **2014**, 1, 400.
[230] A. Sirelkhatim, S. Mahmud, A. Seeni, N. H. M. Kaus, L. C. Ann, S. K. M. Bakhori, H. Hasan, D. Mohamad,*Review on zinc oxide nanoparticles: antibacterial activity and toxicity mechanism*, *Nano-Micro Letters* **2015**, 7, 219.
[231] A. Raghunath, E. Perumal,*Metal oxide nanoparticles as antimicrobial agents: a promise for the future*, *Int. J. Antimicrob. Agents* **2017**.
[232] G. Grass, C. Rensing, M. Solioz,*Metallic copper as an antimicrobial surface*, *Appl. Environ. Microbiol.* **2011**, 77, 1541.
[233] G. M. Whitesides,*Nanoscience, nanotechnology, and chemistry*, *Small* **2005**, 1, 172.
[234] Y. Xia,*Nanomaterials at work in biomedical research*, *Nature materials* **2008**, 7, 758.
[235] M. J. Hajipour, K. M. Fromm, A. A. Ashkarran, D. J. de Aberasturi, I. R. de Larramendi, T. Rojo, V. Serpooshan, W. J. Parak, M. Mahmoudi,*Antibacterial properties of nanoparticles*, *Trends Biotechnol.* **2012**, 30, 499.
[236] J. F. Hernández-Sierra, F. Ruiz, D. C. C. Pena, F. Martínez-Gutiérrez, A. E. Martínez, A. d. J. P. Guillén, H. Tapia-Pérez, G. M. Castañón,*The antimicrobial sensitivity of Streptococcus mutans to nanoparticles of silver, zinc oxide, and gold*, *Nanomed. Nanotechnol. Biol. Med.* **2008**, 4, 237.
[237] R. Mie, M. W. Samsudin, L. B. Din, A. Ahmad, N. Ibrahim, S. N. A. Adnan,*Synthesis of silver nanoparticles with antibacterial activity using the lichen Parmotrema praesorediosum*, *International journal of nanomedicine* **2014**, 9, 121.
[238] S. Pal, Y. K. Tak, J. M. Song,*Does the antibacterial activity of silver nanoparticles depend on the shape of the nanoparticle? A study of the gram-negative bacterium Escherichia coli*, *Appl. Environ. Microbiol.* **2007**, 73, 1712.
[239] K. Bahrami, P. Nazari, M. Nabavi, M. Golkar, A. Almasirad, A. R. Shahverdi,*Hydroxyl capped silver-gold alloy nanoparticles: characterization and their combination effect with different antibiotics against Staphylococcus aureus*, *Nanomedicine Journal* **2014**, 1, 155.
[240] A. Besinis, T. De Peralta, R. D. Handy,*The antibacterial effects of silver, titanium dioxide and silica dioxide nanoparticles compared to the dental*

*disinfectant chlorhexidine on Streptococcus mutans using a suite of bioassays*, *Nanotoxicology* **2014**, 8, 1.
[241] J. T. Seil, T. J. Webster,*Antimicrobial applications of nanotechnology: methods and literature*, *Int J Nanomedicine* **2012**, 7, 2767.
[242] C. Buzea, I. I. Pacheco, K. Robbie,*Nanomaterials and nanoparticles: Sources and toxicity*, *Biointerphases* **2007**, 2, MR17.
[243] F. Haghighi, S. Roudbar Mohammadi, P. Mohammadi, S. Hosseinkhani, R. Shipour,*Antifungal activity of TiO2 nanoparticles and EDTA on Candida albicans biofilms*, *Infection, Epidemiology and Medicine* **2013**, 1, 33.
[244] G. Carré, E. Hamon, S. Ennahar, M. Estner, M.-C. Lett, P. Horvatovich, J.-P. Gies, V. Keller, N. Keller, P. Andre,*TiO2 photocatalysis damages lipids and proteins in Escherichia coli*, *Appl. Environ. Microbiol.* **2014**, 80, 2573.
[245] V. Ravishankar Rai, A. Jamuna Bai,*Nanoparticles and their potential application as antimicrobials*, *Science against microbial pathogens: communicating current research and technological advances. Badajoz, Spain: Formatex Research Center* **2011**, 197.
[246] J. W. Rasmussen, E. Martinez, P. Louka, D. G. Wingett,*Zinc oxide nanoparticles for selective destruction of tumor cells and potential for drug delivery applications*, *Expert opinion on drug delivery* **2010**, 7, 1063.
[247] M. Oves,*Antimicrobial activity of metal oxide nanoparticles against Gram-positive and Gram-negative bacteria: a comparative study*, *Ijnm* **2012**.
[248] M. Ahamed, H. A. Alhadlaq, M. A. Khan, P. Karuppiah, N. A. Al-Dhabi,*Synthesis, characterization, and antimicrobial activity of copper oxide nanoparticles*, *Journal of Nanomaterials* **2014**, 2014, 17.
[249] A. M. Allahverdiyev, E. S. Abamor, M. Bagirova, M. Rafailovich,*Antimicrobial effects of TiO2 and Ag2O nanoparticles against drug-resistant bacteria and leishmania parasites*, *Future Microbiol.* **2011**, 6, 933.
[250] J.-W. Rhim, H.-M. Park, C.-S. Ha,*Bio-nanocomposites for food packaging applications*, *Prog. Polym. Sci.* **2013**, 38, 1629.
[251] S. Pina, J. M. Oliveira, R. L. Reis,*Natural‐Based Nanocomposites for Bone Tissue Engineering and Regenerative Medicine: A Review*, *Adv. Mater.* **2015**, 27, 1143.
[252] A. Farouk, S. Moussa, M. Ulbricht, E. Schollmeyer, T. Textor,*ZnO-modified hybrid polymers as an antibacterial finish for textiles*, *Textile Research Journal* **2014**, 84, 40.
[253] M. Moniruzzaman, K. I. Winey,*Polymer nanocomposites containing carbon nanotubes*, *Macromolecules* **2006**, 39, 5194.
[254] M. Rai, A. P. Ingle, S. Gaikwad, I. Gupta, A. Gade, S. Silvério da Silva,*Nanotechnology based anti‐infectives to fight microbial intrusions*, *J. Appl. Microbiol.* **2016**, 120, 527.
[255] J.-Y. Wu, C.-W. Li, C.-H. Tsai, C.-W. Chou, D.-R. Chen, G.-J. Wang,*Synthesis of antibacterial TiO 2/PLGA composite biofilms*, *Nanomed. Nanotechnol. Biol. Med.* **2014**, 10, e1097.
[256] A. M. Díez-Pascual, A. L. Díez-Vicente,*Nano-TiO2 reinforced PEEK/PEI blends as biomaterials for load-bearing implant applications*, *ACS applied materials & interfaces* **2015**, 7, 5561.
[257] Y. Haldorai, J.-J. Shim,*Multifunctional chitosan-copper oxide hybrid material: photocatalytic and antibacterial activities*, *International Journal of Photoenergy* **2013**, 2013.

[258] W. A. Daoud, J. H. Xin, Y.-H. Zhang,*Surface functionalization of cellulose fibers with titanium dioxide nanoparticles and their combined bactericidal activities*, *SurSc* **2005**, 599, 69.
[259] A. Bonnefond, E. González, J. M. Asua, J. R. Leiza, J. Kiwi, C. Pulgarin, S. Rtimi,*New evidence for hybrid acrylic/TiO 2 films inducing bacterial inactivation under low intensity simulated sunlight*, *Colloids Surf. B. Biointerfaces* **2015**, 135, 1.
[260] V. B. Schwartz, F. Thétiot, S. Ritz, S. Pütz, L. Choritz, A. Lappas, R. Förch, K. Landfester, U. Jonas,*Antibacterial Surface Coatings from Zinc Oxide Nanoparticles Embedded in Poly (N‐isopropylacrylamide) Hydrogel Surface Layers*, *Adv. Funct. Mater.* **2012**, 22, 2376.
[261] S. D. Burnside, V. Shklover, C. Barbé, P. Comte, F. Arendse, K. Brooks, M. Grätzel,*Self-organization of TiO2 nanoparticles in thin films*, *Chem. Mater.* **1998**, 10, 2419.
[262] J. J. Hernández, M. A. Monclús, I. Navarro-Baena, F. Viela, J. M. Molina-Aldareguia, I. Rodríguez,*Multifunctional Nano-engineered Polymer Surfaces with Enhanced Mechanical Resistance and Superhydrophobicity*, *Sci. Rep.* **2017**, 7, 43450.
[263] M. Ul-Islam, W. A. Khattak, M. W. Ullah, S. Khan, J. K. Park,*Synthesis of regenerated bacterial cellulose-zinc oxide nanocomposite films for biomedical applications*, *Cellu* **2014**, 21, 433.
[264] S. Khan, M. Ul-Islam, W. A. Khattak, M. W. Ullah, J. K. Park,*Bacterial cellulose-titanium dioxide nanocomposites: nanostructural characteristics, antibacterial mechanism, and biocompatibility*, *Cellu* **2015**, 22, 565.
[265] A. Kubacka, C. Serrano, M. Ferrer, H. Lünsdorf, P. Bielecki, M. L. Cerrada, M. Fernández-García, M. Fernández-García,*High-performance dual-action polymer-TiO2 nanocomposite films via melting processing*, *Nano Lett.* **2007**, 7, 2529.
[266] A. Kubacka, M. S. Diez, D. Rojo, R. Bargiela, S. Ciordia, I. Zapico, J. P. Albar, C. Barbas, V. A. M. dos Santos, M. Fernández-García,*Understanding the antimicrobial mechanism of TiO2-based nanocomposite films in a pathogenic bacterium*, *Sci. Rep.* **2014**, 4.
[267] L. Tamayo, M. Azócar, M. Kogan, A. Riveros, M. Páez,*Copper-polymer nanocomposites: An excellent and cost-effective biocide for use on antibacterial surfaces*, *Materials Science and Engineering: C* **2016**, 69, 1391.
[268] R. Dutta, B. P. Nenavathu, M. K. Gangishetty, A. Reddy,*Studies on antibacterial activity of ZnO nanoparticles by ROS induced lipid peroxidation*, *Colloids Surf. B. Biointerfaces* **2012**, 94, 143.
[269] S. Dalai, S. Pakrashi, S. Chakravarty, S. Hussain, N. Chandrasekaran, A. Mukherjee,*Studies on interfacial interactions of TiO2 nanoparticles with bacterial cells under light and dark conditions*, *Bull. Mater. Sci.* **2014**, 37, 371.
[270] A. Joe, S.-H. Park, K.-D. Shim, D.-J. Kim, K.-H. Jhee, H.-W. Lee, C.-H. Heo, H.-M. Kim, E.-S. Jang,*Antibacterial mechanism of ZnO nanoparticles under dark conditions*, *Journal of Industrial and Engineering Chemistry* **2017**, 45, 430.
[271] G. Applerot, A. Lipovsky, R. Dror, N. Perkas, Y. Nitzan, R. Lubart, A. Gedanken,*Enhanced antibacterial activity of nanocrystalline ZnO due to increased ROS‐mediated cell injury*, *Adv. Funct. Mater.* **2009**, 19, 842.

[272] Y. Li, W. Zhang, J. Niu, Y. Chen,*Mechanism of photogenerated reactive oxygen species and correlation with the antibacterial properties of engineered metal-oxide nanoparticles*, *ACS nano* **2012**, 6, 5164.
[273] V. Lakshmi Prasanna, R. Vijayaraghavan,*Insight into the mechanism of antibacterial activity of ZnO: surface defects mediated reactive oxygen species even in the dark*, *Langmuir* **2015**, 31, 9155.
[274] B. Zhao, H. C. van der Mei, G. Subbiahdoss, J. de Vries, M. Rustema-Abbing, R. Kuijer, H. J. Busscher, Y. Ren,*Soft tissue integration versus early biofilm formation on different dental implant materials*, *Dent. Mater.* **2014**, 30, 716.
[275] J. L. García, A. Asadinezhad, J. Pacherník, M. Lehocký, I. Junkar, P. Humpolíček, P. Sáha, P. Valášek,*Cell proliferation of HaCaT keratinocytes on collagen films modified by argon plasma treatment*, *Molecules* **2010**, 15, 2845.